

AD\_\_\_\_\_

Award Number: W81XWH-07-1-0099

TITLE: Development of Highly Sensitive Bulk Acoustic Wave Device Biosensor Arrays  
for Screening and Early Detection of Prostate Cancer

PRINCIPAL INVESTIGATOR: Anthony J Dickherber

CONTRACTING ORGANIZATION: Georgia Tech Research Corporation  
Atlanta, GA 30332

REPORT DATE: January 2008

TYPE OF REPORT: Annual Summary

PREPARED FOR: U.S. Army Medical Research and Materiel Command  
Fort Detrick, Maryland 21702-5012

DISTRIBUTION STATEMENT: Approved for Public Release;  
Distribution Unlimited

The views, opinions and/or findings contained in this report are those of the author(s) and should not be construed as an official Department of the Army position, policy or decision unless so designated by other documentation.

<b>REPORT DOCUMENTATION PAGE</b>				Form Approved OMB No. 0704-0188	
Public reporting burden for this collection of information is estimated to average 1 hour per response, including the time for reviewing instructions, searching existing data sources, gathering and maintaining the data needed, and completing and reviewing this collection of information. Send comments regarding this burden estimate or any other aspect of this collection of information, including suggestions for reducing this burden to Department of Defense, Washington Headquarters Services, Directorate for Information Operations and Reports (0704-0188), 1215 Jefferson Davis Highway, Suite 1204, Arlington, VA 22202-4302. Respondents should be aware that notwithstanding any other provision of law, no person shall be subject to any penalty for failing to comply with a collection of information if it does not display a currently valid OMB control number. <b>PLEASE DO NOT RETURN YOUR FORM TO THE ABOVE ADDRESS.</b>					
<b>1. REPORT DATE (DD-MM-YYYY)</b> 01-01-2008		<b>2. REPORT TYPE</b> Annual Summary		<b>3. DATES COVERED (From - To)</b> 1 JAN 2007 - 31 DEC 2007	
<b>4. TITLE AND SUBTITLE</b>  Development of Highly Sensitive Bulk Acoustic Wave Device Biosensor Arrays for Screening and Early Detection of Prostate Cancer				<b>5a. CONTRACT NUMBER</b>	
				<b>5b. GRANT NUMBER</b> W81XWH-07-1-0099	
				<b>5c. PROGRAM ELEMENT NUMBER</b>	
<b>6. AUTHOR(S)</b> Anthony J Dickherber  E-Mail: tonyd@gatech.edu				<b>5d. PROJECT NUMBER</b>	
				<b>5e. TASK NUMBER</b>	
				<b>5f. WORK UNIT NUMBER</b>	
<b>7. PERFORMING ORGANIZATION NAME(S) AND ADDRESS(ES)</b>  Georgia Tech Research Corporation Atlanta, GA 30332				<b>8. PERFORMING ORGANIZATION REPORT NUMBER</b>	
<b>9. SPONSORING / MONITORING AGENCY NAME(S) AND ADDRESS(ES)</b> U.S. Army Medical Research and Materiel Command Fort Detrick, Maryland 21702-5012				<b>10. SPONSOR/MONITOR'S ACRONYM(S)</b>	
				<b>11. SPONSOR/MONITOR'S REPORT NUMBER(S)</b>	
<b>12. DISTRIBUTION / AVAILABILITY STATEMENT</b> Approved for Public Release; Distribution Unlimited					
<b>13. SUPPLEMENTARY NOTES</b>					
<b>14. ABSTRACT</b> In this research, we present several novel contributions to the field of microelectronic acoustic biosensors that approach the goal of developing a cost-effective, highly sensitive and highly selective sensor array for the detection of early cancer proliferation. First we report on the development of a novel solidly mounted shear-mode resonator employing piezoelectric ZnO as an appropriate base device for liquid-phase sensing applications. Second we report on the development of an appropriate chemical surface preparation protocol for the covalent immobilization of monoclonal IgG antibodies to the surface of this device, thereby functionalizing it as a biosensor. Preliminary data employing these sensors for the detection of prostate specific antigen in LnCap conditioned medium as well as progress towards developing a packaged disposable sensor array system is also reported. This research has thus far yielded three journal publications and three conference abstracts, which are provided in the report.					
<b>15. SUBJECT TERMS</b> Prostate cancer, early detection, biosensor, microelectronic acoustics					
<b>16. SECURITY CLASSIFICATION OF:</b>			<b>17. LIMITATION OF ABSTRACT</b>  UU	<b>18. NUMBER OF PAGES</b>  95	<b>19a. NAME OF RESPONSIBLE PERSON</b> USAMRMC
<b>a. REPORT</b> U	<b>b. ABSTRACT</b> U	<b>c. THIS PAGE</b> U			<b>19b. TELEPHONE NUMBER (include area code)</b>

## Table of Contents

Introduction.....	3
Body.....	4
Device design and development .....	4
ZnO solidly mounted resonator .....	4
Device testing.....	5
Surface preparation .....	8
Covalent antibody immobilization.....	8
Sensor array system .....	10
Key Research Accomplishments: .....	13
Reportable Outcomes.....	14
Conclusion .....	15
So what?.....	15
Future work.....	15
References:.....	17
Appendices:.....	19
Journal of Applied Physics 2007 – <i>published manuscript</i> .....	20
2007 AACR Molecular Diagnostics and Therapeutics Conference - <i>abstract</i> .....	27
2007 AACR Conference Press Release .....	28
2007 AACR Conference Press Coverage .....	30
2007 IEEE Sensors Conference - <i>abstract</i> .....	34
Sensors & Actuators A: Physics 2007 – <i>accepted manuscript</i> .....	38
Langmuir 2008 - <i>submitted manuscript</i> .....	63
2008 Annual MeetAACR - <i>abstract</i> .....	90
Anthony Dickherber – <i>curriculum vitae</i> .....	91

## Introduction

Microelectronic acoustic devices have long been recognized as offering great potential as biomedical sensors; specifically microelectronic piezoelectric resonators. Excitation of a thickness shear mode (TSM) in a piezoelectric crystal bulk is ideal for liquid-phase applications (*e.g.* blood or serum) as aqueous solutions cannot support propagation of a shear wave. Therefore, minimal acoustic energy is lost into the liquid media. The resonance condition (or resonance frequency) of the device then becomes a highly sensitive real-time indicator of any changes in surface conditions. The resonator is functionalized as a biosensor by immobilization of a bio- or chemi-specific layer at the surface of the device. Specific binding events at the biolayer interface therefore cause changes in the surface conditions resulting in a change of the resonance frequency, which is an easily monitored parameter. Employing common fabrication methods from the microelectronic device industry, this very cost-effective biosensor could be used for multiple applications. As a screening tool, this sensor device offers the possibility of detecting extremely low concentrations of multiple targets in a physiologically noisy environment at a very low cost. For researchers, it is a powerful tool for conducting basic proteomics research in the laboratory.

The implementation of this biosensor technology towards early cancer detection is reliant upon the discovery of appropriate biomarkers. Prostate cancer is an especially attractive initial focus for this research as much work has already gone into identifying various potential diagnostically relevant biomarkers. Of course early indicators involve the various forms of prostate specific antigen (PSA), but more recently a great deal of excitement has surrounded the relevance of early prostate cancer antigen (EPCA-2) [1].

The purpose of this research is to design and develop a new biosensor array technology that offers near real-time reporting and high specificity simultaneously for multiple targets, with a high degree of specificity, producible at low cost. This proposal builds upon a significant amount of past research that demonstrates the feasibility of this goal, yet has thus far fallen short. A new piezoelectric material to supplant crystal quartz is required to achieve greater sensitivity over the widely used quartz crystal microbalance (QCM) biosensor [2, 3] and allow for miniaturization. A novel surface chemistry is required to immobilize specific capture molecules on the surface of that crystal which likely will not have been developed before. Finally, the biosensor array system will need to be packaged in such a way that liquid samples can be introduced to the sensor surface in a controlled fashion.

## Body

Three primary research goals were submitted in the *statement of work* for this training project. In general, they were as follows:

1. *The design and development of acoustic resonator arrays that could be employed as liquid-phase biosensors;*
2. *The development of a repeatable surface chemistry protocol appropriate for our resonator material for immobilization of specific capture molecules;*
3. *Testing the sensor array system for known prostate cancer biomarkers in an effort to establish a protocol for early cancer detection.*

Substantial progress has been made towards achieving the first two goals of this research along with significant achievements to report on the third.

### ***Device design and development***

Microelectronic biosensors are comprised of a transducer element coupled with a molecularly-specific surface treatment. As indicated in the submitted statement of work, the transducer element selected for this biosensor application is an acoustic resonator. It was decided early that a bulk acoustic wave (BAW) device should be employed rather than a surface acoustic wave (SAW) device for this liquid-phase biosensor application. Past success with BAW devices is demonstrated by the QCM towards liquid-phase biosensor applications swayed this decision, as these devices have already been shown to exhibit strong qualities as liquid biosensors [2, 3]. Furthermore, it is easier to achieve higher resonant frequencies with BAW devices than with SAW devices, which is a requirement for developing acoustic sensors with higher sensitivity.

### **ZnO solidly mounted resonator**

A BAW resonator functions by maintaining the acoustic energy within the piezoelectric crystal film. This occurs by maintaining an apparent acoustic impedance of zero on opposing sides of the crystal film, which is the acoustic impedance of air. Thin film bulk acoustic resonators (FBAR) are generally implemented in the membrane form by etching the supporting material beneath the piezoelectric film yielding a device similar to the one seen in Figure 1 (left). This implementation is a mechanically fragile design and requires difficult and often very expensive fabrication steps. The solidly mounted resonator (SMR) implementation is a solution to this problem originally described by Newell [4] and is achieved through the use of an acoustic mirror; analogous to an optical Bragg reflector. Considering that the device package must be easily fabricated with existing microelectronic fabrication equipment, a SMR package was selected as the base resonator design, as seen in Figure 1 (right).

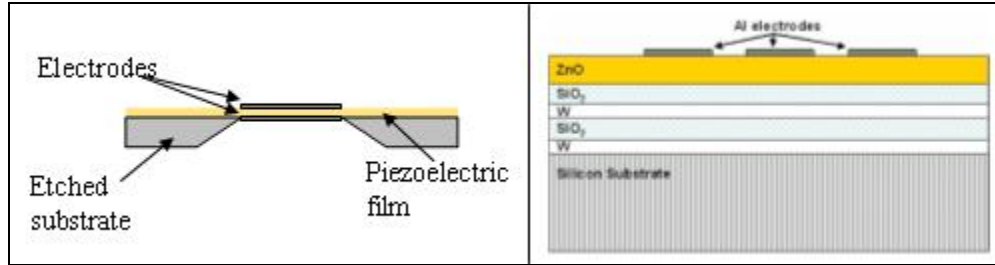


**Figure 1.** Comparison of traditional thin-film bulk acoustic resonator (FBAR) design (left figure) with solidly mounted resonator design (right figure) offers simple and robust fabrication alternative to traditional FBAR approach.

Two piezoelectric crystal species were considered in developing the bulk acoustic resonator device that could be employed for our liquid-phase biosensor. Zinc oxide (ZnO) yielded results far superior to the tantalum pentoxide (Ta<sub>2</sub>O<sub>5</sub>) alternative that was attempted. Preliminary results for the quality of the ZnO resonators achieved were summarized and published in the *Journal of Applied Physics* [5]. Incidentally, the significance of this work was quickly recognized by and jointly published in the *Virtual Journal of Biological Physics Research*. The 2 GHz TSM resonator was achieved by lateral field excitation (LFE) of thin-film (< 1  $\mu\text{m}$ ) *c*-axis oriented ZnO, deposited by RF sputtering. Theoretical treatment of LFE of ZnO to achieve a TSM acoustic resonator has been available since the late 1980s [6] and some attempts published in the research literature prior to this work [7, 8], but these implementations had either very difficult fabrication requirements or yielded dubious results. Furthermore, LFE of ZnO had never been realized in an SMR implementation before this work. While these results are promising, it is felt that the device quality must be higher still than what has been achieved thus far in order to obtain the biosensor sensitivity promised by a device that exhibits such a high operating frequency.

## Device testing

Further testing was performed on the ZnO devices to evaluate their susceptibility to changing temperature and solution conductivity. Thermal testing is a standard resonator evaluation criterion, in which the reported parameter is the standard *temperature coefficient of resonant frequency* (TCF). Conductivity susceptibility tests had to be conducted due to the LFE method employed in this design. Since oppositely polarized electrode materials are deposited plane-parallel on the surface of the piezoelectric thin film and both exposed to the liquid sample under test, it is possible that the conductivity of the fluid might divert significant electrical energy away from the piezoelectric crystal and thereby substantially affect device performance. The results of both of the temperature susceptibility and sample conductivity tests were submitted to the IEEE Sensors 2007 Annual Conference by June of 2007 and presented in October of 2007 [9]. Thermal experiments the resonator demonstrated a low TCF of  $\sim 25$  ppm/ $^{\circ}\text{C}$ , which is desirable for our application. Conductivity tests indicate that solution conductivity did have some effect on device performance as the device quality diminished with increasing solution conductivity. That is to say, that the resonance condition became more difficult

to track with increasing solution conductivity, which is not a surprising result for the reason indicated above. Significantly, however, the solution conductivity did not have a significant effect on the resonance frequency itself, as can be seen from Figure 2 below. Further, it is expected that the degradation in monitoring precision will be substantially improved by further improving device quality factor,  $Q$ .

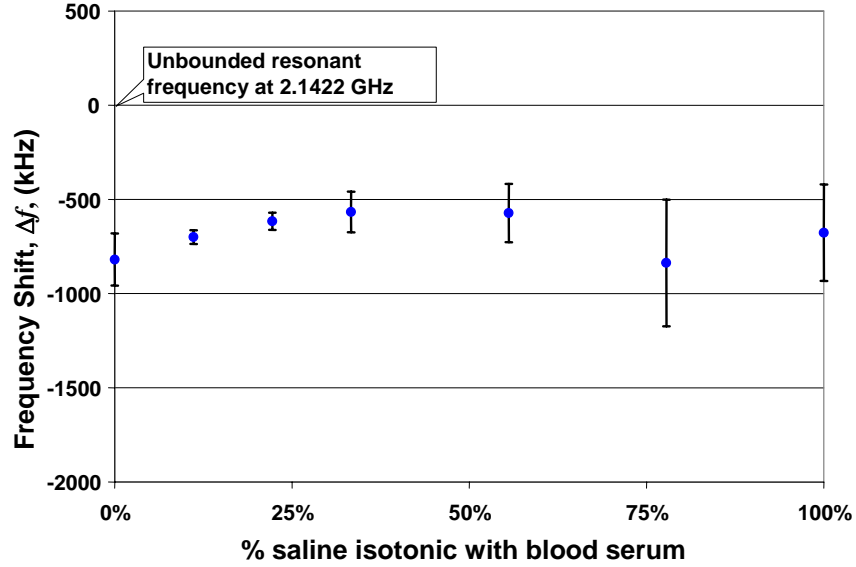


**Figure 2.** Change in resonant frequency as a function of increasing fluid sample conductivity

Tests were performed to evaluate device performance as a function of electrode geometry. Two electrode configurations were attempted (as seen in Figure 3) along with variations in electrode width and ground-signal electrode gap width. These results were summarized and submitted for publication in the *Sensors & Actuators A: Physics* journal [10]. This article has been accepted by the journal editors and is currently pending publication.

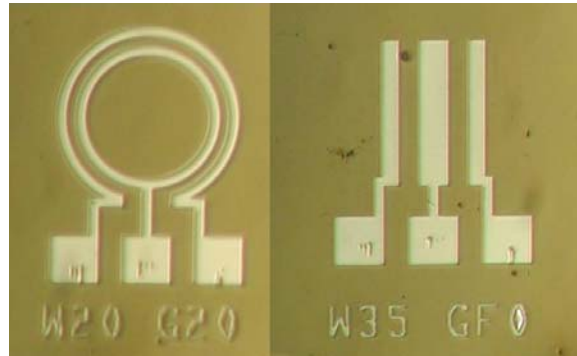


**Figure 3.** Various electrode shapes fabricated in an effort to determine the optimal LFE resonator configuration. [Note the left figure has electrode widths of 20  $\mu\text{m}$  and a gap size of 20  $\mu\text{m}$ , and the right figure has electrode widths of 35  $\mu\text{m}$  and a gap size of 40  $\mu\text{m}$ ]

In general, it was found that there was a marginal trade-off in performance parameters ( $Q$  and coupling coefficient,  $K^2$ ) between the two electrode geometries implemented. Surprisingly, electrode width and inter-electrode gap width had very little effect on device performance. The results of these experiments are summarized in Table 1 below and graphically displayed in Figure 4.

Device	Shape	Electrode Width ( $\mu\text{m}$ )	Electrode Gap ( $\mu\text{m}$ )	# Tested	Average $Q$	Average $K^2$
A	Circular	20	10	92	198	0.86%
B	Circular	20	20	72	195	0.87%
C	Circular	20	40	70	192	0.86%
D	Straight	20	10	69	198	0.84%
E	Straight	35	20	74	217	0.78%
F	Straight	35	40	98	206	0.77%
G	Straight	20	50	25	220	0.74%
H	Straight	35	50	44	221	0.73%

**Table 1.** Assessment of device performance of tested resonators from analysis of collected S11 parameters.

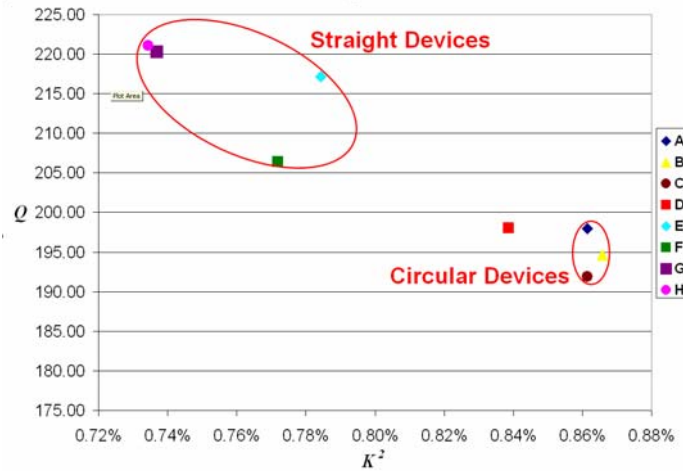


**Figure 4.** Comparison of various electrode configurations using  $Q$  and  $K^2$ .

It was decided that  $Q$  was the most important parameter to optimize, as it is the best predictor of how clearly the resonance condition can be monitored. Therefore the straight finger electrode design was selected for implementation in an eight-device array structure, as seen in Figure 5. It was then necessary to quantify any loss in performance due to the array configuration. It was found that device  $Q$  deteriorated by approximately 30% as a result of the electrode configuration in the array structure. This is not surprising as the additional metallization required to implement the array structure would likely disturb the electric field distribution and thereby reduce the amount of electrical energy focused on stimulating the piezoelectric crystal. These results are also discussed further in the publication in *Sensors & Actuators A* [10].



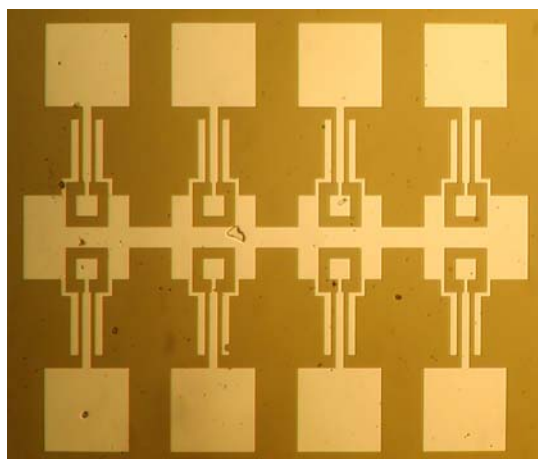


**Figure 5.** Digital image of fabricated 8-device array. Device is designed for probing with Cascade Microtech ACP40 GSG150 probes and with pads large enough for subsequent wire bonding. These devices have electrode widths of 50  $\mu\text{m}$  and a gap size of 20  $\mu\text{m}$ .

Currently, the acoustic mirror performance is being investigated to verify that it performs as theoretical calculations predict it should. As mentioned earlier, the acoustic mirror functions similarly to an optical Bragg reflector. Alternating quarter-wavelength thin films of materials with high acoustic impedance mismatches are deposited as a substrate for the piezoelectric crystal layer in order to mimic an air boundary. That is to say, the acoustic mirror is meant to “appear” as having an acoustic impedance of zero in order to force acoustic energy to remain within the piezoelectric crystal, thereby achieving the resonance function. Preliminary results indicate that the mirror does not perform nearly as well as theoretical calculations predict, which is not a surprising result. Full empirical elucidation of the acoustic mirror performance should yield a configuration for improved device  $Q$ . The result of these experiments is expected by the end of January 2008 and will subsequently be submitted for publication in a suitable journal.

## ***Surface preparation***

It is a requirement of any analytical instrument that the output signal, or response, be repeatable given multiple identical samples under test. One of the most critical aspects in the development of high precision biosensors is the controlled immobilization of appropriate capture molecules to form a molecularly-specific surface on the device. Excessive variation in this process would obviate the achievement of a highly sensitive sensor, as deviations due to inconsistent immobilization would make impossible the ability to compare results from one sensor to any other; a control sensor, for example.

## **Covalent antibody immobilization**

Attachment of antibodies to the surface of ZnO can be achieved through simple adsorption. The resulting surface coverage, uniformity and repeatability from this method

are not sufficient for biosensor applications. Formation of a covalent bond between the antibody and ZnO surface via a chemical crosslinker is the preferred method over adsorption for several reasons. First, the stable bonds that are formed yield a more robust sensor. Further, it is often the case that biosensor experiments require that the sensor be subjected to fluidic flow. Therefore covalent immobilization of antibodies is important to withstand fluidic washing steps for preventing detachment of the antibodies from the surface. Detachment of capture molecules from the surface would erroneously affect the sensor's output signal.

To date, the literature pertaining to functionalizing crystal oxides through covalent methods has largely been focused on SiO<sub>2</sub>. Hydroxyl groups at the surface of an oxide provide sites for reaction with cross-linking molecules to form covalent bonds [11]. One of the more common methods for functionalizing SiO<sub>2</sub> surfaces involves the use of organosilane molecules as primary crosslinkers. Organosilane molecules react at room temperature with surface hydroxides to link the silane molecules to the oxide surface. Success with immobilizing antibodies on silica surfaces has been shown using amine- and thiol-terminal silanes such as 3-Mercaptopropyltrimethoxysilane (MTS). Subsequent binding of a secondary crosslinker, such as N- $\gamma$ -maleimidobutyryloxy succinimide ester (GMBS) [11, 12] serves the purpose of transforming the end group of the silane into a group that will bind covalently with functional groups on an antibody. It was initially intended to adopt methods described by Bhatia *et al* to compare the use of MTS and aminopropyl triethoxysilane (ATS) as the primary crosslinker to the crystalline ZnO surface [11, 12]. Results of these preliminary experiments demonstrated their inadequacy for use with ZnO.

Other work in modifying SiO<sub>2</sub> surfaces has focused on forming self-assembled monolayers using expoxysilanes [13, 14]. One advantage of using an expoxysilane such as (3-glycidoxypropyl)trimethoxysilane (GPS) for forming self-assembled monolayers (SAMs) on oxide surfaces is that it eliminates the need for a heterobifunctional crosslinker between the silane molecule and target antibodies since the exposed epoxy groups react readily with amine groups on lysine residues of the antibody. The usefulness of this antibody immobilization technique has been illustrated on indium-tin oxide (ITO) substrates for the development of *Escherichia coli* O157:H7 sensors [15, 16]. One of the problems with modifying surface oxides using organosilanes is that the quality of surface modification is sensitive to the amount of water in the solvent or adsorbed to the surface of the oxide [17]. In anhydrous conditions, a partial monolayer of organosilane molecules forms. In excess H<sub>2</sub>O, self-condensation can occur between the silane molecules and a multilayer will form. An alternative to organosilanes for surface modification of oxides is the use of phosphonic acids. Phosphonic acids do not suffer from the same susceptibility to hydration levels that organosilanes do. They have been used for the functionalization of ITO electrodes for development of electrochemical sensors [18] and for modifying TiO<sub>2</sub> particles [19]. In another study, phosphonic acids were used to pattern ITO and Indium Zinc Oxide (IZnO) through microcontact printing and subsequent wet etching [20].

A comparison between antibody immobilization protocols on device-quality sputtered ZnO surfaces was conducted with three different primary crosslinking molecules. The results provide a foundation for further research in developing highly uniform antibody immobilization protocols for planar ZnO surfaces. MTS, GPS and mercaptodecyl-phosphonic Acid (MPA) were deposited onto the ZnO surface using both a conventional wet method and an evaporation method. Subsequent secondary crosslinking with GMBS was performed for ZnO surfaces coated with MTS and MPA. To provide visual confirmation of the density and uniformity of antibody immobilization, fluorescently labeled antibodies were incubated with the surface. The results were investigated using water contact angle measurements, atomic force microscopy, and confocal microscopy. As demonstrated in Figure 6 below, the results indicate that MPA immobilized via the liquid protocol provides the highest surface coverage and most repeatable antibody immobilization procedure. It is concluded that thiol-terminated phosphonic acids are therefore a viable option for immobilization of antibodies onto planar crystalline ZnO surfaces. The results of this investigation are currently being submitted to the journal *Langmuir*.

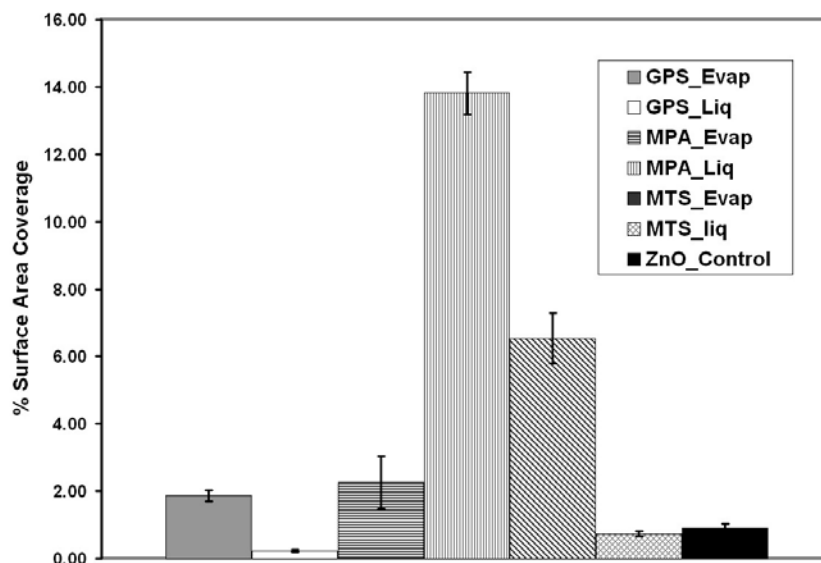


**Figure 6.** Plot of the average overall fluorescent antibody coverage for each of the antibody immobilization procedures. The values were calculated based on image analysis performed on confocal fluorescence images of the surfaces resulting from treatment with fluorescent antibodies. (Error Bars = Standard Error)

## Sensor array system

Prior to optimization of the surface preparation protocol, a preliminary investigation of the efficacy of the sensor array was attempted. A set of twelve eight-device ZnO SMR arrays similar to the one seen in Figure 5 above was fabricated. To functionalize each sensor toward a specific target, a surface-preparation process was performed for covalently binding IgG mAbs to the surface of the ZnO crystal using the MTS-GMBS protocol. The antibody immobilization process required 3 steps and took roughly 2 days to prepare. As mentioned, the immobilization protocol employed MTS as the primary

organosilane crosslinker followed by GMBS as the secondary crosslinker to link the mAbs to the ZnO surface. The surface coverage was assessed via atomic force microscopy, confocal laser scanning microscopy and contact angle measurements. As mentioned earlier, preliminary results had indicated the significant presence of antibodies bound to the surface. Our subsequent investigations have found this protocol to be inferior to the phosphonic acid crosslinking protocol.

Sensor arrays were used to assay for the presence of PSA in conditioned medium from LNCaP prostate cancer cells. Monoclonal antibodies from Santa Cruz Biotechnology<sup>®</sup>, Inc were used to functionalize sensor arrays for detection of PSA (sc-52170), FITC (sc-69871), and alkaline phosphatase (sc-80678). Each array contained 8 devices coated with the same antibody species. Fluorescein Isothiocyanate (FITC) was selected as the negative control since FITC is a synthetic molecule and is not naturally present in human tissue samples. Alkaline phosphatase was employed as a positive control, since it is a well regulated molecule in human tissue and is expected to be present at significant levels. Upon exposure to LNCaP conditioned medium, the PSA-targeted sensor arrays demonstrated a significant response. This response was greater than the FITC-targeted sensor yet less than the alkaline phosphatase-targeted sensor, as expected. Detection of targeted markers in the sample is evident nearly instantaneously once presented to the device surface. The values displayed in Figure 7 represent the average frequency shift after incubation with the LNCaP conditioned medium for several minutes. Binding of PSA from the conditioned medium to the covalently bound monoclonal antibodies yielded a 385 kHz shift on average. Further analysis is required of the LNCaP conditioned medium in order to provide an estimation of absolute sensitivity of the sensor. The results of this study are being presented at the 2008 AACR annual meeting this April.

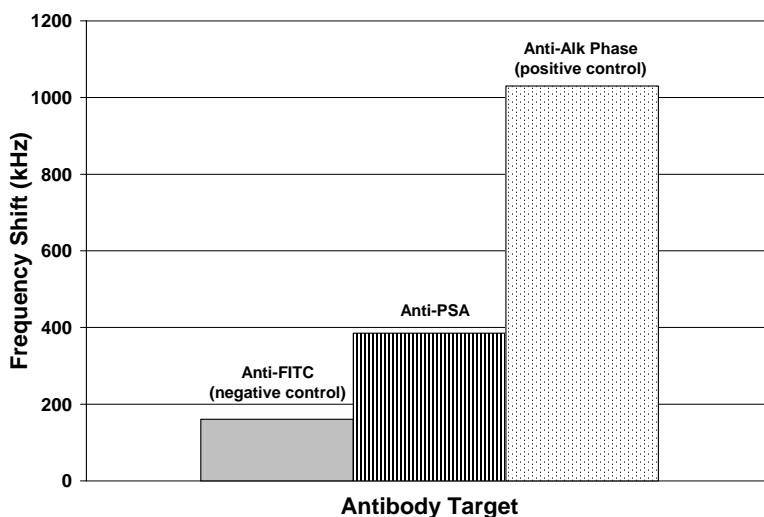


**Figure 7.** Average frequency shift observed when LNCaP conditioned medium is presented to Anti-FITC coated (n=22), Anti-PSA coated (n = 23), and Anti-Alkaline phosphatase coated (n = 21) devices.

As indicated above, subsequent work has been performed to identify a superior surface-preparation protocol that involves the use of a phosphonic acid as the primary crosslinker

which does not suffer from hydration-related formation issues the way organosilanes do. Superior antibody surface coverage and uniformity results achieved with mercapto-decyl-phosphonic acid will further improve the sensitivity of the sensors.

A prototype system has been developed to encompass the sensor array, the fluid sample flow cell and the RF switching and controller interface circuitry, as can be seen in Figure 8. The sensor package currently requires the use of a network analyzer to capture the sensor signals, but in the future this will be replaced with an appropriately designed microelectronic oscillator circuit, completing the portability packaging. The package design contains a disposable chip board that includes the sensor array and flow cell. This board connects via a card-slot connector to the switching board and is monitored by a network analyzer. The data is collected and analyzed by a laptop computer, which simultaneously controls the RF switch IC. The system allows for real-time monitoring of 8 distinct sensors with very high sensitivity and is a significant move towards realization of a disposable, inexpensive, and portable sensor platform.

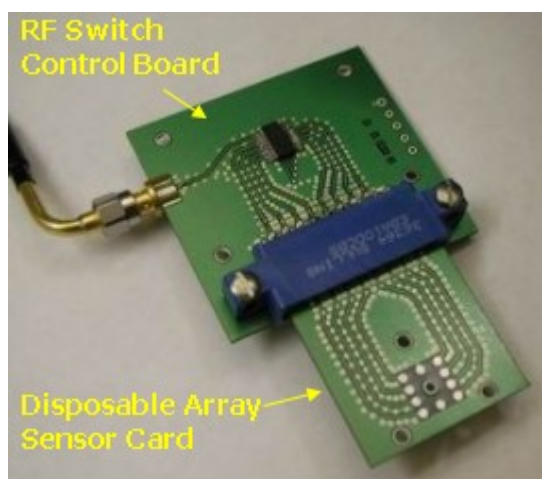


**Figure 8.** Switch board (2.25" x 2") with high-speed low-loss RF switch IC from Hittite and disposable array sensor board (1.4" x 1.6") containing sensor array chip. RF switch to be controlled via USB connection to a laptop running NI LabVIEW software allowing sensor array to be monitored via SMA connection.

## Key Research Accomplishments:

1. Fabrication of ZnO LFE SMRs
  - a. Found to work better than Ta<sub>2</sub>O<sub>5</sub>
    - Published: *Journal of Applied Physics*
    - Jointly published: *Virtual Journal of Biological Physics Research*
2. Device optimization
  - a. By electrode dimensions
  - b. By geometry (straight vs. circular)
  - c. Arrays
    - Pending publication: *Sensors & Actuators A: Physical*
  - d. By mirror...(pending)
    - To be submitted for publication by Feb 2008
3. Device susceptibility testing
  - a. Temperature: TCF of 25 ppm/°C
  - b. Conductivity: ↑ conductivity yields ↓ device quality
    - Presented: *IEEE Sensors 2007 Conference*
4. Surface chemistry
  - a. Surface chemistries attempted: (various protocols for each)
    - i. Aminopropyl triethoxy-silane (APS)
    - ii. Mercaptopropyl trimethoxy-silane (MPS)
    - iii. Mercatodecyl-phosphonic acid (MPA)
    - iv. Glycidoxyl-propyl-trimethoxy-silane (GPS)
    - v. Mercapto undecanoic acid (MUDA)
    - vi. Mercapto-benzoic acid (MBA)
    - vii. Passive adsorption (Control)
  - b. MPA has statistically greater success with ZnO
    - Pending acceptance in *Langmuir*
5. Preliminary biosensor testing
  - a. Poor statistical performance with initial test
    - i. Improved surface chemistry procedure should fix this
    - Pending Presentation: *AACR 2008 Annual Meeting, San Diego CA*
6. Switch packaging
  - a. Fast low-loss RF switch
  - b. Epoxy-bound array chip
  - c. 2-PCB board design for connection with laptop controller and network analyzer for resonance monitoring

## Reportable Outcomes

1. Christopher D. Corso, Anthony Dickherber, and William D. Hunt, "Lateral field excitation of thickness shear mode waves in a thin film ZnO solidly mounted resonator," *Journal of Applied Physics*, vol. 101, pp. 054514, 2007.
  - a. Jointly published in the May edition of the *Virtual Journal of Biological Physics Research*
2. Anthony Dickherber, Christopher D. Corso, William D. Hunt, Ira K. Pastan, Mitchell Ho, Raffit Hassan, "Mesothelin-fc fusion protein detection using a novel microelectronic acoustic sensor platform," presented at *2007 AACR Molecular Diagnostics in Cancer Therapeutic Development Conference*, Atlanta, GA, Sept 17-20, 2007
  - a. Selected for press release by the AACR and featured by WebMD, RxPG News, Dentalplans.com, PhysOrg.com, ScienceDaily, CBC News, Health Central.com, WFIE 14 Indiana (NBC affiliate), LEX 18 Kentucky (NBC affiliate), Forbes, US News & World Report, Health Scout, HealthCentral.com, KOLD News Arizona (CBS Affiliate), and finally the CNN News Room September 19, 2007 Wednesday special report by Dr. Sanjay Gupta
3. Anthony Dickherber, Christopher D. Corso, William D. Hunt, "Stability of a RF sputtered ZnO solidly mounted resonator sensor in varying temperature and conductivity environments," presented at *IEEE Sensors 2007 Conference*, Atlanta, GA USA, Oct 2007
4. Anthony Dickherber, Christopher D. Corso, William D. Hunt, "Optimization of the thickness shear mode in ZnO solidly mounted resonators," *Sensors & Actuators A: Physics*, pending publication Feb 5, 2008
5. Christopher D. Corso, Anthony Dickherber, Peter Hotchkiss, Seth Marder, William D. Hunt, "A comparison of antibody immobilization methods employing organosilanes and phosphonic acids on planar crystalline ZnO surfaces," *pending acceptance by Langmuir*, 2008
6. Anthony Dickherber, Christopher D. Corso, John Petros, Milton W. Datta, William D. Hunt, "A microelectronic bulk acoustic wave biosensor array for the detection of PSA in complex solutions," to be presented at *2008 AACR Annual Conference*, San Diego, USA, April 10-16, 2008

## Conclusion

In summary, significant progress has been made towards completing the goals outlined in the submitted *statement of work*. Given that late June through early September of 2007 was plagued with numerous equipment failures that stalled nearly all progress during that time, it is felt that these accomplishments are substantial. I was able to attend several conferences including the AACR Annual and Molecular Diagnostics Conferences, having presented at the latter. I have continued to attend weekly urology grand rounds at the Winship Cancer Institute, which have helped significantly with my own understanding of the clinical environment surrounding prostate cancer and how the technology being developed through this research could be best adopted. The weekly meetings have further helped in keeping me aware of the latest clinical developments in the field regarding everything from the identification of novel indicators for diagnosis to novel therapies and on-going clinical trials.

### ***So what?***

What has been accomplished to date is the design and development of a novel acoustic resonator array that can be employed for liquid phase biosensing. Some final optimization experiments are currently underway, but this alone is a significant accomplishment that garnered the unsolicited recognition of the editors of the *Virtual Journal of Biological Physics Research* which selected it for publication. An optimized procedure for covalent immobilization of monoclonal IgG antibodies on the planar surface of the ZnO crystal has been developed and is currently being submitted to the *Langmuir* journal. This too is a novel contribution to the field and can be employed for various applications employing planar ZnO. The early use of these biosensor arrays to detect the widely studied cancer biomarker mesothelin-fc was presented at the *AACR Molecular Diagnostics in Cancer Therapeutic Development Conference* where it garnered significant unsolicited media attention, demonstrating widespread interest in this research. The development of interface circuitry and packaging that incorporates the flow cell as well as the switching element makes significant steps towards making the overall system compact and portable.

### ***Future work***

As indicated above, current work is being performed to complete the optimization of device operation. The results of this investigation should result in publishable work that will likely be submitted in February of 2008. Initial biosensor investigations should commence by the end of January, employing the aforementioned optimized antibody immobilization procedure. These investigations will include the use of these newly developed biosensors to scan for free and conjugated forms of PSA in LNCap (widely used prostate cancer cell line) conditioned medium. An effort is currently underway to collaborate with other pioneers in the field of prostate cancer research to obtain antibodies for additional markers such as Dr. Getzenberg's EPCA-2 (early prostate cancer antigen). A novel aspect of our biosensor investigations is the use of both a



positive and negative control sensor to verify the proper detection capability of the sensor. Extensive investigation of the research literature shows that no other biosensor groups employ this very important control protocol to fully validate their results. These investigations should certainly yield publishable results, which shall be submitted in as timely a manner as is possible and responsible.

## References:

- [1] E. S. Leman, G. W. Cannon, B. J. Trock, L. J. Sokoll, D. W. Chan, L. Mangold, A. W. Partin, and R. H. Getzenberg, "EPCA-2: a highly specific serum marker for prostate cancer," *Urology*, vol. 69, pp. 714-20, 2007.
- [2] V. T. S. Matthew A. Cooper, "A survey of the 2001 to 2005 quartz crystal microbalance biosensor literature: applications of acoustic physics to the analysis of biomolecular interactions," *Journal of Molecular Recognition*, vol. 20, pp. 154-184, 2007.
- [3] H. Nakamura and I. Karube, "Current research activity in biosensors," *Anal Bioanal Chem*, vol. 377, pp. 446-68, 2003.
- [4] W. E. Newell, "Face-mounted piezoelectric resonators," *Proceedings of the IEEE*, vol. 53, pp. 575-581, 1965.
- [5] C. D. Corso, A. Dickherber, and W. D. Hunt, "Lateral field excitation of thickness shear mode waves in a thin film ZnO solidly mounted resonator," *Journal of Applied Physics*, vol. 101, pp. 054514, 2007.
- [6] J. F. Rosenbaum, *Bulk acoustic wave theory and devices*. Boston: Artech House, 1988.
- [7] M. Link, M. Schreiter, J. Weber, R. Gabl, D. Pitzer, R. Primig, W. Wersing, M. B. Assouar, and O. Elmazria, "c-axis inclined ZnO films for shear-wave transducers deposited by reactive sputtering using an additional blind," *Journal of Vacuum Science & Technology A: Vacuum, Surfaces, and Films*, vol. 24, pp. 218-222, 2006.
- [8] W. Pang, H. Yu, J. W. Kwon, H. Zhang, and E. S. Kim, "Self-aligned lateral field excitation film acoustic resonator with very large electromechanical coupling [FBAR]," presented at Frequency Control Symposium and Exposition, 2004. *Proceedings of the 2004 IEEE International*, 2004.
- [9] A. Dickherber, C. D. Corso, and W. D. Hunt, "Stability of a RF sputtered ZnO solidly mounted resonator sensor in varying temperature and conductivity environments," presented at IEEE Sensors 2007 Conference, Atlanta, GA USA, 2007.
- [10] A. Dickherber, C. D. Corso, and W. D. Hunt, "Optimization of the thickness shear mode in ZnO solidly mounted resonators," *Sensors & Actuators A*, vol. Publication pending, 2007.
- [11] S. K. Bhatia, L. C. Shriver-Lake, K. J. Prior, J. H. Georger, J. M. Calvert, R. Bredehorst, and F. S. Ligler, "Use of thiol-terminal silanes and heterobifunctional crosslinkers for immobilization of antibodies on silica surfaces," *Anal Biochem*, vol. 178, pp. 408-13, 1989.
- [12] L. C. Shriver-Lake, B. Donner, R. Edelstein, K. Breslin, S. K. Bhatia, and F. S. Ligler, "Antibody immobilization using heterobifunctional crosslinkers," *Biosensors & Bioelectronics*, vol. 12, pp. 1101-1106, 1997.
- [13] I. Luzinov, D. Julthongpiput, A. Liebmman-Vinson, T. Cregger, M. D. Foster, and V. V. Tsukruk, "Epoxy-terminated self-assembled monolayers: Molecular glues for polymer layers," *Langmuir*, vol. 16, pp. 504-516, 2000.

- [14] V. V. Tsukruk, I. Luzinov, and D. Julthongpiput, "Sticky Molecular Surfaces: Epoxysilane Self-Assembled Monolayers," *Langmuir*, vol. 15, pp. 3029-3032, 1999.
- [15] C. M. Ruan, L. J. Yang, and Y. B. Li, "Immunobiosensor chips for detection of *Escherichia coli* O157 : H7 using electrochemical impedance spectroscopy," *Analytical Chemistry*, vol. 74, pp. 4814-4820, 2002.
- [16] L. Yang and Y. Li, "AFM and impedance spectroscopy characterization of the immobilization of antibodies on indium-tin oxide electrode through self-assembled monolayer of epoxysilane and their capture of *Escherichia coli* O157:H7," *Biosens Bioelectron*, vol. 20, pp. 1407-16, 2005.
- [17] P. H. Mutin, G. Guerrero, and A. Vioux, "Organic-inorganic hybrid materials based on organophosphorus coupling molecules: from metal phosphonates to surface modification of oxides," *Comptes Rendus Chimie*, vol. 6, pp. 1153-1164, 2003.
- [18] M. A. Aziz and H. Yang, "Electrochemical immunosensor using the modification of an amine-functionalized indium tin oxide electrode with carboxylated single-walled carbon nanotubes," *Bulletin of the Korean Chemical Society*, vol. 28, pp. 1171-1174, 2007.
- [19] G. Guerrero, P. H. Mutin, and A. Vioux, "Anchoring of phosphonate and phosphinate coupling molecules on titania particles," *Chemistry of Materials*, vol. 13, pp. 4367-4373, 2001.
- [20] T. L. Breen, P. M. Fryer, R. W. Nunes, and M. E. Rothwell, "Patterning Indium Tin Oxide and Indium Zinc Oxide Using Microcontact Printing and Wet Etching," *Langmuir*, vol. 18, pp. 194-197, 2002.

## **Appendices:**

Included in this section are copies of all manuscripts outlined in the “Reportable Outcomes” section of this document, followed by the author’s *curriculum vitae*.

# Lateral field excitation of thickness shear mode waves in a thin film ZnO solidly mounted resonator

Christopher D. Corso

*School of Biomedical Engineering, Georgia Institute of Technology, Atlanta, Georgia 30332*

Anthony Dickherber and William D. Hunt<sup>a)</sup>

*School of Electrical and Computer Engineering, Georgia Institute of Technology, Atlanta, Georgia 30332*

(Received 7 November 2006; accepted 2 January 2007; published online 14 March 2007)

In recent years, interest in the development of highly sensitive acoustic wave devices as biosensor platforms has grown. A considerable amount of research has been conducted on AT-cut quartz resonators both in thickness excitation and in lateral excitation configurations. In this report, we demonstrate the fabrication of a ZnO solidly mounted resonator operated in thickness shear mode (TSM) using lateral field excitation of the piezoelectric film. Theoretical Christoffel equation calculations are provided to explore the conditions for excitation of a TSM wave in *c*-axis-oriented ZnO through lateral excitation. The existence of a TSM wave is verified through the comparison of theoretical and experimentally obtained acoustic velocity values from frequency versus thickness measurements and water loading of the resonators. A major strength of this design is that it incorporates a simple eight-layer, single-mask fabrication process compatible with existing integrated circuit fabrication processes and can be easily incorporated into multidevice arrays. With minimal electrode optimization, we have been able to fabricate resonators with nearly 100% yield that demonstrate *Q* values of up to 550 and  $K^2$  values of 0.88% from testing of more than 30 devices. © 2007 American Institute of Physics. [DOI: 10.1063/1.2562040]

## I. INTRODUCTION AND BACKGROUND

The interest in developing highly sensitive acoustic wave devices for chemical and biological sensing purposes has dramatically increased in the past decade. Acoustic devices offer an attractive alternative to other sensor schemes such as surface plasmon resonance<sup>1</sup> (SPR) and electrochemical sensors<sup>2</sup> because they are small, relatively inexpensive to produce, and offer a potentially superior sensitivity to surface perturbations. The acoustic wave resonating in the piezoelectric cavity acts as a probe querying the surface for any changes in boundary conditions such as mass loading. This is the fundamental concept behind the operation of acoustic biosensors.

In the past, piezoelectric ZnO thin films have been used in the fabrication of thin film bulk acoustic resonators (FBARs) for high frequency filters.<sup>3</sup> Typically, these devices are operated in the thickness-excited longitudinal mode in which the frequency can be tuned simply by varying the thickness of the ZnO thin film. The particle displacement of the propagating acoustic wave in a longitudinal bulk mode is normal to the surface of the film and generates compressional waves in the medium adjacent to the device surface. When operated in an adjacent liquid medium, the longitudinal mode energy is dissipated into the liquid for devices utilizing waves that propagate at a velocity higher than the sound velocity in the liquid. This results in a highly reduced quality factor, *Q*, and poor mass resolution in a sensor application. The thickness shear mode (TSM) is better suited for

liquid sensing applications due to the shear particle displacement of the acoustic wave in the piezoelectric film. Since the adjacent liquid medium cannot effectively support a shear wave, very little energy is transferred into the liquid, and this results in minimal damping of the thickness shear mode.

The most common type of TSM resonator is the quartz crystal microbalance (QCM). QCMs are made from thin plates of AT-cut quartz. These devices have been shown to be highly sensitive as gravimetric sensors in both vapor phase and in liquid phase sensing.<sup>4–7</sup> The frequency dependence of the resonator-based biosensor has been characterized by many, including Sauerbrey,<sup>8</sup> Kanazawa and Gordon,<sup>9</sup> and most recently Hunt *et al.*,<sup>10</sup> but all agree that the frequency sensitivity of these devices is proportional to a power of the fundamental resonant frequency  $f_0$ . QCMs typically operate in the frequency range of 5–35 MHz. In AT-cut quartz plates, it is difficult to further increase the fundamental operating frequency because of its dependence on the thickness of the quartz plate. At very low thicknesses, the quartz plate becomes extremely fragile and is difficult to handle. It is possible to achieve higher frequencies with the QCM by monitoring harmonic modes beyond the fundamental, but these become progressively diminished with increasing harmonic number. Solidly mounted FBARs, on the other hand, do not suffer from this problem because the piezoelectric film is grown directly onto a solid foundation. Solidly mounted resonators (SMRs) are made possible by the fabrication of an acoustic mirror directly below the piezoelectric thin film. This so-called Bragg reflector in effect presents the lower side of the piezoelectric material with an acoustic impedance close to that of air over a fairly broad range of frequencies,<sup>11</sup> resulting in the reflection of the acoustic en-

<sup>a)</sup>Author to whom correspondence should be addressed; electronic mail: bill.hunt@ece.gatech.edu

ergy back into the piezoelectric film. This allows for the utilization of extremely thin piezoelectric sensing layers and, ultimately, very high frequency devices (i.e., gigahertz range) can be produced.

The sensitivity of acoustic waves in AT-cut quartz plates has been widely exploited in QCMs which use thickness excitation (TE) to excite the wave. It has been shown, however, that lateral field excitation (LFE) can be used to excite the TSM wave<sup>12–15</sup> and that the resulting device may be more sensitive to surface perturbations than the standard TE QCM for liquid phase sensing applications.<sup>16–19</sup> The advantages of LFE over TE are mainly attributed to the fact that in LFE, the electrodes that generate the electric field are not directly in the path of the acoustic wave, as in TE. Since the metal material that forms the electrode is a source of acoustic wave scattering and damping, its removal from the acoustic path results in higher  $Q$  values. Other advantages include increased stability at a given harmonic and reduced aging of the crystal since the electrode is absent from the area of greatest vibrational motion.<sup>20</sup> For biosensor applications, removing the electrode from the acoustic path means that biological molecules can be immobilized directly onto the region of highest particle displacement which should result in greater sensitivity of the sensor.

There has been varied interest, thus far, in generating a thickness shear mode in ZnO for acoustic devices. One of the more highly investigated methods involves the growth of inclined  $c$ -axis oriented films<sup>21</sup> coupled with an electrode pattern in which the electrodes are situated on opposite sides of the thin film to produce an electric field through the thickness. Wang and Lakin had excellent success in fabricating oriented films with the  $c$ -axis-oriented  $40^\circ$  to the substrate normal.<sup>22</sup> While their resonator  $Q$  and electromechanical coupling were high, the operating frequency was low ( $\sim 293$  MHz) and the fabrication procedure required bulk etching of the Si wafer to produce the air-backed ZnO membrane resonators. More recently, Link *et al.*<sup>23,24</sup> have revived the inclined ZnO growth research with the intent of developing ZnO TSM resonators for liquid phase sensing. A shortcoming of the inclined ZnO growth method is that the thickness excitation requires that the electrodes be in the path of the acoustic wave. While it offers the benefit of a higher operating frequency than the QCM for sensing, it still suffers from the same pitfalls as the QCM because the electrodes are located in the area of highest sensitivity.

In a study by Wei *et al.* focusing on noninclined  $c$ -axis-oriented ZnO, the thickness shear mode was excited through lateral field excitation.<sup>25</sup> The devices were solidly mounted resonators fabricated through the use of a self-aligning process that involved ZnO lift-off and a spiral electrode structure spanning 2 mm in diameter. Operating close to 4.1 GHz, the devices illustrated the ability for ZnO FBARs to be operated at high frequencies with relative ease. However, an acoustic mirror was not implemented in the design, and the quality factor  $Q$  of the resonators was very low (roughly 35). Acoustic velocity calculations we made from the numbers given in the study come out to  $\sim 3280$  m/s as compared to a theoretical value of  $\sim 2841$  m/s calculated

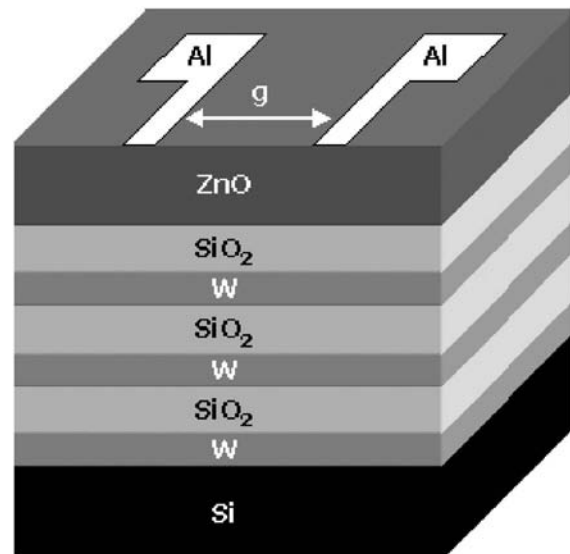


FIG. 1. Electrode and stack configuration.

using bulk stiffness properties of ZnO available in Rosenbaum.<sup>26</sup> This value is reasonable considering variations in ZnO thin film material parameters.

In this paper, we present a laterally excited ZnO thickness shear mode resonator that is both extremely simple to fabricate and highly sensitive to surface perturbations. The resonator configuration consists of a laterally excited, solidly mounted ZnO thin film resonator that incorporates the use of an acoustic mirror. Future investigations will yield optimized electrode designs and even higher performance devices. It should be noted that this device approach is amenable to array format such that multiple target molecules can be simultaneously detected while also providing reference sensors to add statistical significance to the test results. An additional benefit of these devices is the ease of fabrication of repeatable highly  $c$ -axis-oriented ZnO thin films by rf sputtering. We will present data on devices which have been fabricated with a single mask step.

## II. DEVICE FABRICATION AND EXPERIMENTAL PROTOCOL

The overall device design can be seen in Fig. 1. The thin film six-layer stack of alternating W and SiO<sub>2</sub> was deposited by rf magnetron sputtering using the Unifilm PVD-300 sputtering system to create an acoustic reflector analogous to that of a reflector grating in a surface acoustic wave device.<sup>27,28</sup> Scanning electron microscopy (SEM) analysis of the deposition layers demonstrated that we could achieve greater than 90% uniformity of deposition thickness across a 3 in. wafer. The acoustic mirror is designed according to the model described by Lakin.<sup>28</sup> For the desired resonance frequency of approximately 2 GHz, W and SiO<sub>2</sub> thicknesses of 600 and 1200 nm, respectively, were calculated to achieve the desired mirror response. The results of a model simulation based on actual thickness measurements of the fabricated device are shown in Fig. 2. The plot illustrates that over the frequency range of 1.8–2.3 GHz, the reflection coefficient approaches unity. The layers comprising the reflector stack were alternat-

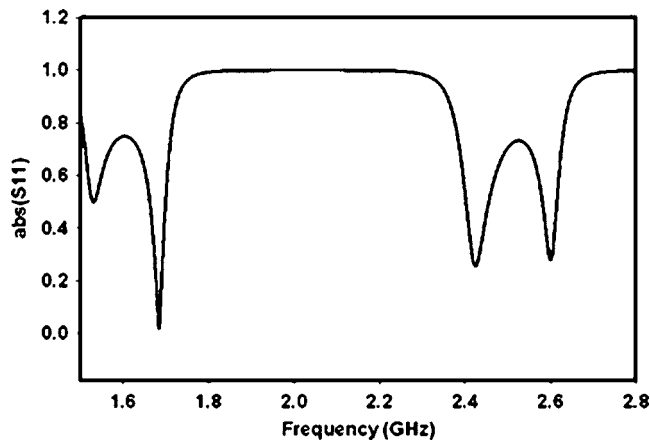


FIG. 2. Simulated reflection coefficient of the acoustic mirror.

ing fused  $\text{SiO}_2$  and W, in which W was the first layer deposited onto a Si (1 0 0) wafer. All sputtering parameters used for the fabrication of these devices are provided in Table I. Following deposition of the stack, a ZnO thin film was sputtered using the Unifilm PVD-300 sputtering system. The final thicknesses of the thin film layers were verified by imaging a cross section of the fabricated wafer using a LEO 1530 thermally assisted field emission (TFE) scanning electron microscope (SEM), and can be seen in Fig. 3. To finish the fabrication procedure, approximately 120 nm of Al was deposited on top of a 30 nm seeding layer of Cr to create the electrodes using a CVC e-beam evaporator and a standard photolithography lift-off process. The electrodes were designed such that the electric field created upon excitation would be perpendicular to the wafer surface normal. This laterally oriented electric field is important for excitation of a bulk acoustic shear wave in the ZnO. To verify the orientation of the electric field resulting from the electrode geometry, electric field simulations were carried out using the COMSOL MULTIPHYSICS<sup>TM</sup> finite element modeling software package. The resonator scattering parameters of the finished devices were obtained using a Cascade Microtech 9000 probe station with Cascade Microtech ACP40-GS/SG probes and analyzed using a HP 8753C network analyzer equipped with a 85047A S parameter test set.

The x-ray diffraction (XRD) data were taken on a Philips X'Pert Materials Research Diffractometer<sup>TM</sup> using a hybrid mirror/monochromator incident optics and a  $1/4$ -degree receiving slit in the diffracted optics beam path. A  $2\theta$ - $\Omega$  rocking-curve scan of the film indicated a strong peak at approximately  $34.26^\circ$ , indicating a (0 0 2) ZnO hexagonal

TABLE I. Sputtering parameters for respective layers using a Unifilm PVD-300 sputterer.

	W	$\text{SiO}_2$	ZnO
Power (W)	0.86 dc	281 rf	142 rf
$\text{O}_2$	NA	2.5%	3%
Ar	100%	97.5%	97%
Temperature ( $^\circ\text{C}$ )	Not heated	Not heated	325
Deposition time (min)	84	139	115
Pressure (torr)	$5.00 \times 10^{-3}$	$5.02 \times 10^{-3}$	$5.10 \times 10^{-3}$

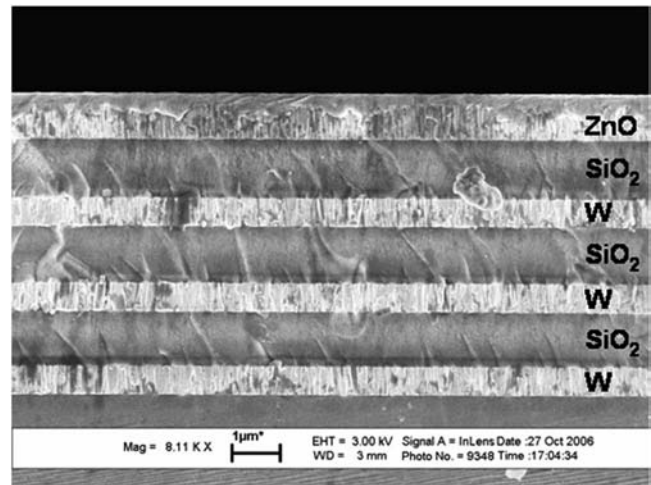


FIG. 3. SEM image of the acoustic mirror and ZnO thin films on a Si substrate.

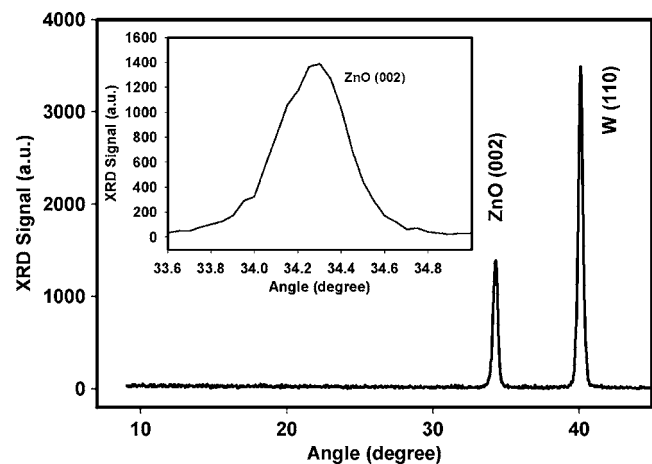
crystal orientation shown in Fig. 4. The peak has a full width at half maximum (FWHM) of  $0.35^\circ$ , indicating a highly oriented  $c$ -axis crystal film. Figure 4 also shows a tight peak at  $40.1^\circ$ , which corresponds to the (1 1 0) orientation of the tungsten layers in the acoustic stack. As expected, no peaks were observed for the  $\text{SiO}_2$  layers in the stack because they are amorphous.

### III. THEORETICAL BACKGROUND AND FINITE ELEMENT MODELING

With the verification of the ZnO crystal orientation in hand, it is possible to solve the Christoffel equation to find the modes of propagation in the bulk given a defined electrical excitation direction. We begin by considering the nonpiezoelectric Christoffel equation

$$(k^2 l_{iK} c_{KL} l_{Lj}) v_j = \rho \omega^2 v_i, \quad (1)$$

where  $k = \tilde{\omega}/v_a$ ,  $\rho$  is the density of the material,  $v_i$  and  $v_j$  are the particle polarization direction vectors, and the  $l_{iK}$  matrix is in the form of

FIG. 4.  $2\theta$ - $\omega$  rocking-curve scan of the ZnO film sputtered on the six-layer W/ $\text{SiO}_2$  acoustic mirror. The inset is a zoomed image of the ZnO peak.



$$l_{iK} = \begin{bmatrix} l_x & 0 & 0 & 0 & l_z & l_y \\ 0 & l_y & 0 & l_z & 0 & l_x \\ 0 & 0 & l_z & l_y & l_x & 0 \end{bmatrix}, \quad (2)$$

where the nonzero terms come from the propagation vector  $\hat{\mathbf{l}} = l_x \hat{\mathbf{i}} + l_y \hat{\mathbf{j}} + l_z \hat{\mathbf{k}}$ . The  $l_{Lj}$  matrix is simply the transpose of  $l_{iK}$ , and  $c_{KL}$  is the material stiffness tensor rotated according to the desired Euler angles. It follows from the XRD data that the ZnO thin films belong to a hexagonal system with a crystal class of 6 mm.

Since the  $c$  axis is oriented normal to the surface, we will arbitrarily choose to align the  $z$  coordinate axis along this crystal axis for our calculations. For thickness shear mode propagation, wave propagation is defined to be in the  $z$  direction, so  $l_x$  and  $l_y$  go to zero and  $l_z$  goes to 1.

Equation (1) is used to solve for directions and velocities of bulk waves propagating in the substrate, but it does not account for the piezoelectric properties of a material nor the possibility of the generation of these waves by an electric field. For this reason, we turn to the piezoelectric Christoffel equation

$$k^2 \left\{ l_{iK} \left[ c_{KL}^E + \frac{(e_{Kj} m_j)(m_i e_{iL})}{m_i \varepsilon_{ij}^S m_j} \right] l_{Lj} \right\} v_j = \rho \omega^2 v_i, \quad (3)$$

where  $e_{Kj}$  is the piezoelectric coupling tensor,  $\varepsilon_{ij}^S$  is the  $3 \times 3$  permittivity tensor at constant strain,  $m$  is the vector corresponding to the direction of the electric excitation field, and now  $c_{KL}^E$  corresponds to the  $6 \times 6$  stiffness tensor at a constant electric field. As can be seen, Eq. (3) is similar to Eq. (1) but for the inclusion of the piezoelectric and permittivity tensors, which apply piezoelectric “stiffening” to the stiffness tensor.

For the lateral field excitation of the  $c$ -axis-oriented ZnO, we desire the electric excitation field to be orthogonal to the wave propagation. Therefore, if the wave propagation is in the direction of the  $z$  axis, the electric field is in the  $x$ - $y$  plane. Here, we will describe the coupling and acoustic wave propagation for the general case of an electric field along any direction within the  $x$ - $y$  plane. The electric field vector  $m_j$  is of the form

$$m_j = \begin{bmatrix} m_x \\ m_y \\ m_z \end{bmatrix}. \quad (4)$$

Solving the piezoelectrically stiffened Christoffel equation for laterally excited ZnO, we set  $m_z = 0$  and  $m_x^2 + m_y^2 = 1$ . The 6 mm hexagonal system stiffness tensor is of the form

$$c = \begin{bmatrix} c_{11} & c_{12} & c_{13} & 0 & 0 & 0 \\ c_{12} & c_{11} & c_{13} & 0 & 0 & 0 \\ c_{13} & c_{13} & c_{33} & 0 & 0 & 0 \\ 0 & 0 & 0 & c_{44} & 0 & 0 \\ 0 & 0 & 0 & 0 & c_{44} & 0 \\ 0 & 0 & 0 & 0 & 0 & c_{66} \end{bmatrix}, \quad (5)$$

and the form of the piezoelectric matrix is

$$e = \begin{bmatrix} 0 & 0 & 0 & 0 & e_{15} & 0 \\ 0 & 0 & 0 & e_{15} & 0 & 0 \\ e_{31} & e_{31} & e_{33} & 0 & 0 & 0 \end{bmatrix}. \quad (6)$$

The resulting Christoffel matrix is of the form

$$\Gamma = \begin{bmatrix} c_{44} + e_{15}^2 m_x^2 / \varepsilon_{11} & e_{15}^2 m_x m_y / \varepsilon_{11} & 0 \\ e_{15}^2 m_x m_y / \varepsilon_{11} & c_{44} + e_{15}^2 m_y^2 / \varepsilon_{11} & 0 \\ 0 & 0 & c_{33} \end{bmatrix}. \quad (7)$$

The eigenvalues of this matrix correspond to terms that can be used to solve for  $v_a$ , the acoustic velocity in each of the three wave propagation modes, while the corresponding eigenvectors relate to the direction of particle displacement. Solving for the eigenvectors and eigenvalues of  $\Gamma$  gives

$$x_1 = \begin{bmatrix} -m_y \\ m_x \\ 0 \end{bmatrix}, \quad \lambda_1 = c_{44}; \quad x_2 = \begin{bmatrix} m_x \\ m_y \\ 0 \end{bmatrix}, \quad (8)$$

$$\lambda_2 = c_{44} + \frac{e_{15}^2}{\varepsilon_{11}}; \quad x_3 = \begin{bmatrix} 0 \\ 0 \\ 1 \end{bmatrix}, \quad \lambda_3 = c_{33}.$$

From these results, we find that only one mode is piezoelectrically excited (defined by  $x_2$  and  $\lambda_2$ ) and that the particle displacement will be directly aligned with the electric field, regardless of the orientation of the field with respect to the  $x$ - $y$  plane. This mode is a pure shear thickness mode and is the mode we seek. Another pure shear mode exists (defined by  $x_1$  and  $\lambda_1$ ) with particle displacement also in the  $x$ - $y$  plane at an angle perpendicular to that of the piezoelectrically excited mode; however, it is piezoelectrically inactive. The longitudinal mode (defined by  $x_3$  and  $\lambda_3$ ), importantly, is also piezoelectrically inactive. These results indicate that an electric field in the  $x$ - $y$  plane will excite a pure shear thickness mode with particle displacement aligned with the electric field. The acoustic velocity for this mode can be calculated from

$$v_a = \sqrt{\frac{c_{44} + e_{15}^2 / \varepsilon_{11}}{\rho}}. \quad (9)$$

Using bulk values for ZnO from Rosenbaum,<sup>26</sup>  $e_{15} = -0.48$ ,  $c_{44} = 43 \times 10^9$  N/m<sup>2</sup>,  $\varepsilon_{11} = 8.6$  (rel.), and  $\rho = 5700$  kg/m<sup>3</sup>, the theoretical acoustic velocity for the piezoelectrically stiffened thickness shear mode is approximately 2841 m/s. Since most ZnO thin films include various dopants and are not of pure crystal uniformity, they will have stiffness, density, and piezoelectric constants that are different from these bulk values. This calculated acoustic velocity is therefore an approximate figure and not an absolute value from which to evaluate an experimentally obtained mode. The theoretical piezoelectric coupling constant for the ZnO LFE resonator is given by



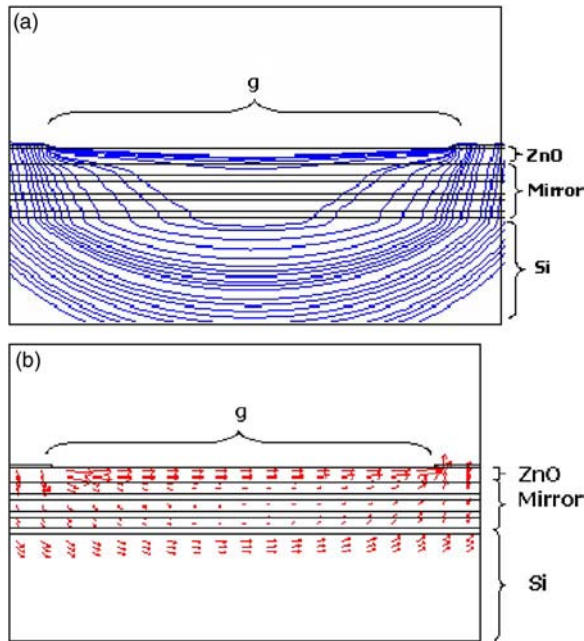


FIG. 5. (Color online) Finite element simulation plots illustrating the electric field characteristics resulting from the electrode configuration in Fig. 1. (a) shows the electric field streamline plot and (b) shows an arrow plot where the electric field direction is indicated by the direction of the arrow, and the relative strength of the electric field (C/m) is indicated by the size of the arrow.

$$K^2 = \frac{e_{15}^2}{c_{44}\epsilon_{11}}, \quad (10)$$

which is calculated to be approximately 0.07 or 7% for the case of the thickness shear mode.

All of the above calculations rely on the assumption that the lateral excitation field is aligned in the  $x$ - $y$  plane. Therefore, it is important to verify that a given electrode structure generates an electric field consisting of a primarily lateral component. To accomplish this, the electromagnetics module of the COMSOL MULTIPHYSICS® finite element modeling software package was used to evaluate the electrode configuration. While multiple electrode geometries have been investigated, only the most basic structure, as shown in Fig. 1, will be discussed here for the sake of simplicity.

Figure 5(a) shows a streamline plot of the electric field lines produced from the simple electrode geometry with a gap of  $20\ \mu\text{m}$ . The streamlines visualize the direction of the electric field lines with no information about the strength of the vector field. Figure 5(b) is an image of the electric field produced by the gap depicted through arrows which illustrate the direction (orientation of arrow) and relative intensity of the electric field (size of arrow) in the ZnO. The plots specify that the electric field is aligned parallel to the surface in the area between the gaps, while it is aligned primarily normal to the surface in the area directly below the electrodes. The relative sizes of the arrows in Fig. 5(b) show that the relative strength of the electric field within the electrode gap is approximately twice that of the electric field directly beneath the electrodes (data not shown). These plots indicate that the electric field generated by the proposed electrode configuration will generate a laterally oriented field in the active area

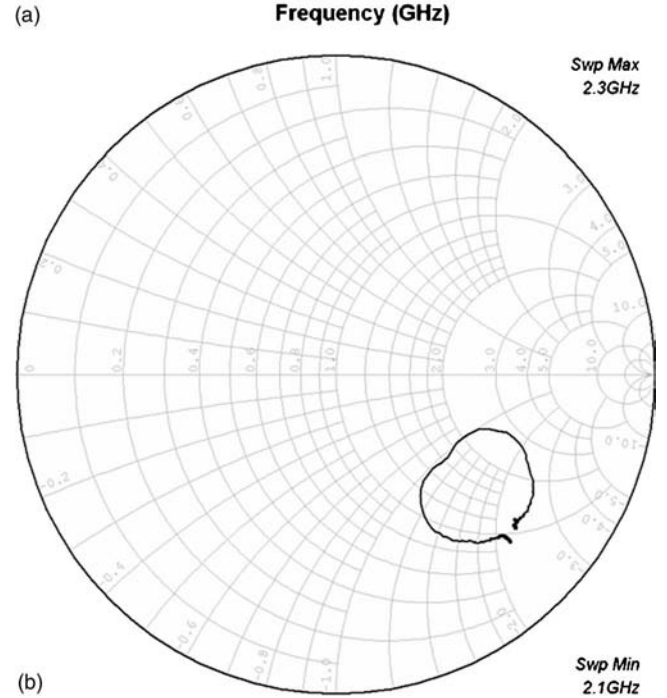
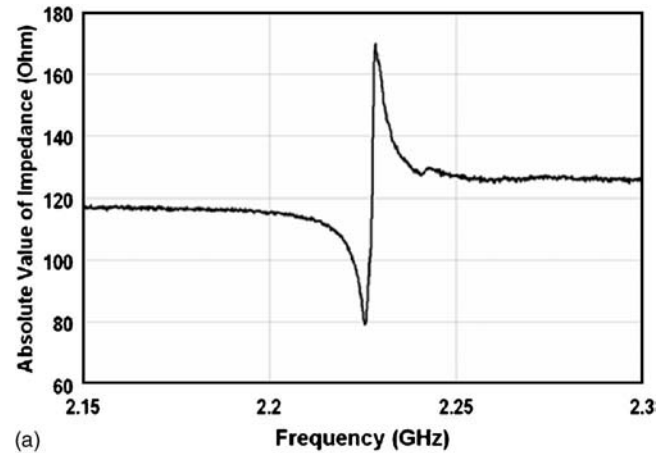


FIG. 6. Network analyzer probe measurements showing (a) the magnitude of the impedance response as a function of frequency and (b) the  $S_{11}$  Smith chart plot.

of the device with a minimal surface-normal component which is a requisite for lateral field excitation. Further, it is indicated that a weak response due to thickness excitation of the longitudinal mode is expected.

#### IV. RESULTS AND DISCUSSION

RF probing of individual devices yielded thickness shear mode activity in the ZnO devices over a range of ZnO thin film thicknesses. Testing the acoustic response by fabricating wafers with multiple thicknesses of ZnO is important for verifying that the  $S_{11}$  response is due to an acoustic phenomenon rather than some electromagnetic resonance. This can be done by verifying that as the film thickness changes, the resonant frequency changes accordingly. Probing of more than 30 devices yielded impedance and  $S_{11}$  responses similar to those shown in Fig. 6. As can be seen from the Smith chart [Fig. 6(b)], a clear loop pattern, indicative of resonant activity, is present. An average unloaded  $Q$  of these resonators is

TABLE II. Result of changing ZnO thickness on resonator response.

Measured ZnO thickness (nm)	$f_0$ (GHz)	Extracted acoustic velocity (m/s)
790	2.0	3160
710	2.2	3130
660	2.35	3100

approximately 340 and the  $K^2$  is approximately 0.4%, with peak values of 550 and 0.88%, respectively. The calculations used to assess  $Q$  and  $K^2$  are<sup>26,28</sup>

$$Q = \left( \frac{f}{2} \right) \frac{d \angle Z}{df}, \quad (11)$$

$$K^2 = \left( \frac{\pi}{2} \right)^2 \frac{f_p - f_s}{f_p}. \quad (12)$$

The acoustic velocity was empirically determined to be on the average of 3130 m/s. This is somewhat close to the theoretical value of 2841 m/s, but much closer to the experimental value of 3280 m/s, as calculated from the results of Woo Wai *et al.*<sup>29</sup> The theoretical longitudinal velocity for ZnO is approximately 6300 m/s. This value is much higher than the experimentally obtained acoustic velocity, and is therefore a good indicator that it is the shear mode that is being excited and not the longitudinal. Interestingly, no longitudinal peak was found to exist throughout the frequency spectrum of the resonators and may be attributed to poor reflection characteristics of the mirror at the longitudinal frequency. This can also be explained by the weak electric field component normal to the surface generated by the electrode configuration. To further confirm acoustic wave resonance, we altered the thickness of the ZnO to demonstrate that increasing the film thickness resulted in a corresponding decrease in resonant frequency. The results of these tests are summarized in Table II. We feel that the resonance could be significantly improved through optimization of the electrode configuration to enhance piezoelectric coupling of the electric field energy to the crystal and to provide energy trapping for the acoustic wave.

Aside from comparing the experimentally obtained acoustic velocity to the TSM and longitudinal velocities, another way to further establish the existence of a thickness shear mode is to expose the resonators to water at the surface. If the acoustic activity were longitudinal, application of de-ionized water at the surface would decimate the acoustic resonance observed in the device since water can support a longitudinal wave, but not a shear wave. Figure 7 shows the response before (triangles) and after (squares) application of de-ionized water to the surface. As can be seen, the water had only small effects on the suppression seen in the  $S_{11}$  magnitude response, and a negative frequency shift occurred after water was applied to the device of approximately 1.1 MHz. According to Sauerbrey,<sup>8</sup> this response is to be expected from a TSM device, roughly described in his equation

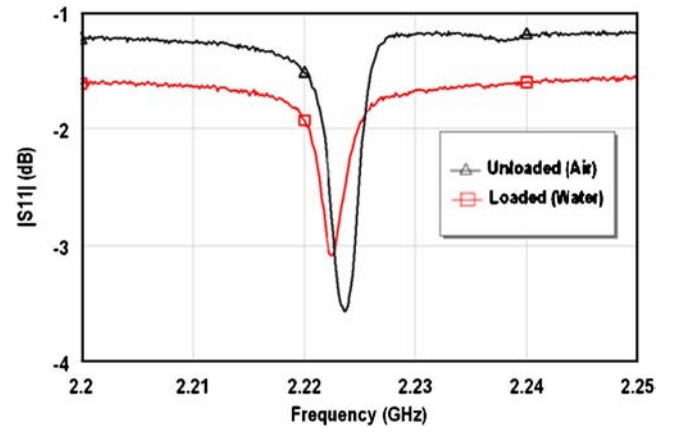


FIG. 7. (Color online) Frequency shift observed in  $S_{11}$  measurement in response to loading the surface of the resonator with de-ionized  $H_2O$ . Some deterioration of the resonance was observed resulting in the decrease of the  $Q$  factor.

$$\Delta f = \left( \frac{-2f_0^2}{A\sqrt{\rho_q\mu_q}} \right) \Delta m_q, \quad (13)$$

where  $f_0$  is the resonant frequency of the device,  $A$  is the relevant area,  $\rho_q$  is the material density,  $\mu_q$  is the material stiffness, and  $\Delta m_q$  is the change in mass at the surface. It is reasonable to assume that the observed frequency shift indicates a mass loading on the surface of the device by the de-ionized water. This would also confirm the prediction made by analysis of the Christoffel matrix that the wave is a TSM wave. The response to the water test was shown to be repeatable across different devices in various locations about the wafer.

## V. CONCLUSIONS

Theoretical analysis of the Christoffel equation has shown that a TSM wave can be excited in  $c$ -axis-oriented ZnO with an in-plane excitation field oriented in any direction on the wafer. Further, it has been shown that the shear particle displacement will be parallel to the excitation field, assuming an entirely lateral field.

To implement the theoretical findings, a solidly mounted resonator consisting of alternating layers of W and  $SiO_2$  were grown on a  $p$ -doped  $\langle 1\ 0\ 0 \rangle$  Si substrate with ZnO as the active piezoelectric layer at the surface. The acoustic mirror was designed to have a reflection coefficient closest to unity near the frequency of operation. The acoustic mirror frequency response was simulated to provide assurance of the frequency range coverage given a fixed number of alternating pairs of W and  $SiO_2$ . Finite element modeling was also performed to predict the electric field of an electrode configuration consisting of two long electrodes positioned on the top of the ZnO with a gap between them. Simulations showed that the electric field within the gap between the electrodes was primarily laterally oriented, while the electric field directly beneath the electrodes was shown to be reduced in magnitude with an orientation normal to the surface of ZnO.

To verify the thickness shear mode operation of the devices, we investigated the experimentally extracted acoustic

velocity and the effects of water loading on the resonance. Without these tests it is difficult to adequately determine that a resonance is necessarily TSM. We have presented evidence of a TSM wave through exposure of the device to de-ionized water, comparison of extracted acoustic velocity with theoretical acoustic velocity, and varying the piezoelectric film thickness to yield respective changes in the frequency response.

On the basis of these results, it is expected that with an appropriate chemical surface preparation, these devices could be used as a platform for biosensor applications. The simple fabrication and small device size make this an appropriate candidate for fabrication of sensor arrays. The results of our investigation indicate that the lateral excitation of a thickness shear mode in solidly mounted ZnO FBARs is realizable both theoretically and experimentally. In the future, we will experiment with multiple electrode geometries in order to improve device response and performance.

## ACKNOWLEDGMENTS

This work was supported by the Georgia Tech/Emory Fund for Innovative Cancer Technologies which derives its funds from The V Foundation and the Georgia Cancer Coalition. In addition, Chris Corso was supported by a NSF Graduate Research Fellowship. Further, we must acknowledge the support of Dr. Colin Wood of the Office of Naval Research under the MURI program "Epitaxial Multifunctional Materials and Applications." We would also like to thank John Perng and Brent Buchine for their time and help with obtaining the SEM images. The support of all of these organizations is very much appreciated.

<sup>1</sup>J. W. Chung, J. M. Park, R. Bernhardt, and J. C. Pyun, *J. Biotechnol.* (2006).

<sup>2</sup>M. S. Wilson and W. Nie, *Anal. Chem.* **78**, 6476 (2006).

<sup>3</sup>S. L. Pinkett, W. D. Hunt, B. P. Barber, and P. L. Gammel, *IEEE Trans. Ultrason. Ferroelectr. Freq. Control* **49**, 1491 (2002).

<sup>4</sup>A. Shons, F. Dorman, and J. Najarian, *J. Biomed. Mater. Res.* **6**, 565 (1972).

<sup>5</sup>X. L. Su and Y. Li, *Biosens. Bioelectron.* **19**, 563 (2004).

<sup>6</sup>Z. Y. Wu, G. L. Shen, S. P. Wang, and R. Q. Yu, *Anal. Sci.* **19**, 437 (2003).

<sup>7</sup>C. D. Corso, D. D. Stubbs, S. H. Lee, M. Goggins, R. H. Hruban, and W. D. Hunt, *Cancer Detect. Prev.* **30**, 180 (2006).

<sup>8</sup>G. Sauerbrey, *Z. Phys.* **155**, 206 (1959).

<sup>9</sup>K. K. Kanazawa and J. G. Gordon, *Anal. Chem.* **57**, 1770 (1985).

<sup>10</sup>W. D. Hunt, D. D. Stubbs, and L. Sang-Hun, *Proc. IEEE* **91**, 890 (2003).

<sup>11</sup>S. L. Pinkett, Ph.D. thesis, Georgia Institute of Technology, 2003.

<sup>12</sup>J. V. Atanasoff and P. J. Hart, *Phys. Rev.* **59**, 85 (1941).

<sup>13</sup>R. Bechmann, 14th Annual Symposium on Frequency Control (US Army Electronics Research and Development Laboratory, Atlantic City, NJ, 1960), pp. 68–88.

<sup>14</sup>E. R. Hatch and A. Ballato, *Ultrason. Symp. Proc. (IEEE Group on Sonics & Ultrasonics, Atlanta, GA, 1983)*, p. 512.

<sup>15</sup>A. W. Warner, 17th Annual Symposium on Frequency Control (US Army Electronics Research and Development Laboratory, Atlantic City, NJ, 1963), pp. 248–266.

<sup>16</sup>H. Yihe, L. A. French, Jr., K. Radecsky, M. Pereira da Cunha, P. Millard, and J. F. Vetelino, *IEEE Trans. Ultrason. Ferroelectr. Freq. Control* **51**, 1373 (2004).

<sup>17</sup>H. Yihe, L. A. French, Jr., K. Radecsky, M. Pereira da Cunha, P. Millard, and J. F. Vetelino *IEEE Trans. Ultrason. Ferroelectr. Freq. Control* **51**, 1373 (2004).

<sup>18</sup>W. Pinkham, M. Wark, S. Winters, L. French, D. J. Frankel, and J. F. Vetelino, *Proc.-IEEE Ultrason. Symp.* **4**, 2279 (2005).

<sup>19</sup>C. York, L. A. French, P. Millard, and J. F. Vetelino, *Proc.-IEEE Ultrason. Symp.* **1**, 44 (2005).

<sup>20</sup>A. Ballato, E. R. Hatch, M. Mizan, and T. J. Lukaszczek, *IEEE Trans. Ultrason. Ferroelectr. Freq. Control* **33**, 385 (1986).

<sup>21</sup>S. V. Krishnaswamy, B. R. McAvoy, W. J. Takei, and R. A. Moore, *Ultrason. Symp. Proc. (IEEE Group on Sonics & Ultrasonics, San Diego, CA, 1982)*, p. 476.

<sup>22</sup>J. S. Wang and K. M. Lakin, *Ultrason. Symp. Proc. (IEEE Group on Sonics & Ultrasonics, San Diego, CA, 1982)*, p. 480.

<sup>23</sup>M. Link *et al.*, *J. Vac. Sci. Technol. A* **24**, 218 (2006).

<sup>24</sup>M. Link, M. Schreiter, J. Weber, R. Primig, D. Pitzer, and R. Gabl, *IEEE Trans. Ultrason. Ferroelectr. Freq. Control* **53**, 492 (2006).

<sup>25</sup>P. Wei, Y. Hongyu, K. Jae Wan, Z. Hao, and K. Eun Sok, *Proceedings of the 2004 IEEE International Frequency Control Symposium and Exposition*, (IEEE UFFC Society, Montreal, Canada, 2004) pp. 558–561.

<sup>26</sup>J. F. Rosenbaum, *Bulk Acoustic Wave Theory and Devices* (Artech House, Boston, 1988).

<sup>27</sup>W. E. Newell, *Proc. IEEE* **53**, 575 (1965).

<sup>28</sup>K. M. Lakin, G. R. Kline, and K. T. McCarron, *IEEE Trans. Microwave Theory Tech.* **43**, 2933 (1995).

<sup>29</sup>L. Woo Wai, S. Yonghua, and K. Eun Sok, *Proceedings of the 1996 IEEE International Frequency Control Symposium (IEEE UFFC Society, New Brunswick, NJ, 1996)*, pp. 558–562.

# Title: Mesothelin-fc fusion protein detection using a novel microelectronic acoustic sensor platform

## *Abstract*

Advances in the proteomics of cancer proliferation are yielding many new potential targets, or biomarkers, for identifying a malignancy at the earliest stages of development. These markers have been difficult to find as they exist in extremely low concentrations in circulating blood. In order to make use of these discoveries at a clinical level, ultra-sensitive biosensors exhibiting high degrees of specificity will be required to identify these proteins in clinical samples, such as patient blood plasma or serum. Further, a sensing technology that identifies a multi-protein signature is most likely to minimize false positives and false negatives. A sensor array incorporating these aspects could have an impact at multiple levels including early detection screening, post-therapy monitoring, as well as on the proteomic discovery process.

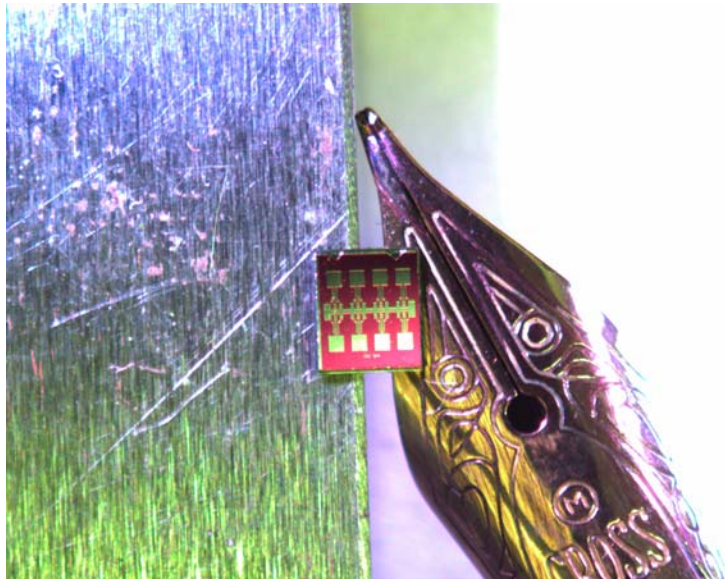
The research presented here involves the development of such a tool and its application towards detecting mesothelin, a cell-surface protein that is highly expressed in mesothelioma, ovarian cancer, pancreatic cancer, and some other malignancies. The acoustic resonator array design consists of electrodes fabricated on the surface of a piezoelectric ZnO thin-film. To functionalize the resonators for mesothelin detection, MB Mabs were immobilized on the surface, which have an affinity for mesothelin at 0.6 nmol/L. The Mabs were bound to the surface using a thiol-terminated silane surface chemistry. Reference device arrays coated with anti-FITC antibodies, specific to a molecule not present in the analyte, were also prepared. The goal of the investigation was therefore to gauge the sensitivity of the sensors to the molecular binding of mesothelin. A total of  $n=16$  mesothelin-targeted devices and  $n=16$  reference devices were tested by exposing them to a 10  $\mu\text{g/ml}$  solution of purified mesothelin-rfc protein in PBS buffer for 25 minutes. The devices were washed and the final operating frequencies were measured. The frequency shifts were then compared with the initial “unloaded” operating frequencies. The reference sensors showed a mean shift of 540 kHz while the mesothelin-coated sensors showed a mean shift of 1.25 MHz. ANOVA was performed on the results which indicate a statistically significant difference ( $p < 0.001$ ) in the overall frequency shifts associated with the mesothelin-target sensors and the reference sensors.

The magnitude of these preliminary results promises a detection limit at much lower target concentrations than those tested; potentially well below the ng/ml threshold upheld in the literature as the necessary limit. An important feature of these devices is that the sensitivity of the sensor platform is scaleable by a simple adjustment of the fabrication parameters. The device design also incorporates standard fabrication practices from the microelectronic device industry, allowing for mass production of extremely low-cost sensors. Work is on-going to demonstrate the efficacy of these devices under realistic physiological conditions and for lower concentrations of target.



## A New Technology for Cancer Screening Listens for the Signs of Cancer

ATLANTA – Cancer-sensing devices built as cheaply and efficiently as wristwatches – using many of the same operating principles – could change the way clinicians detect, treat and monitor cancer in patients. Researchers from the Georgia Institute of Technology have created an acoustic sensor that can report the presence of small amounts of mesothelin, a molecule associated with a number of cancers including mesothelioma, as they attach to the sensor's surface.



According to the researchers, the study is a proof of principle, demonstrating a technique that might work for the detection of nearly any biomarker – a collective term for a molecular signal that denotes the presence of disease. They present their findings today in Atlanta, Georgia at the American Association for Cancer Research's 2<sup>nd</sup> Annual International Conference on Molecular Diagnostics in Cancer Therapeutic Development.

“It is one thing to be able to identify biomarkers for a disease, but it is another to be able to find them in blood quickly and easily at very low concentrations,” said Anthony Dickherber, a graduate student in the School of Electrical and Computer Engineering at Georgia Tech. “We envision that, one day, doctors can use an array of our sensors as a sort of laboratory in their office, where they could use a quick blood sample to detect or monitor the signs of cancer.”

According to Dickherber, such a device would be a boon to healthcare practice, allowing physicians to screen patients for signs of disease before opting for more expensive or invasive diagnostic techniques. Responding to the growing need for such sensors in both research and clinical practice, Dickherber, along with fellow Georgia Tech graduate student Christopher Corso and research adviser William D. Hunt, Ph.D., conceived of and developed the ACμRay™ (pronounced *ak'-u-rā*) chip, standing for ACoustic micro-arRAY – a device that shares more in common with an inexpensive wristwatch than the sort of cutting edge molecule-sorting apparatuses currently used by researchers and clinical laboratory technicians.

The array consists of a series of electrodes deposited on the surface of a thin film of zinc oxide, which allows the device to resonate, or vibrate, at a specific frequency when a current is applied, much like the quartz timing devices used in many clocks and watches.

“The sensor itself is built on a base of silicon, like a computer chip, and could be mass-produced using very well known and inexpensive microelectronic fabrication techniques,” Dickherber said.

To turn this array into a sensor, the Georgia Tech researchers coated the zinc oxide surface with mesothelin-specific antibodies generated in the lab of Ira Pastan, M.D., at the National Cancer Institute. These molecules are engineered versions of the antibodies the immune system creates to identify foreign intruders, such as microbial parasites. In this study, the researchers coated the sensor with antibodies for mesothelin, a cell-surface protein that is highly expressed in mesothelioma, ovarian cancer, pancreatic cancer and other malignancies.

When the mesothelin binds to an antibody, the added mass changes the frequency at which the acoustic wave passes between the electrodes on the surface of the device. The device is able to “hear” the pitch change due to nanomolar concentrations of mesothelin (just a few molecules amid billions) binding to antibodies on the chip. The technology has the potential of detecting biomarkers in even lower concentrations than those tested, Dickeherber said.

“It is really an elegant engineering solution to a very complicated problem,” said Hunt, a professor of electrical and computer at Georgia Tech and lead researcher on the project. “With refinement, this technology could readily lead to an inexpensive, ubiquitous technology for researchers, physicians and the clinical laboratory.”

This research is supported by grants from the U.S. Army Medical Research & Materiel Command Prostate Cancer Research Program, the National Science Foundation, The V Foundation, the National Cancer Institute and the Georgia Cancer Coalition.

**AACR 2007 Conference on Molecular Diagnostics in Cancer Therapeutic Development**  
**September 17-20<sup>th</sup>, Atlanta, Ga.**

Coverage for Tony Dickherber, Christopher Corso, and William Hunt “A New Technology for Cancer Screening Listens for the Signs of Cancer”\*

From our press release:

RxPG News

[http://www.rxpgnews.com/research/A-new-technology-for-cancer-screening-listens-for-the-signs-of-cancer\\_64056.shtml](http://www.rxpgnews.com/research/A-new-technology-for-cancer-screening-listens-for-the-signs-of-cancer_64056.shtml)

Dentalplans.com

<http://www.dentalplans.com/articles/25102/>

PhysOrg.com

<http://www.physorg.com/news109349930.html>

ScienceDaily

<http://www.sciencedaily.com/releases/2007/09/070918144313.htm>

**Original Stories:**

WebMD (Dan DeNoon)

“Sensor Hears Cancer's Call; Tiny Biosensors Detect ‘Song’ of Cancer Markers, Say Researchers”

<http://www.webmd.com/cancer/news/20070918/sensor-hears-cancers-call>

From the WebMD story above:

Medicine.net

<http://www.medicinenet.com/script/main/art.asp?articlekey=83974>

**From the Amanda Gardner HealthDay story “Tiny Sensor Could Spot Cancer Early”:**

CBC News

<http://www.cbc.ca/cp/HealthScout/070918/6091806AU.html>

Health Central.com

<http://www.healthcentral.com/newsdetail/408/608331.html>

WFIE 14 Indiana (NBC affiliate)

<http://www.14wfie.com/Global/story.asp?S=7094493&nav=3w6r>

LEX 18 Kentucky (NBC affiliate)

<http://www.lex18.com/Global/story.asp?S=7094493&nav=EQls>

Forbes

<http://www.forbes.com/forbeslife/health/feeds/hscout/2007/09/18/hscout608331.html>

US News & World Report

<http://health.usnews.com/usnews/health/healthday/070918/tiny-sensor-could-spot-cancer-early.htm>

Dentalplans.com

<http://www.dentalplans.com/articles/25095/>

Health Scout

<http://www.healthscout.com/news/1/608331/main.html>

HealthCentral.com

<http://www.healthcentral.com/newsdetail/408/608331.html>

KOLD News Arizona (CBS Affiliate)

<http://www.kold.com/global/story.asp?s=7094493>

CNN News Room

(Please see page 3 for transcript)

\* We will continue to monitor coverage



CNN

September 19, 2007 Wednesday

**SHOW: CNN NEWSROOM 3:00 PM EST**

Bail Set For O.J. Simpson; Ahmadinejad to Visit Ground Zero?; Al Sharpton's Planned Protest in Jena, Louisiana

BYLINE: Joe Johns, Paul Vercammen, Deborah Feyerick, Susan Roesgen, Ed Lavandera, Don Lemon, Fredricka Whitfield, Jeffrey Toobin, Sanjay Gupta, Susan Lisovicz, Wolf Blitzer

SECTION: NEWS; International

WHITFIELD: Straight ahead, a high tech computer chip smaller than a penny that can detect cancer. Details on that straight ahead in "THE NEWSROOM".

WHITFIELD: A computer chip could one day make diagnosing cancer as easy as telling time.

Here's CNN's chief medical correspondent, Dr. Sanjay Gupta.

DR. SANJAY GUPTA, CNN CORRESPONDENT: This is something that really fascinates me quite a bit. This is a little chip that I'm holding up here. I'm actually holding it in a pair of tweezers this thing is so small. It's called the ACuRay and it's not something that's going to be widely available quite yet. But researchers have been focusing on this particular chip as a way to detect cancer very, very early.

Again, it's called the ACuRay. You can take it at there. What it is specifically is 140 different electrodes actually bound together by zinc oxide. The theory a simple one -- basically, if you have cancer molecules in your blood and you wash your blood over the sensor, the way that those cancer molecules bind to this

ACuRay gives off a certain resonance, a certain frequency that can be measured. If you have cancer molecules, it's going to sound different than if you don't have cancer molecules in your blood. The whole idea is that you want to detect cancer as early as possible.

Now what does this all mean?

There could be a day when doctors have several different little devices like this in their office and you walk in, you give a drop of blood and they immediately screen to tell if you have any cancer molecules in your bloodstream. It could be used, perhaps, in the future for infectious diseases, as well.

Again, as I mentioned, it's not something we may see in our lifetimes as a general way of practicing, but this whole idea you might be able to find cancer early, earlier than ever before, before it shows up on a C.T. scan or an MRI, when it's just a few still a few molecules in your blood is sort of the holy grail of cancer detection and screening.

Could this be the answer?

Possibly one day. It's something that we're certainly going to keep an eye on -- back to you.

LEMON: All right, Sanjay.

It's time now to check in with CNN's Wolf Blitzer.

WHITFIELD: Yes, in "THE SITUATION ROOM" -- what do you have on tap?

WOLF BLITZER, HOST, "THE SITUATION ROOM": All right, guys, thanks very much.

The Republican presidential candidate, Rudy Giuliani, has a message for MoveOn.org -- bring it on. He talks about his high profile spat with the liberal anti-war group in an exclusive one-on-one interview with our chief national correspondent, John King. That's coming up.

Also, Reverend Jesse Jackson says Democratic presidential candidate Barack Obama -- and I'm quoting now -- "is acting like he's white." We'll show you what's behind that controversial comment.

Also, carefree lives in the face of unimaginable suffering. There are some disturbing newly released images of the men and women who ran the Nazi Auschwitz death camp. All that and a lot more coming up right here in "THE SITUATION ROOM" -- back to you.

LEMON: All right, Wolf, we'll be watching.

Thank you. WHITFIELD: All right, the closing bell and a wrap of the action on Wall Street straight ahead.

# Stability of a RF sputtered ZnO solidly mounted resonator sensor in varying temperature and conductivity environments

*Anthony Dickherber<sup>†</sup>, Christopher D. Corso<sup>‡</sup>, and William Hunt<sup>†</sup>*

<sup>†</sup>Dept of Electrical and Computer Engineering, Georgia Inst. of Technology, Atlanta, GA 30332

<sup>‡</sup>Dept of Biomedical Eng, Georgia Inst. of Technology, Atlanta, GA 30332

Email: tonyd@gatech.edu

**Abstract**—It has been demonstrated that thickness shear mode acoustic wave devices have been extremely useful for liquid phase sensing applications, especially as biosensors. The quartz crystal microbalance is likely the strongest demonstration of this application to date. Recently, we reported on a ZnO-based TSM device that is easily fabricated and operates at significantly higher frequencies than the QCM. To further validate the usefulness of the ZnO resonator as a strong candidate for biosensor applications, we report the stability of the device over varying temperature and sample conductivity. A modest thermal coefficient of resonant frequency is reported at  $\sim 25$  ppm/ $^{\circ}$ C. Further, it is demonstrated that the resonator demonstrates reasonable stability over a range of sample conductivities (0.0 to 0.9 % wt/vol NaCl in DI H<sub>2</sub>O).

## I. INTRODUCTION

To date, the quartz crystal microbalance (QCM) resonator has best demonstrated the potential of bulk acoustic wave (BAW) biosensors. QCM resonators excite a thickness shear mode (TSM) bulk wave through the thickness of the crystal wafer, which is necessary for application of the resonator in a liquid-phase medium. This is what makes the device so attractive for biosensor applications, especially in the field of medical diagnostics. The QCM is additionally attractive as it demonstrates excellent temperature stability.

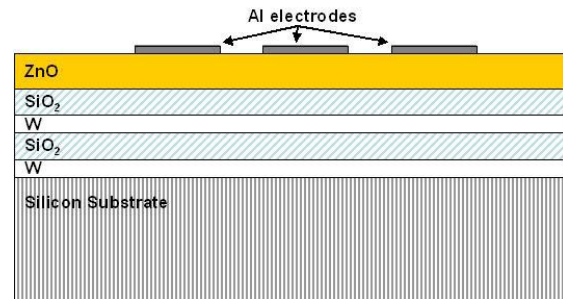
Thin film bulk acoustic wave resonators (FBARs) are employed widely from front-end filtering applications to resonator-based biosensors. Recently, we reported on a ZnO-based TSM FBAR device that is easily fabricated and operates at significantly higher frequencies than the QCM. Additionally, these resonators have been fabricated in a solidly mounted resonator (SMR) configuration, which allows them to be imbedded in existing silicon or gallium arsenide-based fabrication processes with a very small footprint ( $<1000 \mu\text{m}^2$  per device). Finally, these devices

have been fabricated as multi-device arrays in a progression towards functionalizing these as ultra-sensitive biosensor arrays.

TSM operation of the resonator is achieved by lateral field excitation (LFE) of the piezoelectric layer, requiring that both the signal and ground electrodes are on the surface of the ZnO. The mechanics of the ZnO SMR achieved by LFE of the TSM is thoroughly treated by Corso, *et al.*[1] Exposure of these SMRs to biological environments translates to varying conductivity and possibly varying thermal conditions at the surface of the resonator. Similar work has been done to characterize QCMs employing LFE for biosensor applications.[2] This investigation similarly reports on the response of ZnO SMRs to a range of thermal and surface conductivity conditions.

## II. DEVICE DESIGN

SMRs were fabricated by first depositing an acoustic mirror, analogous to an optical Bragg reflector, onto a mechanical grade silicon wafer (University Wafer). The acoustic mirror consisted of alternating layers of SiO<sub>2</sub> (low acoustic impedance) and W (high acoustic impedance). Highly *c*-axis oriented ZnO was then deposited onto the mirror followed by aluminum electrodes, as seen in Figure 1. SiO<sub>2</sub> and ZnO were deposited by RF sputtering, while the W and Al electrodes were deposited by DC sputtering. Electrodes were



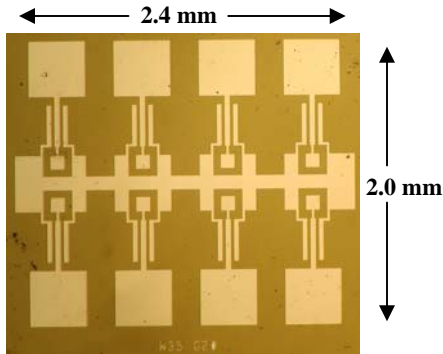
**Figure 1.** Cross section of the acoustic resonator solidly mounted on a W/SiO<sub>2</sub> acoustic mirror.

Table 1. Sputtering Parameters				
	Pressure (Torr)	Temp.	% Ar	% O <sub>2</sub>
SiO <sub>2</sub>	5.02 x 10 <sup>-3</sup>	Ambient	80	20
W	5.00 x 10 <sup>-3</sup>	Ambient	100	0
ZnO	5.10 x 10 <sup>-3</sup>	325°C	80	20
Al	5.02 x 10 <sup>-3</sup>	Ambient	100	0

fabricated on the surface of the piezoelectric ZnO film by standard photolithography methods. All sputtering depositions were performed by a Unifilm PVD-300 multi-target sputtering system, using the sputtering parameters summarized in Table 1. (All sputtering targets were obtained from PureTech, Inc.) Figure 2 shows one of the 8-device arrays occupying roughly 5 mm<sup>2</sup> of surface space. Resonators were probed using a Cascade Microtech 9000 Analytical Probe Station and scattering (S) parameters were gathered using a HP 8753C Network Analyzer outfitted with a HP 85047A S-Parameter Test Set. A ThermoChuck (Temptronic Corp.) system was set up on the probestation in order to control the wafer temperature. Finally, saline solutions were prepared using 99.5% NaCl (Sigma) and HPLC-grade deionized H<sub>2</sub>O (Burdick & Jackson) and mixed for at least 30 seconds on a mini vortexer (VWR Scientific Products). Saline solutions were deposited on the resonator surface by hand-pipetting ~2 µl directly onto the surface while being probed.

### III. RESULTS

It was first empirically verified that the resonator design displayed in Figure 2 performed as well in the array configuration as individual devices with the same electrode layout. That is to say, it was confirmed that the array structure did



**Figure 2.** Digital image of fabricated 8-device array. Device is designed for probing with Cascade Microtech ACP40 probes and with pads large enough for subsequent wire bonding.

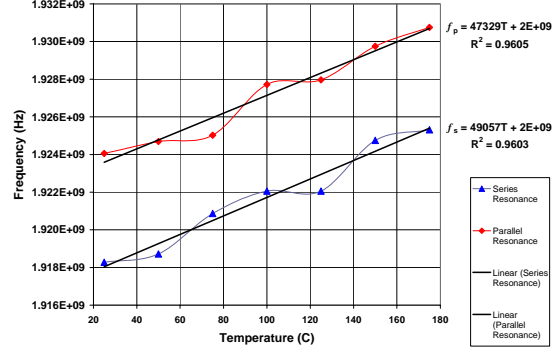


**Figure 3.** Frequency drift of parallel and series resonance frequency with increasing temperature.

not bear any beneficial nor detrimental effects on the resonator's performance. A broad sampling of devices ( $n > 20$  each) showed the maximum and average coupling coefficients,  $K^2$ , and quality factor,  $Q$ , were consistently about equal for both the array layout and the individual resonator layout.

With the goal of employing these resonators in biosensor applications, the arrays were tested over a temperature range of 20°C to 175°C. The equation used to calculate the thermal coefficient of resonant frequency (TCF) was

$$TC(f_x) = \frac{df_x}{dT} \cdot \frac{1}{f_{x,RT}} \quad (1)$$

where  $T$  is the temperature,  $f_x$  is the relevant resonant frequency and  $RT$  represents room temperature (25°C). The results yielded an empirically derived TCF for the series and parallel resonance of 24.6 ppm/°C and 25.6 ppm/°C, respectively. These results are demonstrated in Figure 3.

From the collected reflection scattering parameters ( $S_{11}$  responses),  $K^2$  and  $Q$  were determined as follows: [3]

$$K^2 = \left( \frac{\pi}{2} \right)^2 \frac{f_p - f_s}{f_p} \quad (2)$$

$$Q = \left( \frac{f}{2} \right) \frac{d\angle\Phi_Z}{df} \quad (3)$$

where  $p$  denotes parallel and  $s$  denotes series of the resonance,  $f$ , and  $\Phi_Z$  is phase of the impedance. It was found that the  $K^2$  remained very stable over the temperature range tested, varying by only 0.1% over the 155°C range. The  $Q$  drift of the resonator was slightly more significant, varying by roughly 42% over the 155°C temperature range. For application in a bench-top biosensor application, the  $Q$  remained stable enough to consider negligible, exhibiting an average 0.28 point shift per degree Celsius (<0.2%)

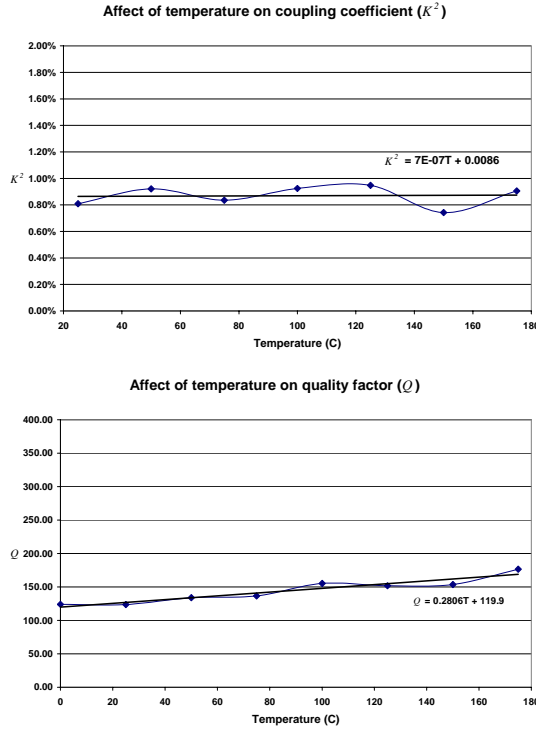


**Figure 4.** Variation observed over a wide temperature range for the resonator coupling coefficient,  $K^2$ , (top) and the resonator quality factor,  $Q$  (bottom).

per degree). The results for the temperature stability of  $K^2$  and  $Q$  are summarized in Figure 4.

With the idea of employing these resonators in biosensor applications with biological fluid samples, the resonators were tested over a range of sample conductivities loading the surface with 0.0% to 0.9% wt/vol of NaCl in DI  $H_2O$ . It is common in the literature to see 0.9% NaCl in DI  $H_2O$  as an equivalent salinity to blood. Results indicated that the magnitude of resonator frequency shift varied little in relation to loading with pure water alone, as indicated in Figure 5. As can be seen, the percentage of frequency shift with

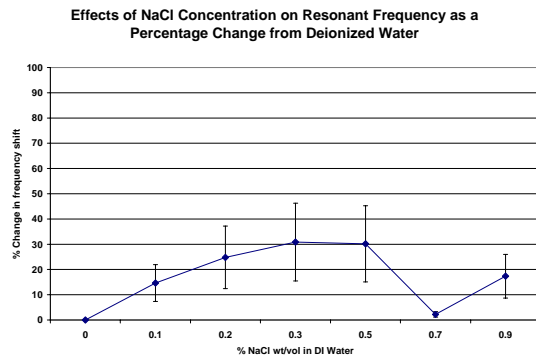


**Figure 5.** Percent change in resonant frequency as a function of increasing sample conductivity.

increasing sample conductivity was just slightly more significant than the noise level. Because these devices are not high- $Q$ , the resonance peak is slightly broad, and incidental fluctuations in the reflection parameters will cause the monitor to register a variance in the resonance. Note the error bars indicate the measured variance due to these incidental fluctuations. A further indicator of this can be seen in Figure 6, which represents the results of a typical experiment when sample is deposited on the device surface then subsequently washed with DI  $H_2O$ .

#### IV.DISCUSSION

A similar investigation of the TCF for ZnO SMRs excited by thickness excitation was performed by Pinkett, *et al.*[4] These resonators excited a longitudinal acoustic wave, as opposed to the TSM waves seen in this investigation, which yielded a steady decrease in resonance with increasing temperature. It was posited by Pinkett *et al* that the frequency increase was due to an expansion of the ZnO thickness, resulting in a longer acoustic path length, and therefore a lower resonant frequency. The frequency of the resonant wave is determined by the following:[3]

$$f = \frac{v_a}{2d} \quad (4)$$

where  $d$  is the material film thickness and the acoustic velocity,  $v_a$ . This term is determined by

$$v_a = \sqrt{\frac{c}{\rho}} \quad (5)$$

where  $c$  is the relevant material stiffness and  $\rho$  is the material density. Since the two investigations were carried out over a similar temperature range, it must be assumed that any expansion of the ZnO film was overtaken by an increase in the shear stiffness over and changes in the longitudinal stiffness.

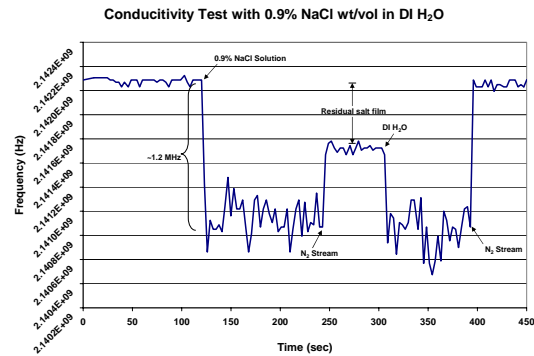


**Figure 6.** Demonstration of a typical conductivity experiment with 0.9% NaCl in DI  $H_2O$ .

As demonstrated in the conductivity experiments, the noise level of the resonator frequency response is significant. In order to reduce this, the  $S_{11}$  response of the resonator should have as narrow and smooth a peak as possible, so as to result in an easily tracked resonance condition. This parameter is gauged by the  $Q$  of the resonator, which can be explained as a ratio of the energy stored versus the energy dissipated per cycle of resonance. If the resonator transduces a wider frequency band, it is likely that the varying wave frequencies will compete for the available energy and also interfere destructively with each other's propagation.

The QCM demonstrates extraordinarily high  $Q$ , often in the 10's of thousands, and therefore has an easily tracked resonance. Such a high  $Q$  is not required for tracking, however, as demonstrated by various other acoustic wave based sensors.[5, 6] Optimization of the ZnO-based resonator presented in this research will be required to stabilize this response and provide a viable ultra-sensitive biosensor. Optimizing the individual device  $Q$  should result in the resonator only transducing the electrical driving energy about a tight band and therefore yield a reduced noise level.

## V. CONCLUSION

In this investigation, it has been shown that ZnO solidly mounted resonators can be fabricated in an array configuration without loss of performance. Further, it has been shown that these resonators can operate stably in biologically equivalent environments. Specifically, these resonators have been shown to exhibit low susceptibility to changes in temperature and conductivity. In order to achieve sensors of greater quality, however, it will be necessary to optimize the device  $Q$ .

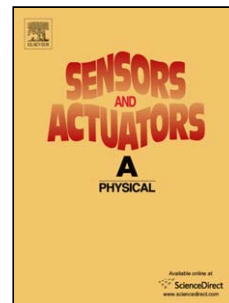
## REFERENCES:

- [1] C. D. Corso, A. Dickherber, and W. D. Hunt, "Lateral field excitation of thickness shear mode waves in a thin film ZnO solidly mounted resonator," *Journal of Applied Physics & Virtual Journal of Biological Physics Research*, vol. 101, 2007.
- [2] Y. Hu, L. A. French, Jr., K. Radecsky, M. P. DaCunha, P. Millard, and J. F. Vetelino, "A lateral field excited liquid acoustic wave sensor," presented at 2003 IEEE Symposium on Ultrasonics, Orono, ME, USA, 2003.
- [3] J. F. Rosenbaum, *Bulk acoustic wave theory and devices*. Boston: Artech House, 1988.
- [4] S. L. Pinkett and W. D. Hunt, "Temperature Characteristics of ZnO-Based Thin Film Bulk Acoustic Wave Resonators," presented at 2001 IEEE Ultrasonics Symposium, 2001.
- [5] F. Josse, F. Bender, and R. W. Cernosek, "Guided Shear Horizontal Surface Acoustic Wave Sensors for Chemical and Biochemical Detection in Liquids," *Anal. Chem.*, vol. 73, pp. 5937-5944, 2001.
- [6] S.-H. Lee, D. D. Stubbs, W. D. Hunt, and P. J. Edmonson, "Vapor phase detection of plastic explosives using a SAW resonator immunosensor array," 2005.

## Accepted Manuscript

Title: Optimization and characterization of a ZnO biosensor array

Authors: Anthony Dickherber, Christopher D. Corso, William D. Hunt



PII: S0924-4247(08)00014-9  
DOI: doi:10.1016/j.sna.2008.01.007  
Reference: SNA 6190

To appear in: *Sensors and Actuators A*

Received date: 2-8-2007  
Revised date: 2-1-2008  
Accepted date: 2-1-2008

Please cite this article as: A. Dickherber, C.D. Corso, W.D. Hunt, Optimization and characterization of a ZnO biosensor array, *Sensors and Actuators: A Physical* (2007), doi:10.1016/j.sna.2008.01.007

This is a PDF file of an unedited manuscript that has been accepted for publication. As a service to our customers we are providing this early version of the manuscript. The manuscript will undergo copyediting, typesetting, and review of the resulting proof before it is published in its final form. Please note that during the production process errors may be discovered which could affect the content, and all legal disclaimers that apply to the journal pertain.

# Optimization and characterization of a ZnO biosensor array

*Anthony Dickherber, Christopher D. Corso, William D. Hunt*

Microelectronics Research Center, Georgia Institute of Technology, 791 Atlantic Dr., Atlanta GA 30332

Accepted Manuscript



***Abstract***

Practical usage of acoustic biosensors has revealed that high quality factor,  $Q$ , is an important attribute of a highly sensitive acoustic sensor. In this research, we present performance optimization of ZnO thin-film bulk acoustic resonators (FBARs) operating in the thickness shear mode through characterization of a variety of electrode geometries. The resulting average  $Q$  and  $K^2$  from each of the electrode geometries were calculated and compared. Based on these results, a preferred electrode configuration was selected, and fabricated into an 8-device array. The arrays were tested in physiologically relevant environments to illustrate the effects of temperature and solution conductivity on the stability of the resonators. The devices demonstrated a temperature coefficient of frequency of  $\sim 25$  ppm/ $^{\circ}\text{C}$ . The resonators also exhibited reasonable stability under varying levels of solution conductivity as tested by exposing the devices to solutions containing a varied amount of NaCl in deionized  $\text{H}_2\text{O}$ .

## 1. Introduction

Thin film bulk acoustic wave resonators (FBARs) are employed widely from front-end filtering applications to resonator-based biosensors. To date, the quartz crystal microbalance (QCM) resonator has best demonstrated the potential of bulk acoustic wave (BAW) biosensors [1]. QCM resonators excite and support a thickness shear mode (TSM) bulk wave through the thickness of the crystal wafer, which is necessary for operation of the resonator in a liquid-phase medium. This is what makes the device so attractive for biosensor applications, especially in the field of medical diagnostics where most clinically relevant samples to be tested are in the liquid phase. The QCM is additionally attractive because it demonstrates excellent frequency stability over a significant frequency range as a result of the AT-cut crystal structure that comprises the QCM [2].

Recently, we reported on a ZnO-based TSM FBAR device that is easily fabricated and operates at significantly higher frequencies than the QCM [3]. Theory predicts that higher operating frequency is desirable as it translates to greater sensitivity to perturbation of the sensor [1]. Additionally, these resonators have been fabricated in a solidly mounted resonator (SMR) configuration, which allows them to be imbedded in existing silicon or gallium arsenide-based fabrication processes with a very small footprint ( $<0.05 \text{ mm}^2$  per device as compared to a QCM which is roughly  $150 \text{ mm}^2$  per device). A SMR configuration involves fabricating the device onto a solid support, which typically includes an acoustic Bragg reflector, comprised of quarter-wavelength alternating high and low impedance materials to reflect the acoustic wave. This acoustic mirror helps to maintain resonance in the piezoelectric film due to an impedance mismatch at the boundary. The very small size and ability to fabricate the devices using standard

fabrication processes has made it possible to integrate these resonators into multi-device arrays. The motivation for this stems from the growing consensus in the medical field that the ability to make an accurate diagnosis about a specific disease, such as prostate cancer, depends on the expression levels of multiple biomarkers, rather than a single principal indicator [4]. With the array configuration, it becomes possible to monitor any sample for multiple targets simultaneously in a consistent manner.

Acoustic resonators become liquid sensors by exposing the surface of the device to a fluid sample to be tested. The acoustic wave resonating within the piezoelectric crystal film acts as a probe that effectively queries the crystal surface for changes in the boundary conditions. Certain changes in the boundary conditions register as a shift in the resonant frequency, which is an easily monitored quantity. If a chemical layer that specifically binds a known target molecule is immobilized at the surface (comprised of antibodies or aptamers for example) the resonator is functionalized as a biosensor. Several models exist to describe the relationship between changes in the resonant condition for a TSM acoustic wave and changes in the boundary conditions. The first significant work attempting to characterize the sensitivity of a TSM acoustic wave sensor was described by Sauerbrey as part of his dissertation research in the late 1950's [5]. This analysis has been shown to be insufficient for operation of the sensor in a liquid phase environment, so a better description comes from Kanazawa and Gordon regarding operation of the QCM in a liquid [6]:

$$\Delta f = -f_o^{3/2} \sqrt{\frac{\eta_l \rho_l}{\pi \mu_q \rho_q}} \quad (1)$$

where  $\mu_q$  and  $\rho_q$  are the stiffness and density of the crystal,  $\rho_l$  and  $\eta_l$  are the density and viscosity of the liquid, and  $f_o$  is the unloaded resonant frequency of the device. This equation predicts that the resonant frequency of a QCM is affected by the density-viscosity product of the contacting liquid. Further research has been performed to illustrate the QCMs efficacy as a viscosity sensor [7]. Starting from the reciprocity relation (as described by Auld [8]) Hunt *et al.* derived the following expression to further characterize the factors affecting the TSM resonance using time-dependent perturbation theory [9]:

$$t \frac{\partial \Delta \omega}{\partial t} + \Delta \omega = - \frac{\omega_u^2 \cdot h_f}{\pi \sqrt{\rho_q \mu_q}} \left[ \Delta \rho_f - \frac{\Delta \mu_f}{V_s^2} \right] + i \cdot \frac{\omega_u \cdot h_f}{\pi \sqrt{\rho_q \mu_q}} \left[ \frac{\partial \Delta \rho_f}{\partial t} - \frac{1}{V_s^2} \cdot \frac{\partial \Delta \mu_f}{\partial t} \right] \quad (2)$$

where the subscript “u” denotes the unperturbed field condition, the subscript “f” denotes the properties relating to the adjacent molecularly specific film,  $\omega$  is the radian frequency,  $V_s$  is the velocity of the shear acoustic wave, and  $h_f$  is the height of the immobilized surface film. If one were to assume that  $\Delta \omega$ ,  $\Delta \rho$  and  $\Delta \mu$  were independent of time, then we would find that (2) reduces to

$$\Delta f = \frac{-2 \cdot f_u^2 \cdot h_f}{\sqrt{\rho_q \mu_q}} \left[ \Delta \rho_f - \frac{\Delta \mu_f}{V_s^2} \right]. \quad (3)$$

This equation is similar to the Sauerbrey equation with the exception that a term is included taking into account the stiffness of the surface film. This indicates that a change in the resonance condition is subject to both changes in the surface stiffness as well as mass loading at the surface.

TSM operation of the resonator is achieved by lateral field excitation (LFE) of the piezoelectric layer, requiring that both the signal and ground electrodes are plane-parallel on the exposed surface of the ZnO film. The mechanics of the ZnO SMR achieved by LFE of the TSM is thoroughly treated in ref. [3]. The LFE configuration contrasts with the typical thickness field excitation (TFE) configuration of other BAW devices like the QCM, in which electrodes are on opposite sides of the piezoelectric crystal. The LFE case results in electric field propagation through the adjacent medium, which is in contrast to the TFE configuration. Exposure of these LFE devices to biological environments implies potential field diversions through the adjacent medium as it will exhibit varying degrees of conductivity. This must be considered when assessing the sensor's capabilities in this environment.

When designing sensors for use with physiological samples, it is important to assess the sensor's performance under varying thermal and sample conductivity conditions. Hu *et al.* characterized the effects of sample conductivity on QCMs employing LFE rather than the typical TFE for biosensor applications [10]. Presented here is a similar investigation of the characteristics of the TSM in ZnO, analyzing both the impact of the electrode configuration/shape and the stability of the resonator in varying conductivity and temperature conditions.

## 2. Experimental

### a. Device fabrication

Solidly mounted resonators were fabricated by first depositing an acoustic mirror, analogous to an optical Bragg reflector, onto a mechanical grade <1 0 0> silicon wafer (University Wafer)

as described by Newell [11]. The acoustic mirror consisted of alternating  $\frac{1}{4}$ -wavelength layers of  $\text{SiO}_2$  (low acoustic impedance) and W (high acoustic impedance). Highly  $c$ -axis oriented ZnO was then deposited onto the mirror followed by aluminum electrodes. An illustration showing the overall device design is shown in Figure 1.  $\text{SiO}_2$  and ZnO were deposited by RF sputtering using a  $\text{SiO}_2$  target and a ZnO target, respectively, while the W and Al electrodes were deposited by DC sputtering. Electrodes were fabricated on the surface of the piezoelectric ZnO film by standard photolithography methods. All sputtering depositions were performed by a Unifilm PVD-300 multi-target sputtering system. Resonators were probed using a Cascade Microtech 9000 Analytical Probe Station with ACP40 GSG probes and reflection scattering ( $S_{11}$ ) parameters were gathered using a HP 8753C Network Analyzer outfitted with a HP 85047A S-Parameter Test Set.

*b. Susceptibility testing*

To test the susceptibility of the devices to varying sample conductivities, saline solutions were prepared using 99.5% NaCl (Sigma) and HPLC-grade deionized  $\text{H}_2\text{O}$  (Burdick & Jackson) and mixed for at least 30 seconds on a mini vortexer (VWR Scientific Products) at room temperature. The device arrays were exposed to the saline solutions by hand-pipetting  $\sim 1 \mu\text{l}$  directly onto the resonator array surface while being probed.

To test the temperature stability of the resonators, a ThermoChuck (Temptronic Corp.) system was set up on the probe station in order to control the wafer temperature. The temperature was varied from  $25^\circ\text{C}$  up to  $175^\circ\text{C}$  in increments of  $25^\circ\text{C}$  and the resonant frequency was measured after the system was allowed to stabilize at each temperature point for at least 10 minutes.

### 3. Results and Discussion

#### a. Device optimization

A total of eight different electrode configurations were tested using the two electrode shapes depicted in Figure 2. Among these electrode shapes, the electrode width and the gap between electrodes were varied in an effort to determine the optimal electrode configuration. Devices were evaluated based on quality factor,  $Q$ , and coupling coefficient,  $K^2$ , as calculated from the  $S_{11}$  response of each device.  $K^2$  and  $Q$  were determined as described by Rosenbaum [12]:

$$K^2 = \left( \frac{\pi}{2} \right)^2 \frac{f_p - f_s}{f_p} \quad (5)$$

$$Q = \left( \frac{f}{2} \right) \frac{d\Phi_z}{df} \quad (6)$$

where  $\Phi_z$  is phase of the impedance, and 'p' and 's' denotes the parallel and series of the resonance frequency,  $f$ , respectively. Results obtained from ANOVA analysis of these results demonstrate that a statistically significant gap ( $p < 0.01$ ) emerges between the performance of the circular shaped devices (Figure 2A) and the straight electrode devices (Figure 2B) when analyzing their  $K^2$  and  $Q$  results. It is evident that the average  $Q$  is higher for the straight electrode configuration while the effective  $K^2$  is lower. One possible explanation for this is that the circular electrode configuration has a larger surface area over which excitation of the crystal occurs. Therefore, the coupling of the electric field to the crystal over grain boundaries and

crystal non-uniformities is more efficient overall while the added mass of the larger electrodes acts to reduce the  $Q$ . These results are demonstrated in Table 1 and summarized in Figure 3.

As indicated by the strong correlation between devices G and H, it is readily apparent from the data that the electrode widths fabricated had no statistically significant impact on the device performance as assessed by  $Q$  and  $K^2$ . We had initially hypothesized that greater distribution of the electric field from a constant *power* source to the piezoelectric crystal would result in a more distributed and efficient coupling of electrical energy into acoustic wave energy. Since  $Q$  is a ratio of energy conserved to energy dissipated per cycle, it would seem that the  $Q$  factor should improve as a reflection of this. This result was not substantiated by the data, however, as the size of the gap between electrodes had no clear functional relationship with the device performance. Gap size does have some impact, however, as can be seen from device D in Table 1. Compared with the other straight electrode configurations, the 10  $\mu\text{m}$  gap exhibits a significantly lower  $Q$  and higher  $K^2$ , on average. It appears that beyond a particular threshold between 10  $\mu\text{m}$  and 20  $\mu\text{m}$  between straight electrodes, there was a notable improvement in  $Q$ . No clear pattern emerges beyond this, however. Rosenbaum asserts that effective implementation of an LFE resonator requires that the gap width between electrodes must be many times greater than the thickness of the film [12]. It could be that this requirement is met somewhere between 12 and 24 times the crystal thickness.

Having determined that the straight electrode configuration yielded higher  $Q$  devices, which has been identified as the desired parameter, 8-element arrays of these devices were fabricated in order to verify that the resonator design displayed in Figure 2 performed as well in the array configuration as individual devices. That is to say, it was our goal to confirm that the array structure did not bear any beneficial nor detrimental effects on the resonator's performance.



Sampling 88 arrayed devices similar to those seen in Figure 4 showed that there in fact was a statistically significant difference in device performance. A 30% decrease in  $Q$  and a 15% decrease in  $K^2$  was observed for devices with a 20  $\mu\text{m}$  gap fabricated in the array configuration versus the isolated configuration. For devices fabricated with a 50  $\mu\text{m}$  gap, again a decrease of 30% was observed in  $Q$  but only a 5% decrease in  $K^2$ . One explanation for the decrease in performance is the addition of a significant amount of conductor material surrounding the active devices for bonding pads and ground-bus connections. The added mass from the electrodes provide a lossy material at the surface boundary which can act to scatter the acoustic energy.

*b. Device susceptibility*

In order to evaluate these devices for potential biosensor applications, the arrays were tested over a temperature range of 25°C to 175°C to assess their thermal stability. The following equation was used to calculate the thermal coefficient of resonant frequency (TCF):

$$TC(f_x) = \frac{df_x}{dT} \cdot \frac{1}{f_{x,RT}} \quad (7)$$

where  $T$  is the temperature,  $f_x$  is the relevant resonant frequency and  $RT$  represents room temperature (25°C). The results yielded an empirically derived TCF for the series and parallel resonance of 24.6 ppm/°C and 25.6 ppm/°C, respectively. These results are demonstrated in Figure 5.

Past investigations of ZnO BAW resonators by Pinkett, *et al*, yielded a negative TCF of -30 ppm/°C [13]. The difference between these two findings can be explained by the fact that the two

device designs employ very different acoustic modes. The devices reported in this research employ a thickness shear mode while the Pinkett *et al* devices employ a longitudinal mode acoustic wave achieved by TFE. Given that the resonant frequency for both devices are described by the following relationship

$$f = \frac{v_a}{2d} \quad (8)$$

where  $v_a$  is the propagating acoustic wave velocity,  $d$  is the piezoelectric film thickness and  $f$  is the resonant frequency. For the TFE longitudinal case, it is conceivable that increased temperature results in a thickness expansion that outpaces any increase in wave velocity, yielding the negative TCF. The opposite condition could then explain the positive TCF for the LFE case, in which the increased wave velocity outpaces the film expansion. It is important to note that the velocity is a function of the square root of the ratio of the material stiffness to the material density. Given that the lateral (a-axis) thermal expansion of ZnO is significantly greater than the longitudinal (c-axis) thermal expansion, [14] it is conceivable that the shear stiffness coupling is increased with increasing temperature because of the relative expansion coefficients in either direction. A greater expansion in the lateral axis than in the longitudinal axis will result in an overall “apparent” stiffening in the longitudinal direction. This would result in an increase in the apparent stiffness tensor value pertaining to the shear coupling ( $c_{44}$ ) with increasing temperature. An alternative possibility is rather that  $c_{44}$  decreases because of thermal expansion, but the density is decreased by a greater amount per unit temperature change which results in a higher acoustic velocity overall.

It was found that the  $K^2$  remained very stable over the temperature range tested, varying by only 0.1% over the 155°C range. The  $Q$  drift of the resonator was more significant, varying

by roughly 42% over the 155°C temperature range. For use in bench-top biosensor applications, the  $Q$  remained stable enough to consider negligible, exhibiting an average 0.28 point shift per degree Celsius (<0.2% per degree). The results for the temperature stability of  $K^2$  and  $Q$  are summarized in Figure 6.

Considering the goal of employing these resonators in biosensor applications with biological fluid samples, the resonators were tested over a range of sample conductivities loading the surface with 0.0% to 0.9% wt/vol of NaCl in DI H<sub>2</sub>O. It is common in the literature to see 0.9% NaCl in DI H<sub>2</sub>O described as an equivalent salinity to blood. Results indicate that the magnitude of resonator frequency shift varied little in relation to loading with pure water alone, as indicated in Figure 7. A substantial increase in frequency instability was observed, however, with increasing sample conductivity. These devices do not exhibit the high- $Q$  characteristic of the QCM, which translates to a broad resonance peak as observed through the S11 response. Incidental fluctuations in the reflection parameters will therefore cause the resonance frequency monitor to register a variance in the resonance. The error bars in Figure 7 indicate the measured variance due to these incidental fluctuations. A further indicator of this can be seen in Figure 8, which demonstrates the results of a typical experiment when a 0.9% saline sample (isotonic with human blood) is deposited on the device surface then subsequently washed with DI H<sub>2</sub>O.

#### 4. Conclusion

In this investigation, it has been shown that thickness shear mode ZnO solidly mounted resonators can be fabricated in an array configuration with only a modest impact on device performance. It is believed that further electrode optimization could mitigate some of this

performance loss. Further, it has been shown that these resonators can operate stably in biologically equivalent environments. Specifically, these resonators have been shown to exhibit low susceptibility to changes in temperature and conductivity. In order to achieve sensors of greater quality, however, it will be necessary to improve the overall device  $Q$  through experimental optimization of the acoustic mirror.

### **Acknowledgments**

This work was supported by the Georgia Tech/Emory Fund for Innovative Cancer Technologies which derives its funds from the V Foundation and the Georgia Cancer Coalition (GCC). Anthony Dickherber is supported by the Congressionally Directed Medical Research Program Prostate Cancer Training Program and Christopher Corso is supported by a National Science Foundation Graduate Research Fellowship. We would further like to acknowledge the assistance of Georgia Tech undergraduates George Steven Ruff and Alice Wang who developed the monitoring software used in conjunction with the HP Network Analyzer.

## References:

- [1] A. Janshoff, H.-J. Galla, and C. Steinem, "Piezoelectric Mass-Sensing Devices as Biosensors - An Alternative to Optical Biosensors?," *Angewandte Chemie*, vol. 39, pp. 4004-4032, 2000.
- [2] D. Salt, *Hy-Q Handbook of Quartz Crystal Devices*. Berkshire, England: Van Nostrand Reinhold (UK) Co. Ltd, 1987.
- [3] C. D. Corso, A. Dickherber, and W. D. Hunt, "Lateral field excitation of thickness shear mode waves in a thin film ZnO solidly mounted resonator," *Journal of Applied Physics & Virtual Journal of Biological Physics Research*, vol. 101, 2007.
- [4] M. F.-P. Cecilia, "Selection of appropriate cellular and molecular biologic diagnostic tests in the evaluation of cancer," *Cancer*, vol. 69, pp. 1607-1632, 1992.
- [5] G. Sauerbrey, "Use of quartz vibrator for weighting thin films on a microbalance," *Z. Phys.*, vol. 155, pp. 206-210, 1959.
- [6] K. K. Kanazawa and J. G. Gordon, "Frequency of a quartz microbalance in contact with liquid," *Anal. Chem.*, vol. 57, pp. 1770-1771, 1985.
- [7] W. A. Gee, K. M. Ritalahti, W. D. Hunt, and F. E. Loeffler, "QCM viscometer for bioremediation monitoring," 2002.
- [8] B. A. Auld, *Acoustic fields and waves in solids*, 2nd ed. Malabar, Fla.: R.E. Krieger, 1990.
- [9] W. D. Hunt, D. D. Stubbs, and L. Sang-Hun, "Time-dependent signatures of acoustic wave biosensors," *Proceedings of the IEEE*, vol. 91, pp. 890-901, 2003.
- [10] Y. Hu, L. A. French, Jr., K. Radecsky, M. P. DaCunha, P. Millard, and J. F. Vetelino, "A lateral field excited liquid acoustic wave sensor," presented at 2003 IEEE Symposium on Ultrasonics, Orono, ME, USA, 2003.
- [11] W. E. Newell, "Face-mounted piezoelectric resonators," *Proceedings of the IEEE*, vol. 53, pp. 575-581, 1965.
- [12] J. F. Rosenbaum, *Bulk acoustic wave theory and devices*. Boston: Artech House, 1988.
- [13] S. L. Pinkett and W. D. Hunt, "Temperature Characteristics of ZnO-Based Thin Film Bulk Acoustic Wave Resonators," presented at 2001 IEEE Ultrasonics Symposium, 2001.
- [14] J. Albertsson, S. C. Abrahams, and A. Kvik, "Atomic displacement, anharmonic thermal vibration, expansivity and pyroelectric coefficient thermal dependences in ZnO," *Acta Crystallographica Section B*, vol. 45, pp. 34-40, 1989.

**Anthony Dickherber** earned his Bachelor's degree in Electrical Engineering from Georgia Tech in Atlanta in 1999. He worked for Georgia Tech Research Institute in their Information Technology and Telecommunications Laboratory for the next 4 years, while going to Georgia Tech part time to earn his Master's degree in Electrical and Computer Engineering. Tony is currently a Ph.D. candidate in the school of Bioengineering at Georgia Tech and a Sam Nunn Security Program Fellow. His research interests involve developing sensors for early detection of prostate cancer.

**Christopher D. Corso** graduated from Georgia Tech in 2004 with a bachelor's degree in Computer Engineering. He is now a graduate student in the joint MD/PhD program between Georgia Tech and Emory. Chris is currently working on his Ph.D. in Bioengineering after which he will attend Emory for medical school. His research interests involve the development of acoustic wave devices for medical diagnostics.

**William D. Hunt** received the B.S. degree in electrical engineering from the University of Alabama, Tuscaloosa, in 1976, the M.S. degree in electrical engineering from the Massachusetts Institute of Technology, Cambridge, in 1980, and the Ph.D. degree in electrical engineering from the University of Illinois, Urbana-Champaign, in 1987. From 1976 to 1978, he was an Engineer with Harris Corporation. From 1980 to 1984, he was a Staff Engineer at Bolt Beranek and Newman Corporation, Arlington, VA. In 1987, he joined the Electrical Engineering Faculty at Georgia Institute of Technology, Atlanta. His area of expertise is in the area of microelectronic acoustic devices for wireless applications as well as chemical and biological sensors based on this technology. He has published over 70 papers in refereed journals and conference proceedings. He holds four U.S. patents and five provisional patents.

Device	Shape	Electrode Width ( $\mu\text{m}$ )	Electrode Gap ( $\mu\text{m}$ )	# Tested	Average $Q$	Average $K^2$
A	Circular	20	10	92	198	0.86%
B	Circular	20	20	72	195	0.87%
C	Circular	20	40	70	192	0.86%
D	Straight	20	10	69	198	0.84%
E	Straight	35	20	74	217	0.78%
F	Straight	35	40	98	206	0.77%
G	Straight	20	50	25	220	0.74%
H	Straight	35	50	44	221	0.73%

**Table 1.** Assessment of device performance of tested resonators from analysis of collected S11 parameters.

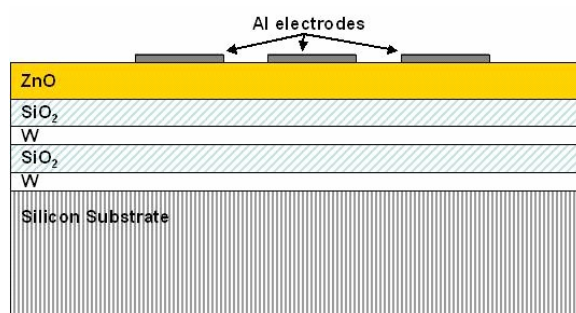


**Figure 1.** Profile of device fabrication.



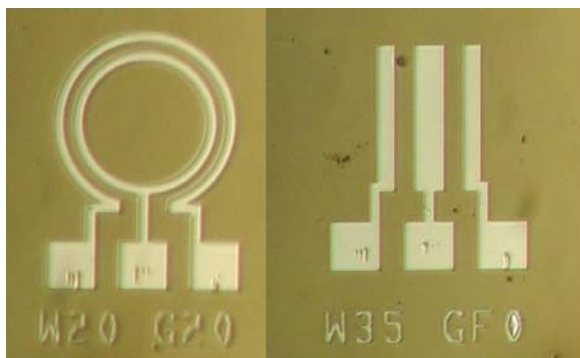


**Figure 2.** Various electrode shapes fabricated in an effort to determine the optimal LFE resonator configuration. [Note the left figure has electrode widths of 20  $\mu\text{m}$  and a gap size of 20  $\mu\text{m}$ , and the right figure has electrode widths of 35  $\mu\text{m}$  and a gap size of 40  $\mu\text{m}$ .]

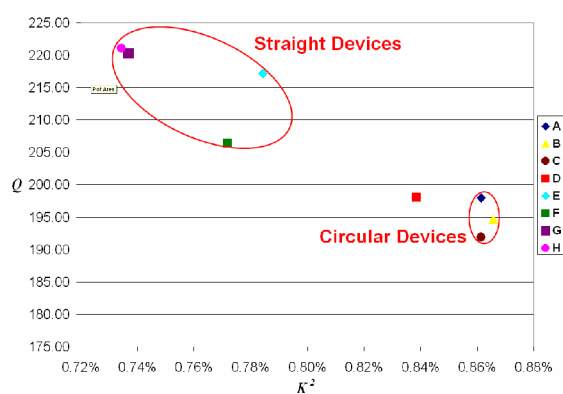


**Figure 3.** Comparison of various electrode configurations using  $Q$  and  $K^2$

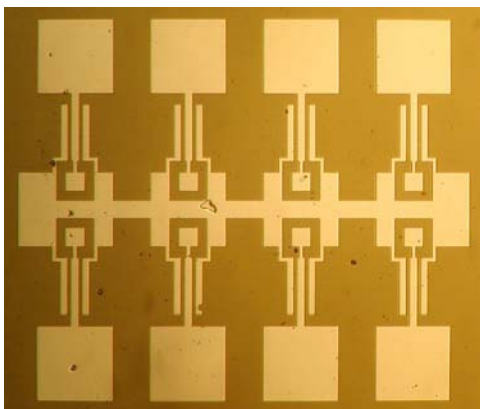


**Figure 4.** Digital image of fabricated 8-device array. Device is designed for probing with Cascade Microtech ACP40 GSG150 probes and with pads large enough for subsequent wire bonding. These devices have electrode widths of 50  $\mu\text{m}$  and a gap size of 20  $\mu\text{m}$ .

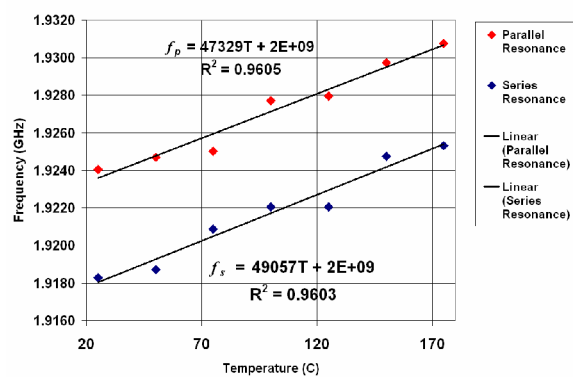


**Figure 5.** Frequency drift of parallel and series resonance frequency with increasing temperature.

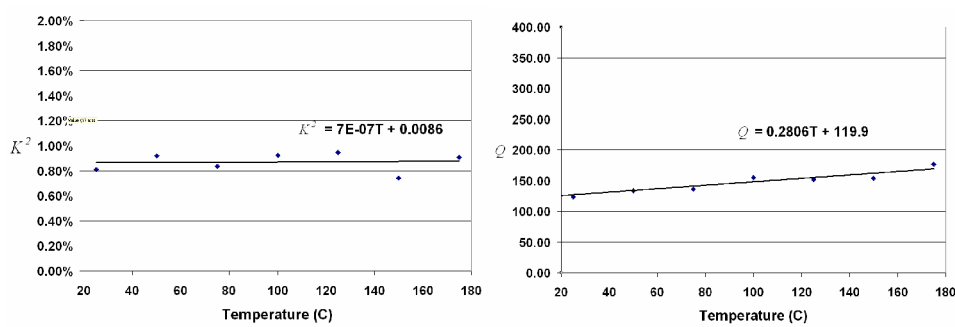


**Figure 6.** Variation observed over a wide temperature range for the resonator coupling coefficient,  $K^2$ , (left) and the resonator quality factor,  $Q$  (right).

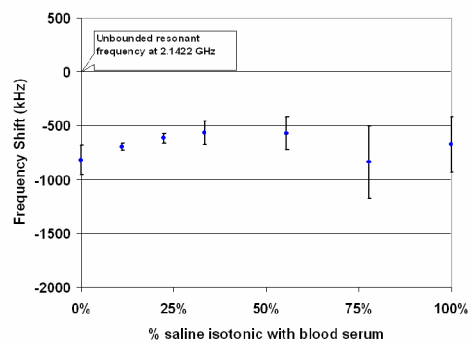


**Figure 7.** Change in resonant frequency as a function of increasing fluid sample conductivity.

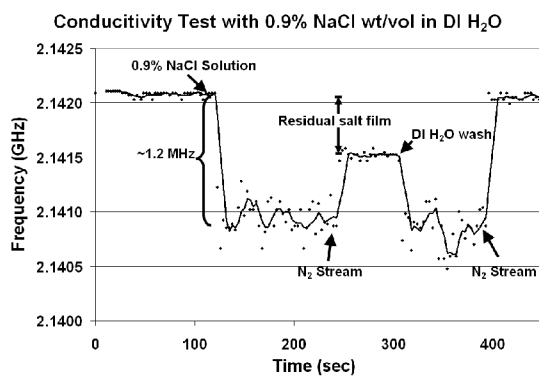


Figure 8. **Demonstration of a typical conductivity experiment with 0.9% NaCl in DI H<sub>2</sub>O.**

# A comparison of antibody immobilization methods employing organosilanes and phosphonic acids on planar crystalline ZnO surfaces

*Christopher D. Corso<sup>1</sup>, Anthony Dickherber<sup>2</sup>, Peter Hotchkiss<sup>3</sup>, Seth R. Marder<sup>3</sup>, William D. Hunt<sup>\*2</sup>*

Georgia Institute of Technology, Atlanta, GA 30332

**RECEIVED DATE January 24<sup>th</sup>, 2008**

\*Corresponding Author – Phone: (404) 894-2945. Fax: (404) 894-xxxx. Email:  
[bill.hunt@ee.gatech.edu](mailto:bill.hunt@ee.gatech.edu).

<sup>1</sup> School of Biomedical Engineering, Georgia Institute of Technology

<sup>2</sup> School of Electrical Engineering, Georgia Institute of Technology

<sup>3</sup> Center for Organic Photonics and Electronics (COPE), School of Chemistry and Biochemistry,  
Georgia Institute of Technology

**ABSTRACT:** One critical aspect for the development of label-free immunosensors is the employment of highly uniform and repeatable antibody immobilization techniques. With the increasing interest in the use of crystalline ZnO for sensor applications, it is useful to make a detailed comparison of antibody immobilization methods. In this study, we compared the use of three different molecules, (3-Glycidyloxypropyl)trimethoxysilane,(GPS), (3-Mercaptopropyl)trimethoxysilane (MTS), and 10-Mercaptodecanylphosphonic acid (MPA) as the primary crosslinkers for the immobilization of



fluorescently labeled IgG antibodies to ZnO surfaces. The modification of ZnO utilizing each primary crosslinker was compared using both an evaporation method and a more conventional wet method in which the samples were immersed in the crosslinker solution for 24 hrs. MTS and MPA coated samples were subsequently reacted with the hetero-bifunctional crosslinker N- $\gamma$ -maleimidobutyryloxy succinimide ester (GMBS) to transform the thiol end-groups into groups that will readily react with amine-terminal residues on an IgG antibody. The chemical modification of the surfaces was investigated using water contact angle measurements and atomic force microscopy. Following incubation with a 200  $\mu$ g/mL solution of Alexa Fluor-labeled IgG antibodies, the samples were imaged using confocal microscopy and analyzed for total antibody surface coverage. The results indicate that the immobilization protocol employing the conventional wet method for deposition of the crosslinkers MPA and GMBS provided a significantly higher surface coverage (14%) than any of the other methods tested. The wet phosphonic acid-based antibody immobilization technique offers the highest uniformity and repeatability of any of the other methods tested and represents a good alternative to silane immobilization methods for ZnO-based biosensors.

**KEYWORDS.** Phosphonic Acids, Organosilane, Antibody Immobilization, ZnO

## INTRODUCTION

Piezoelectric resonators are the base transducer elements of acoustic wave sensors, which operate by maintaining a propagating mechanical elastic wave. Acoustic wave biosensors function by detecting changes in the path over which the propagating wave travels. When a target molecule binds to the biolayer immobilized at the surface of the device, the boundary conditions change as a result of the binding events. This perturbation alters the motion of particles at the surface of the resonating crystal which affects the propagating elastic wave and results in a resonant frequency shift. These devices are often referred to as gravimetric sensors since the sensing mechanism is related to the addition or subtraction of mass. As with most types of biosensors, the ability to obtain repeatable results from an

acoustic sensor is directly related to the repeatability of the biolayer. This molecularly-specific biolayer typically consist of antibodies, RNA/DNA, or enzymes depending on the sensor application. A common example of an acoustic sensor is the quartz crystal microbalance (QCM). Due to their sensitivity to physical perturbation, QCMs have been successfully implemented in a wide variety of sensor systems, including biological sensor systems <sup>1-4</sup>. A requirement for such high precision biosensors is that the output signal, or response, be repeatable given multiple identical samples and on different sensor elements prepared in the same manner. Therefore controlled, reproducible immobilization of appropriate capture molecules to form a molecularly-specific surface on the device is necessary to preclude device to device signal variations.

Recent interest in developing highly sensitive acoustic biosensors for a wide variety of industrial applications has prompted research into the use of piezoelectric materials other than quartz in an effort to circumvent some of the shortcomings of quartz-based devices such as the low electromechanical coupling. The use of zinc oxide (ZnO) has growing interest because it possesses many qualities that make it a good candidate for sensor applications. Primarily, ZnO thin-films can be deposited with excellent c-axis orientation using by RF magnetron sputtering techniques which allows for integration into standard IC fabrication processes. Furthermore, ZnO possesses a relatively strong piezoelectric coupling coefficient of approximately 7-8% and is capable of supporting both longitudinal and thickness shear mode waves <sup>5</sup>, as well as surface acoustic waves <sup>6,7</sup>. The wide bandgap of ZnO further makes this material useful for developing optoelectronic and acousto-optic devices <sup>8,9</sup>. Additionally, ZnO has become a material of interest because of the ability to grow single crystal ZnO nanostructures with a variety of useful properties <sup>10-12</sup>.

Attachment of antibodies to the surface of oxides can be achieved through simple adsorption. However, for biosensor applications, formation of a covalent bond between the antibody and the oxide surface via a chemical crosslinker is the preferred method over adsorption for several reasons. First, the stable bonds that are formed yield a more robust sensor due to the relative strength of covalent bonds. The resulting immobilization of target molecules allows for potentially harsher experimental conditions

and expanded use. Additionally, biosensor experiments often require that the sensor be subjected to fluidic flow. Therefore, covalent immobilization of antibodies is important for preventing detachment of the antibodies from the surface under fluid flow which would erroneously affect the sensor's output signal.

To date, the literature pertaining to functionalizing oxides through covalent methods has largely been focused on SiO<sub>2</sub>. Hydroxyl groups at the surface of an oxide provide sites for reaction with cross-linking molecules to form covalent bonds<sup>13</sup>. One of the more common methods for functionalizing SiO<sub>2</sub> surfaces involves the use of organosilanes. Organosilanes react at room temperature with surface hydroxides to link the silane molecules to the oxide surface. Success with immobilizing antibodies on silica surfaces has been shown using amine- and thiol-terminal silanes such as 3-Mercaptopropyltrimethoxysilane (MTS) with a variety of heterobifunctional crosslinkers including N-γ-maleimidobutyryloxy succinimide ester (GMBS)<sup>13, 14</sup>. Heterobifunctional crosslinkers serve the purpose of transforming the end group of the silane into a group that will bind covalently with functional groups on an antibody. Bhatia *et al.* reported that antibody immobilization with a number of different organosilanes yielded a comparable amount of antibodies immobilized from one silane to the next and that the resulting covalently bound biofilm maintained similar overall antigen binding capacity. They also found that there was minimal loss of antibody function after immobilizing the antibodies to the silica surface<sup>13, 14</sup>.

Other work in modifying SiO<sub>2</sub> surfaces has focused on forming self-assembled monolayers using expoxysilanes<sup>15, 16</sup>. One advantage of using an expoxysilane such as (3-glycidoxypropyl)trimethoxysilane (GPS) for forming self-assembled monolayers (SAMs) on oxide surfaces is that it eliminates the need for a heterobifunctional crosslinker between the silane molecule and target antibodies since the exposed epoxy groups react readily with amine groups on lysine residues of the antibody. The usefulness of this antibody immobilization technique has been illustrated on indium-tin oxide (ITO) substrates for the development of *Escherichia coli* O157:H7 sensors<sup>17, 18</sup>. However, one of the problems with modifying surface oxides using organosilanes is that the quality of

surface modification is sensitive to the amount of water present during the modification reaction<sup>19</sup>. In anhydrous conditions, a partial monolayer of organosilane molecules forms resulting in incomplete coverage of the substrate. In excess H<sub>2</sub>O, self-condensation can occur between the silane molecules and a multilayer can form, often accompanied by gelling of the silane. An alternative to organosilanes for surface modification of oxides is the use of phosphonic acids. Phosphonic acids do not suffer from the same susceptibility to hydration levels that organosilanes do and do not easily self-condense. They have been used for the functionalization of ITO electrodes for development of electrochemical sensors<sup>20</sup> and for modifying TiO<sub>2</sub>, BaTiO<sub>3</sub>, and ZnO particles<sup>21-23</sup>. In another study, phosphonic acids were used to pattern ITO and Indium Zinc Oxide (IZnO) through microcontact printing and subsequent wet etching<sup>24</sup>.

Despite the amount of research that has been performed on various oxides, including SiO<sub>2</sub>, there have been relatively few studies involving surface functionalization of ZnO. One such study reports the use of an amine-terminated silane, 3-aminopropyltriethoxysilane (APS) and glutaraldehyde as a crosslinker to bind a protein, Interleukin-6, to the ZnO surface<sup>25</sup>. One drawback to the use of glutaraldehyde, however, is that it is known to form large polymers which may bind many residues and form multiprotein complexes. Studies by Thomsen and Watts *et al.* highlight issues to consider regarding the adsorption of amine-terminated silanes to oxidized Zn sheet surfaces (as opposed to deposited crystalline ZnO)<sup>26, 27</sup>. It is shown that the degree to which each moiety of the SAM (the silane or the amine) binds to the ZnO surface is largely dependent upon the pH of the solution. A molecular dynamics study confirms that silane molecules with polar head groups, such as amines, prefer a more stable conformation parallel to the surface rather than aligned perpendicular to the surface<sup>28</sup>. These studies tend to indicate that amine-terminated silanes may not be the optimal surface treatments when further conjugation steps such as linking antibodies to the surface are required.

Apart from surface treatment with silanes, there have been very few other reports of surface modification studies performed on ZnO. In a study by Sadik *et al.*, adsorption of alkane-thiols to Zn and O terminated ZnO surfaces to form SAMs was investigated, but the study did not involve further functionalization with antibodies or any other type of protein<sup>29</sup>. Other studies have described methods

for functionalizing ZnO nanostructures, however they are of limited use for translation to planar ZnO surface chemistry because of the morphological and crystalline differences between RF sputtered ZnO surfaces and single crystal nano-structures. In a study by Liu *et al.*, ZnO nanorods were functionalized using dimercaptosuccinic acid followed by EDC to bind amine groups located on the antibody <sup>30</sup>. Another study outlined the use of a pH 5 solution of 11-triethoxysilylundecanal to coat ZnO nanoparticles leaving an amine-reactive aldehyde group for subsequent conjugation with antibodies <sup>31</sup>.

The focus of this study is to provide a comparison between antibody immobilization protocols on device-quality sputtered ZnO surfaces with three different primary crosslinking molecules. The results will provide a foundation for further research in developing highly uniform antibody immobilization protocols for planar ZnO surfaces. MTS, GPS and 10-Mercaptodecanylphosphonic Acid (MPA) were deposited onto the ZnO surface using both a conventional wet method and an evaporation method. Subsequent secondary crosslinking with GMBS was performed for ZnO surfaces coated with MTS and MPA. To provide visual confirmation of the density and uniformity of antibody immobilization, fluorescently labeled antibodies were incubated with the surface. The results were investigated using water contact angle measurements, atomic force microscopy, and confocal microscopy.

## METHODS

### ZnO Preparation

ZnO samples were prepared by depositing 500 nm of ZnO onto 3" (100) silicon wafers (University Wafer) by RF magnetron sputtering using the Unifilm PVD-300 sputtering system. We have previously reported X-ray diffraction (XRD) measurements of the sputtered ZnO films which indicate a strong (0 0 2) ZnO hexagonal *6mm* crystal orientation <sup>5</sup>. The wafers were diced into 1 cm by 1 cm squares for surface functionalization experiments. Prior to surface functionalization, the ZnO samples were sonicated in acetone for 5 minutes in an ultrasonic bath before being cleaned using an ion beam mill. The samples were etched in a 20% oxygen / 80% argon atmosphere for 5.5 minutes. This was done

to remove any adsorbed chemical species from the surface and to provide a reactive surface for the primary crosslinker to bind.

### Crosslinking Solution Preparation

The three primary crosslinker solutions for treating the ZnO samples were prepared under a nitrogen atmosphere: a 4% solution by volume of MTS (Fluka) in dry toluene (Sigma); a 4% solution of GPS (Sigma) in dry toluene; and a 1 mM solution of MPA in 95% ethanol (Sigma). MPA was synthesized in accordance with the procedures from the literature<sup>32</sup>.

### Antibody Immobilization Procedure

#### *Wet Method*

Immediately following the ion etching procedure to clean the ZnO surface, samples were placed in vials containing 2 mL of either the silane or phosphonic acid solution, sealed, and placed in a nitrogen environment for 24 hours. The samples were then removed from the vials and rinsed with ethanol followed by sonication for 5 minutes in ethanol. The samples were then dried with a stream of N<sub>2</sub>. At this point, water contact angle measurements and AFM scans were performed. Samples treated with either the 4% MTS or the 1 mM MPA were then placed in vials containing 2 mL of 2 mM GMBS (Fluka) in ethanol and sealed for 24 hours. The GPS-treated samples do not require treatment with a secondary crosslinker because the terminal epoxy groups react directly with the antibody. Following sonication in ethanol, GPS coated samples were immediately treated with the antibody solution as described below. Following GMBS treatment, the MTS and MPA coated samples were removed from the solution and sonicated in ethanol for 5 minutes. The activated ZnO surfaces were then used for covalent attachment of antibodies.

#### *Evaporation Method*

Following the ion etching of the ZnO samples, the devices were immediately placed in vials containing 2 mL of the respective primary crosslinker solutions. They were then transferred to a nitrogen glove box where they were placed in aluminum weighing dishes covered by 2 mL of the crosslinking solution. The solutions were left to evaporate overnight. Following the complete evaporation of the solutions, the dies were rinsed and sonicated in ethanol for at least 5 minutes. MTS and MPA-treated devices were then placed again in weighing dishes with 2 mL of the 2 mM GMBS solution and allowed to evaporate overnight. Following the complete evaporation of the solution, the dies were again rinsed with ethanol and sonicated in ethanol for 5 minutes. The activated surfaces were then used for covalent attachment of antibodies.

#### *Covalent Antibody Attachment*

The activated surfaces were treated with 548 nm Alexa-Fluor labeled Goat anti-rabbit IgG antibodies (Invitrogen). 20  $\mu$ L of a 200  $\mu$ g/mL solution of the fluorescently labeled antibodies in PBS buffer (pH 7.4) was pipetted onto the surface of the samples. The antibody solution was incubated for 3 hours in a nitrogen environment at room temperature, after which the substrate was rinsed with aliquots of PBS buffer followed by ultra-pure water to remove any unbound antibodies from the surface. At no point was the antibody solution allowed to evaporate during the antibody reaction protocol.

#### Water Contact Angle Measurements

Water contact angle measurements were performed using an SEO Phoenix 150 Contact Angle Analyzer. The contact angles for each of the 3 surface treatments were evaluated by averaging the contact angles from at least five separate measurements for each surface treatment following reaction with the primary crosslinker. Silane and phosphonic acid-coated samples were measured and compared to a control sample consisting of ZnO with no surface treatments other than ion etching to clean the surface of any adsorbed species and sonication in ethanol to simulate the rinse process. The

measurements were used as a semi-quantitative method of determining the film quality and reproducibility as well as to confirm that the surface was being chemically modified.

### AFM Measurements

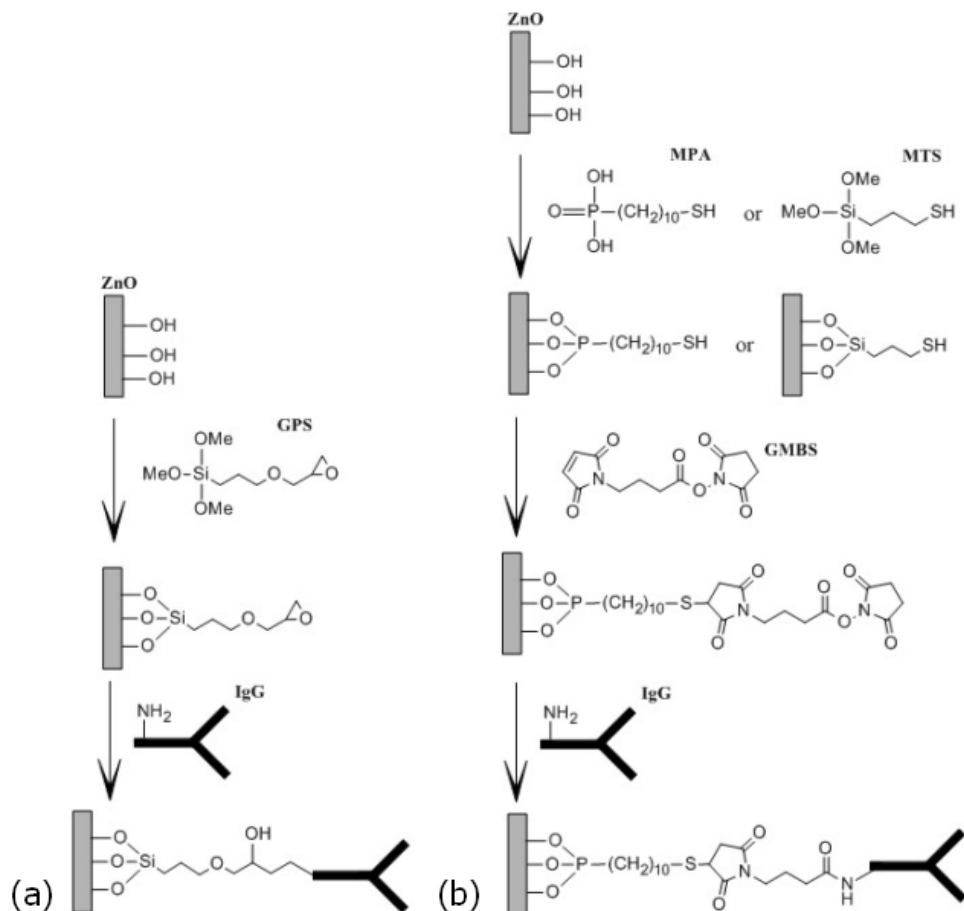
Samples were measured after treatment with the primary crosslinker and again after treatment with the secondary crosslinker (in the case of MTS and MPA treated samples) using a Digital Instruments (DI) 3000 AFM in tapping mode. Separate samples were prepared for each test, meaning that the surface chemistry steps were not interrupted by measurements since this would disrupt the environment-sensitive protocol. That is to say, the surface chemistry protocol was performed on each sample, step-wise and uninterrupted, up to the point of measurement. After each measurement, samples were subsequently discarded. AFM probe tips were obtained from Veeco Instruments (FESP). Multiple scans of each sample were taken to ensure uniformity in the measurements across each  $1\text{ cm} \times 1\text{ cm}$  sample. The scans were evaluated for surface roughness and overall average particle height and diameter using the DI Nanoscope software. Both  $5\text{ }\mu\text{m} \times 5\text{ }\mu\text{m}$  and  $1\text{ }\mu\text{m} \times 1\text{ }\mu\text{m}$  scans were taken at each location on all samples and used for the calculation of the surface morphology metrics. For AFM data collected on samples prepared from different ZnO wafers, control scans were performed on untreated ZnO samples from each wafer. This is a requirement because overall ZnO grain sizes and heights can vary from wafer to wafer undergoing separate ZnO depositions, despite being uniform across a single wafer.

### Confocal Microscopy

Following the antibody conjugation reaction, the devices were dried with a stream of  $\text{N}_2$  and fixed to a glass slide in preparation for confocal microscopy analysis. A Zeiss Laser Scanning Microscope (LSM) 510 microscope with a HeNe laser (543 nm excitation) was used to visualize the fluorescently labeled antibodies. Each sample was viewed at  $10\times$  magnification and  $1\text{ mm} \times 1\text{ mm}$  images were taken at random locations throughout the area of antibody deposition. The images were analyzed using software written in MATLAB to estimate the overall antibody coverage. The algorithm uses a thresholding



technique to include all pixels containing a fluorescence value above that of 30 - 50% of the peak value. The actual thresholding level was determined separately for each image depending on the background fluorescence in the image because it is desirable for the thresholding algorithm to include fluorescence due to immobilized antibodies while discarding less significant fluorescence due to background noise.



**Scheme 1.** The immobilization procedure for covalent attachment of IgG antibodies to the ZnO surface by the three primary crosslinkers. The hydroxylized ZnO surface is treated with (a) (3-glycidypropyl)trimethoxysilane, (b) 10-Mercaptodecanylphosphonic acid or (3-Mercaptopropyl)trimethoxysilane followed by the secondary crosslinker N- $\gamma$ -maleimidobutyryloxy succinimide ester.

## RESULTS & DISCUSSION

A summary of the reactions for covalently attaching antibodies to the ZnO surface is shown in Scheme 1. The deposition of the silanes and phosphonic acid are achieved through reaction of the head groups with hydroxyl groups at the ZnO surface. Regarding the MTS and MPA reactions (Scheme 1(b)), the thiol group on the MTS and MPA molecules react with the maleimide region of the secondary crosslinker GMBS in organic solvent. This reaction leaves the succinimide residue of the GMBS available for antibody attachment. The succinimide residue then binds to an available amino group of the antibody to form a covalent bond between the antibody and the ZnO surface. It is important to note, however, that targeting amine-groups on the antibodies does not promote any specific orientation of the antibodies since amine-containing residues such as lysine can be located on many parts of the antibody. Despite this, it has been shown that antibodies immobilized using this approach still maintain a significant amount of activity, albeit less than with oriented immobilization techniques such as those that target the carbohydrate group on the F<sub>c</sub> region of the IgG antibody<sup>14</sup>. Additionally, the ease and simplicity of the immobilization protocols studied here make them more suitable for biosensor applications than oriented immobilization techniques which often require numerous steps, harsh experimental conditions, and high antibody losses prior to immobilization.

### Water Contact Measurements

The results from the water contact angle (WCA) measurements after the samples were coated with the primary crosslinkers MTS, GPS, and MPA are provided in Table 1. The data shows that the average WCA for each of the crosslinkers deposited with both the wet and evaporation methods were greater than the WCA of the control, indicating an increase in surface hydrophobicity. Samples coated with MTS using the wet method exhibited drastically different results from the non-treated case. The WCA is on average about 5 degrees higher (77°) than the control (72°). The evaporated MTS sample similarly shows a difference in the WCA, however it is much more pronounced than its liquid-phase counterpart. Samples coated with MTS using the evaporation method were found to exhibit a much more hydrophobic surface. The difference could be explained by higher surface coverage by the evaporated

MTS over the liquid deposited MTS. Alternatively, it could be explained by the fact that the MTS is forming a monolayer or near-monolayer in one case, but not in the other.

**Table 1.** Water Contact Angle Measurements for Surface Treatments

Surface Treatment	Avg. WC Angle (degrees)
Untreated ZnO	$72 \pm 2$
GPS (wet)	$80 \pm 5$
GPS (evap)	$78 \pm 9$
MTS (wet)	$77 \pm 1$
MTS (evap)	$85 \pm 3$
MPA (wet)	$83 \pm 5$
MPA (evap)	$77 \pm 1$

The WCA measurements performed with the 4% GPS solutions also suggest that the surface is being chemically modified. The samples coated with GPS using the wet method yielded a significant increase in average WCA of 80°. Samples where the GPS solution was deposited through evaporation only yielded an average WCA of 78°, which is only slightly higher than the control case and exhibited the highest variation among the measurements. An interesting phenomenon was observed for samples coated with GPS by either method, however. Immediately after the water droplet is placed onto the sample surface, it was observed that the WCA is much higher than the control case indicating that the surface is hydrophobic. However, the WCA changes as a function of time in a manner that seems to be unrelated to evaporation phenomena. The WCA values reported in the Table 1 are the values taken immediately the drop was placed on the surface. Over the time period of 20 to 30 seconds the water contact angle is reduced anywhere by about 5-7 degrees and then stabilizes. This phenomenon was only observed on samples treated with the GPS solution and was not observed for either of the protocols

performed with MTS or MPA. Water droplets on ZnO surfaces treated with MTS or MPA formed stable water droplets with WCA that changed very little, if at all, over a 30 second time period. This potentially points to an unstable surface with the GPS film that is disrupted by H<sub>2</sub>O. One possible explanation for this phenomenon is that the water droplets react with the exposed epoxy groups, hydrolyzing the ring to form surface hydroxyl groups which would result in a more hydrophilic surface. Due to the relative smoothness of the GPS surface as indicated by AFM measurements, it is unlikely that this phenomenon is due to surface roughness.

The WCA data for the MPA treated samples confirms that the surface is undergoing a chemical change. Similar to the samples treated with GPS, the samples treated with MPA using the wet method exhibit a WCA on average to be approximately 83°. Samples treated with the evaporation protocol exhibited a lower WCA of, on average, 77° which is still roughly 5° greater than the control. This indicates that in both cases, the surface has become more hydrophobic and implies that the surface is being modified with the chemical treatment. The same conclusion can be drawn for the GPS and MTS surface treatments as well. The contact angle results for surfaces coated with MPA and MTS seem to agree well with previous WCA investigations of dithiol self-assembled monolayers on gold which were reported to be approximately 83.5° on average<sup>33</sup>. Further investigation of the surface morphology using atomic force microscope measurements were performed to more thoroughly assess the surfaces following each of these treatments.

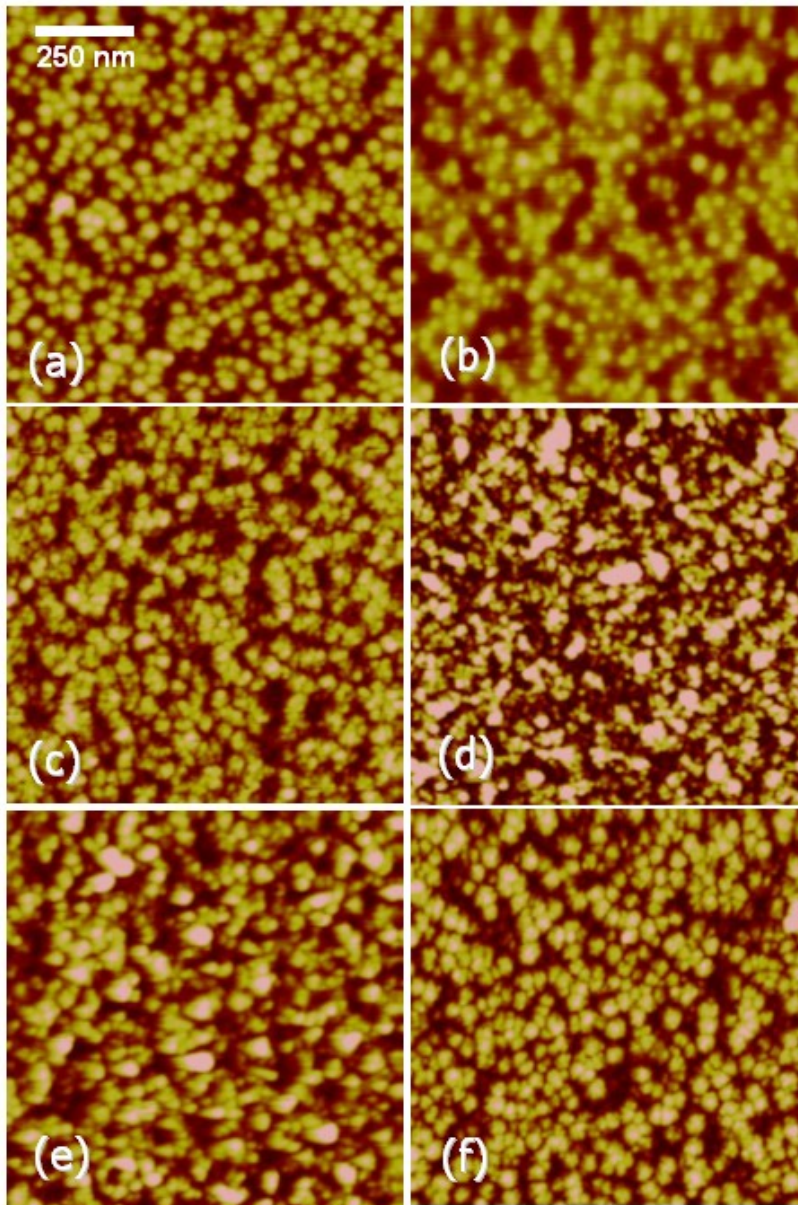


**Figure 2.** Atomic Force Microscope topographical scans of (a) the untreated ZnO surface and samples treated with the wet method for deposition of (b) GPS, (c) MTS (d) MTS+GMBS, (e) MPA, and (f) MPA+GMBS. The scan sizes are  $1\ \mu\text{m} \times 1\ \mu\text{m}$  with a vertical scale of 15.0 nm. The bright parts correspond to higher features while the dark parts correspond to lower features.

### AFM Measurements

#### *Wet Method*

AFM was also used to probe the change in surface morphology after each of the relative surface treatments. This was required to differentiate whether monolayers are being formed, or if large conglomerates of crosslinker are forming at the surface. AFM measurements are especially useful for monitoring the morphological changes at the surface that result from reaction of the primary crosslinker with the GMBS for surfaces treated with MTS and MPA. Figure 2 shows representative AFM scans for each surface after treatment using wet protocols. Figure 2(a) reveals the characteristic cobblestone appearance of the surface of the un-treated control ZnO sample, with round grains that have fairly well defined boundaries. Table 2 shows the mean surface roughness, mean particle height and mean particle diameter for each of the liquid-phase surface treatments. For the control case, the mean surface roughness is approximately  $2.2 (\pm 0.1)$  nm while the particle heights and diameters are  $2.8 (\pm 0.4)$  nm and  $43.4 (\pm 4.6)$  nm, respectively. The scan of the surface after liquid-phase GPS treatment in Figure 2(b) shows a surface that is morphologically different from that of the controlled case, with surface roughness decreasing on average by 33%. This implies an overall smoothening of the surface which is similarly suggested by the appearance of the scan. One likely explanation is that the GPS molecules have been deposited into the gaps in-between the grains to fill some of the grain boundaries. The result could be observed at many locations across the sample, and was repeatable after many re-scans of the same area with no variation in the result.

**Table 2.** AFM Surface Analysis for Wet Method Surface Treatments

Surface Treatment	Roughness (nm)	Avg. Particle Height (nm)	Avg. Particle Diameter (nm)
Untreated ZnO	$2.2 \pm 0.1$	$2.8 \pm 0.4$	$43.4 \pm 4.6$
GPS	$1.5 \pm 0.4$	$2.9 \pm 0.6$	$54.3 \pm 5.9$
MTS	$2.4 \pm 0.1$	$3.0 \pm 0.4$	$43.8 \pm 7.1$
MTS + GMBS	$4.3 \pm 0.1$	$6.6 \pm 0.9$	$40.8 \pm 3.0$
MPA	$3.1 \pm 0.2$	$4.4 \pm 0.1$	$45.5 \pm 4.2$
MPA + GMBS	$2.8 \pm 0.1$	$3.5 \pm 0.1$	$49.8 \pm 5.9$

The AFM scans of the samples treated with MTS in Figure 2(c) and MTS+GMBS in Figure 2(d) show significant differences in the surface morphology as compared to the GPS. Rather than a decrease in surface roughness, we see a slight increase in surface roughness with the MTS treated sample and a much larger roughness increase in the samples treated with MTS+GMBS. The average particle height for the MTS+GMBS treated samples was increased to  $6.6 (\pm 0.9)$  nm indicating an increase in particle size due to deposition of the crosslinker GMBS. Visually, the AFM plots support these statistics. Figure 2(c) resembles the control case, but with grains that are not as well defined or uniform in shape and size as the control case. Many of the typically smooth grains are now slightly enlarged with more surface details which add to the overall surface roughness. Figure 2(d) clearly shows the subsequent treatment with GMBS yields particles on the surface that have a larger average height than in the control case. The data from these scans along with the WCA measurements provides confidence that the surface is being chemically modified and that it is different from the control case both before and after treatment with the GMBS. Further, the surface morphology data in particular suggests that the GMBS is forming polymerized clumps.

Representative AFM scans of the samples treated with MPA and MPA+GMBS are shown in Figures 2(e) and 2(f), respectively. The surface in Figure 2(e) indicates an increase both in overall surface roughness and particle height. These notions are supported by the average calculated roughness of  $3.1 (\pm 0.2)$  nm, which is approximately 38% greater than the control case, and the increased average particle height of  $4.4 (\pm 0.1)$  nm. The surface scans of the samples treated with MPA followed by GMBS, however, indicate an overall decrease in surface roughness and particle height from that of the MPA-only treated samples. This is unexpected, given the evidence of increasing roughness and overall particle size for the MTS+GMBS samples. The water contact angles confirm that the surface is seemingly being modified prior to the GMBS treatment, however, and the overall surface metrics are still statistically different from the control case. One explanation is that the GMBS treatment is forming a more uniform coating on the surface of MPA rather than forming clumps as may be the result in the MTS+GMBS scans.



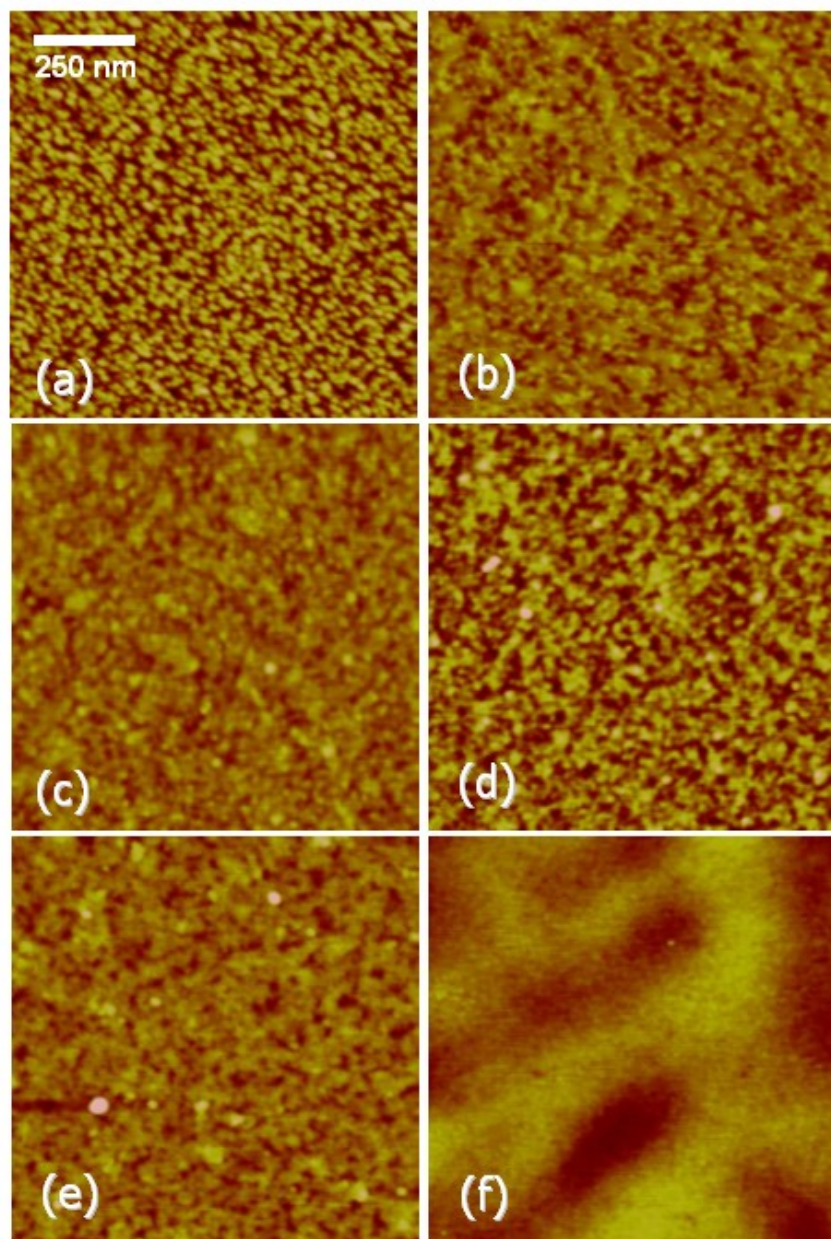


**Figure 3.** Atomic Force Microscope topographical scans of (a) the untreated ZnO surface and samples treated with the evaporation deposition of (b) GPS, (c) MTS (d) MTS+GMBS, (e) MPA, and (f) MPA+GMBS. The scans sizes are  $1\ \mu\text{m} \times 1\ \mu\text{m}$  with a vertical scale of 15.0 nm. The bright parts correspond to higher features while the dark parts correspond to lower features.

**Table 3.** AFM Surface Analysis for Evaporation Method Surface Treatments

Surface Treatment	Roughness (nm)	Avg. Particle Height (nm)	Avg. Particle Diameter (nm)
-------------------	----------------	---------------------------	-----------------------------



Untreated ZnO	$1.5 \pm 0.2$	$1.7 \pm 0.3$	$29.8 \pm 1.6$
GPS	$1.0 \pm 0.1$	$0.9 \pm 0.1$	$32.1 \pm 1.8$
MTS	$0.8 \pm 0.1$	$1.3 \pm 0.2$	$29.2 \pm 2.4$
MTS + GMBS	$1.3 \pm 0.3$	$1.5 \pm 0.7$	$31.8 \pm 1.9$
MPA	$0.9 \pm 0.3$	$0.8 \pm 0.2$	$17.5 \pm 9.0$
MPA + GMBS	$1.5 \pm 0.6$	$0.6 \pm 0.2$	$20.0 \pm 2.3$

### *Evaporation Method*

The AFM measurements of samples undergoing evaporation deposition of the primary and secondary crosslinkers are shown in Figure 3. Since ZnO samples were taken from a different wafer than the samples used in the wet method AFM study, untreated ZnO control samples from this wafer were measured to establish a new baseline from which to compare the rest of the treated samples. A representative scan shown in Figure 3(a) indicates that the surface has similar characteristic well-defined grains, though decidedly smaller, as compared to Figure 3(a). The statistics from the scans are provided in Table 3. The roughness of the untreated ZnO surface is on the order of  $1.5 (\pm 0.2)$  nm and the average particle height is  $1.7 (\pm 0.3)$  nm. Figure 3(b) shows a scan of a sample that was prepared through evaporation deposition of the GPS solution. Visual inspection indicates that the sample shows an overall loss of strong grain boundary definition. This implies that the areas in-between the grains are being coated with GPS molecules. The average surface roughness is measured to be approximately  $1.0 (\pm 0.1)$  nm which supports this visual evidence that the grain boundaries are more poorly defined and that the surface is smoother overall following the deposition of GPS. Coupled with the slight increase in WCA observed with GPS coated samples, it is possible to conclude that the surface is undergoing both chemical and morphological changes as a result of crosslinker deposition. Further analysis with fluorescent antibodies will show if the resulting surface is functionally useful for antibody immobilization.

The samples coated with both MTS and MTS+GMBS by evaporation deposition also exhibit morphological differences from the control case. Figure 3(c) shows the ZnO sample coated with MTS only. The morphology looks similar to the GPS-coated samples with an overall loss of grain-boundary definition and a smoother surface. The surface roughness on average is reduced by 48% and the average particle height is also reduced from the control case by approximately 25%. Following the deposition of GMBS, the surface roughness increased by about 60% and the particle height increased by approximately 23%.  $5\text{ }\mu\text{m} \times 5\text{ }\mu\text{m}$  AFM scans of the evaporation coated MTS+GMBS samples as well as visual inspection under a microscope revealed the presence of larger round particles ( $\sim 200$  to  $1,000\text{ nm}$ ) deposited intermittently across the surface. This heterogeneity is undesirable for antibody immobilization procedures because it detracts from the uniformity of the crosslinking layers and can result in inconsistent antibody surface coverage.

Perhaps the most drastic morphological changes resulting from treatment of the ZnO samples with any crosslinker were observed after evaporation deposition of the MPA crosslinker followed by GMBS. Figure 3(f) depicts a surface coating that seems to cover the underlying ZnO grains completely resulting in a non-uniform amorphous film. The overall surface roughness of the scan shown in Figure 3(f) is fairly low ( $\sim 1.0\text{ nm}$ ), but the average surface roughness calculated over multiple scans is very similar to the untreated control case primarily because larger scans indicate a more heterogeneous surface containing larger conglomerates of molecules. The heterogeneity of this surface, as with the MTS+GMBS surface, is not conducive to repeatable and uniform immobilization of antibodies. Another issue with the evaporation method that was most apparent with the MTS+GMBS and MPA+GMBS samples is the issue of recrystallization at the ZnO surface. During the evaporation process, recrystallization of the crosslinker can yield a visible film on the sample surface. Since this film is neither a monolayer, nor uniform, it must be removed through sonication. Even with thorough washing steps, this recrystallized layer often proved difficult to remove and therefore yielded fewer samples that could be reasonably tested. An optically thick and non-uniform film like this is extremely undesirable

for use with acoustic sensors because the added amorphous mass on the surface of the device can dampen the acoustic signal which results in a loss of sensitivity.

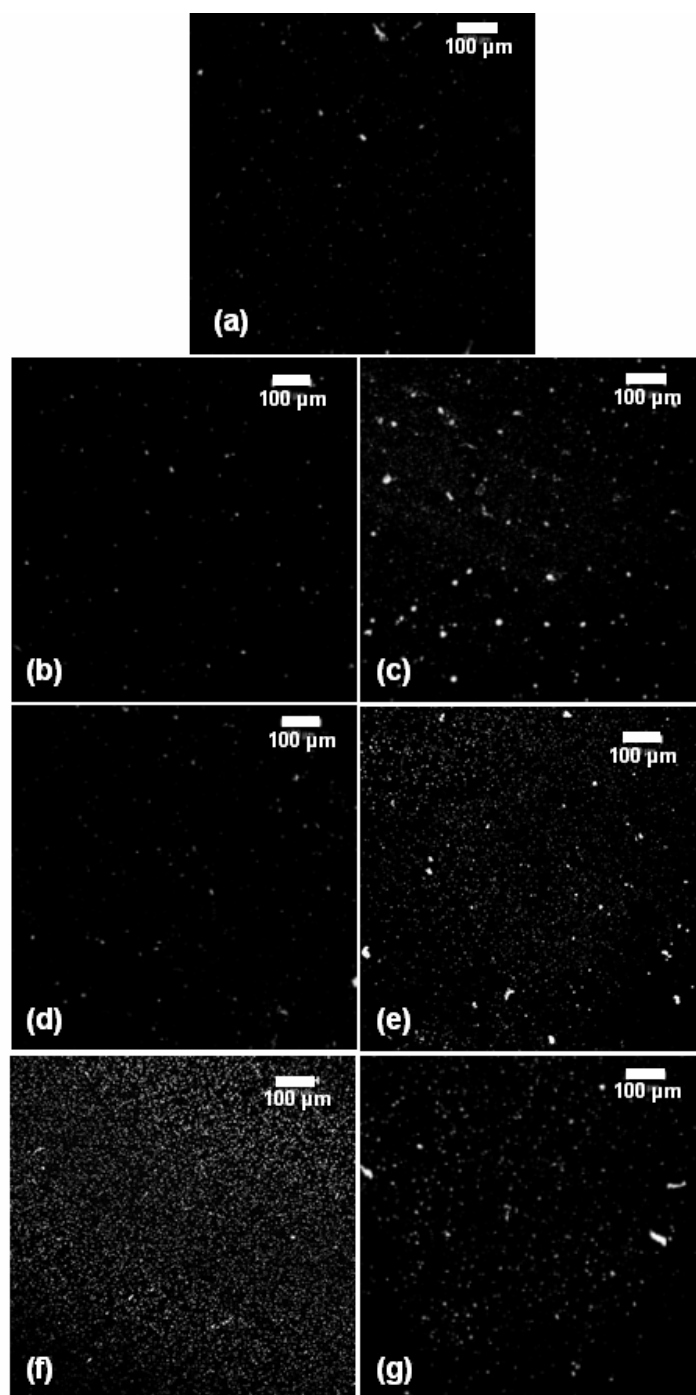


**Figure 4.** Contrast-enhanced fluorescence microscope images of surfaces after immobilization of Alexa-Fluor labeled IgG antibodies. (a) The untreated ZnO surface with passive antibody adsorption (b) Liquid-phase GPS with Abs (c) Evaporated GPS with Abs (d) Liquid-phase MTS+GMBS with Abs (e) Evaporated MTS+GMBS with Abs (f) Liquid-phase MPA+GMBS with Abs, and (g) Evaporated

MPA+GMBS with Abs. The bright spots correspond to areas of high fluorescent signal which is indicative of antibody binding.

### Antibody Surface Coverage

The results of the water contact angle and AFM measurements indicate that the ZnO surfaces are being modified by each of the crosslinkers for both the wet and evaporation deposition methods. However, the main goal of this study is to characterize the spatial distribution of covalently bound antibodies on the surface of the ZnO. Prior studies characterizing antibody immobilization techniques have generated a variety of methods for analyzing the amount of antibodies bound to the surface of a material<sup>13, 14, 18</sup>. As acoustic biosensors become increasingly more compact, the antibody immobilization surface coverage becomes increasingly more important. If the antibody coverage on the sensor is insufficient, a small biosensor may be unable to “sense” the event of antigen binding even if the target molecule is present in a high concentration in the sample under test. It is necessary to compare the surface treatments quantitatively, which is demonstrated in this study through an analysis of the fluorescence. It is also important, however, to determine exactly where the antibodies are deposited and how uniform the surface coverage is from one location on the sample to the next. Figure 4 illustrates representative images for each of the surface treatment methods after 3 hours of incubation with Alexa Fluor-labeled IgG antibodies. The images have been contrast enhanced to decrease the level of background fluorescence and improve the visibility of the fluorescence due to the presence of antibodies. The fluorescence depicted in the images should only be interpreted as a representation of the “apparent” antibody coverage for each of the tested cases. The thresholding method, which only counts pixels from the image with fluorescent signals above a percentage of the peak fluorescence, may exclude antibodies in which the fluorescence signal is too low to be considered above the background. This would lead to a lower estimated surface coverage than the actual value. Imaging the surface at higher magnification, however, did not indicate the presence of any antibody signals that were not visible at the 10× setting.

As a result, it is believed that this method is sufficient for comparing the apparent surface coverage for each of the immobilization methods. Figure 4(a) depicts an untreated ZnO surface that has been exposed to antibodies. The presence of fluorescence in the image is due to simple adsorption of antibodies to the surface. The surface coverage by antibodies was calculated to be approximately 0.90% of the total ZnO surface area. As can easily be seen from Figure 4(a), the surface coverage is fairly low. This is insufficient for uniform and repeatable biosensor immobilization. Figure 5 shows a comparison of the average surface coverage by each of the 7 immobilization methods. For MTS and GPS, the evaporation methods tended to result in higher overall surface coverage than the liquid-phase immobilization methods. The liquid-phase GPS and MTS procedures were shown to statistically perform even worse than immobilization through simple adsorption to the ZnO surface. The MPA liquid-phase method shown in Figure 4(f), however, resulted in the highest surface coverage of all methods tested with an average coverage of 14% of the total area. Upon visual inspection, the resulting antibody layer is both more dense and more uniform than the other methods. It must be noted that the area in the lower-left corner of Figure 4(f) in which an absence of fluorescence can be observed is due to an inability of the microscope to focus on the entire  $1\text{ mm} \times 1\text{ mm}$  area of that image. When brought into focus, this area shows the same surface coverage and density as the rest of the image. An important point that should not be overlooked is that the spatial distribution of the antibodies is fairly uniform and relatively dense. This is critical for the development of sensors because spotty or incomplete surface coverage can result in poor sensor performance. Due to the lack of studies in the literature employing a similar analysis method, it is difficult to compare the surface coverage value (14%) to those obtained in prior work. However, based on our own experience, the surface coverage obtained here is sufficient for use with most acoustic sensors given the distribution of the antibodies. The fluorescence microscopy technique used for evaluating antibody surface coverage allows for visualization of the exact locations of the antibodies. Other techniques that have been used for calculating antibody coverage including scintillation counting of radiolabeled antibodies may give quantitative values, however at the expense of information about the distribution of those antibodies.

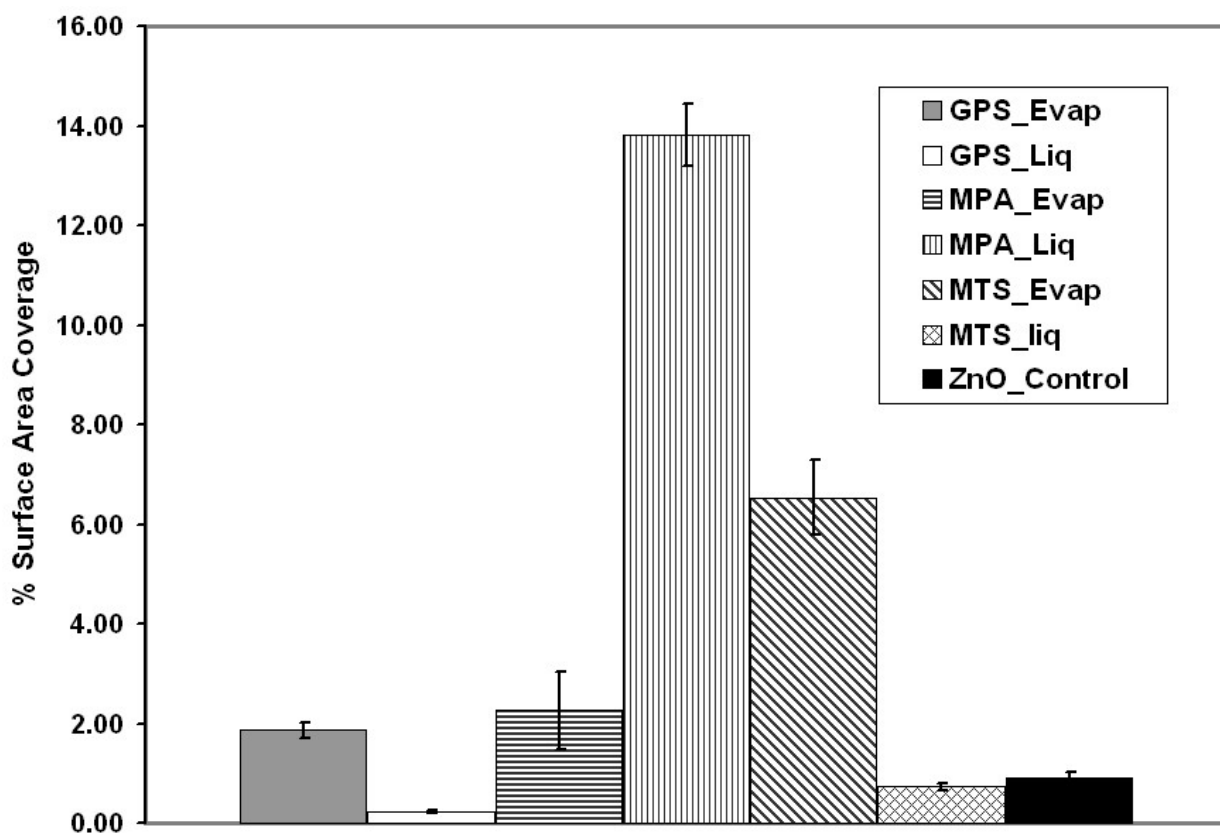


**Figure 5.** Plot of the average fluorescent antibody coverage for each of the antibody immobilization procedures. The values were calculated based on image analysis performed on confocal fluorescence images of the surfaces resulting from treatment with fluorescent antibodies. (Error Bars = Std. Error)

It is fortunate that the phosphonic acid deposited using the wet method resulted in the highest surface coverage, given the recrystallization issues associated with the evaporation method. This method of immobilization is easy to perform, and can be carried out in less than 72 hours. There is essentially 100% yield associated with this technique because the liquid-phase deposition does not run the risk of recrystallization of the crosslinker molecules. Proper functionalization of biosensors requires that the surface chemistry be as simple and repeatable as possible while offering a high yield. Further work should be completed to investigate the optimal reaction times which may produce higher surface coverage and uniformity than is presented here.

## CONCLUSIONS

We have provided a comparison of two antibody immobilization techniques using three different primary crosslinkers on planar ZnO surfaces. The surfaces were analyzed using water contact angle measurements, atomic force microscopy, and fluorescence microscopy to determine the surface characteristics and overall antibody surface coverage. We have achieved relatively high antibody coverage on the ZnO surface through the use of a thiol-terminated phosphonic acid with GMBS as the secondary crosslinker. Crystalline ZnO samples coated with IgG antibodies using MPA+GMBS showed the highest overall surface coverage of 14% as compared to 0.9% with the passive adsorption method. This is the first study detailing the use of a phosphonic acid for functionalizing ZnO surfaces and comparing the use of multiple crosslinkers for immobilizing antibodies onto ZnO. The primary advantage of using phosphonic acids over silanes lies in the stability of the chemical surface coating to hydration levels. This is important for biosensor applications, where an ideal antibody immobilization technique would be unaffected by varying hydration levels in biological samples under test. However, it has been demonstrated in the past with alkane-thiol SAMs that as the chain length decreases, the monolayer becomes increasingly disordered with lower packing density and coverage<sup>34</sup>. Since the MPA chain length is longer than those of MTS and GPS, improved surface coverage obtained with MPA may, in part, be attributed to this difference.

This study is offered as an initial study for immobilization of antibodies on planar ZnO surfaces. Functionalization of crystalline ZnO surfaces is becoming an increasingly important topic as new biosensor platforms are being developed with this material and current investigations are underway for studying the formation and properties of phosphonic acid coatings on ZnO. Further work should build upon the studies detailed here for improving the density and uniformity of covalent antibody immobilization procedures. It is concluded that phosphonic acids, such as MPA, offer a promising alternative to conventional silanization methods for the controlled immobilization of IgG antibodies.

**ACKNOWLEDGMENTS** This work was supported by the Georgia Tech/Emory Fund for Innovative Cancer Technologies which derives its fund from the V Foundation and the Georgia Cancer Coalition. It is also supported by the Office of Naval Research. Chris Corso is supported by a NSF Graduate Research Fellowship, and Anthony Dickherber is supported by the Congressionally Directed Medical Research Prostate Cancer Training Program. The authors thank Debin Wang for his assistance with making water contact angle measurements.

1. Rosler, S.; Lucklum, R.; Borngraber, R.; Hartmann, J.; Hauptmann, P., Sensor system for the detection of organic pollutants in water by thickness shear mode resonators. *Sensors and Actuators B (Chemical)* **1998**, B48, 415-24.
2. Pascal-Delannoy, F.; Sorli, B.; Boyer, A., Quartz crystal microbalance (QCM) used as humidity sensor. *Sensors and Actuators A (Physical)* **2000**, A84, (3), 285-91.
3. Cao, L.; Zhou, X. C.; Li, S. F. Y., Enantioselective sensor based on microgravimetric quartz crystal microbalance with molecularly imprinted polymer film. *Analyst* **2001**, 126, (2), 184-188.
4. Zhou, X. C.; Huang, L. Q.; Li, S. F. Y., Microgravimetric DNA sensor based on quartz crystal microbalance: comparison of oligonucleotide immobilization methods and the application in genetic diagnosis. *Biosensors & Bioelectronics* **2001**, 16, (1-2), 85-95.
5. Corso, C. D.; Dickherber, A.; Hunt, W. D., Lateral field excitation of thickness shear mode waves in a thin film ZnO solidly mounted resonator. *Journal of Applied Physics* **2007**, 101, (5), 54514-1.
6. Yamazaki, O.; Mitsuyu, T.; Wasa, K., ZnO thin-film SAW devices. *IEEE Transactions on Sonics and Ultrasonics* **1980**, SU-27, (6), 369-79.
7. Fernandez, M. J.; Fontecha, J. L.; Sayago, I.; Aleixandre, M.; Lozano, J.; Gutierrez, J.; Gracia, I.; Cane, C.; del Carmen Horrillo, M., Discrimination of volatile compounds through an electronic nose based on ZnO SAW sensors. *Sensors & Actuators: B. Chemical* **2007**, 127, (1), 277-83.
8. Ozgur, U.; Ya, I. A.; Liu, C.; Teke, A.; Reshchikov, M. A.; Dogan, S.; Avrutin, V.; Cho, S. J.; Morkoc, H., A comprehensive review of ZnO materials and devices. *Journal of Applied Physics* **2005**, 98, (4), 041301.
9. Koch, M. H.; Janos, M.; Lamb, R. N.; Sceats, M. G.; Minasian, R. A., All-fiber acoustooptic phase modulators using chemical vapor deposition zinc oxide films. *Lightwave Technology, Journal of* **1998**, 16, (3), 472-476.
10. Hughes, W. L.; Wang, Z. L., Formation of piezoelectric single-crystal nanorings and nanobows. *J Am Chem Soc* **2004**, 126, (21), 6703-9.
11. Nie, L.; Gao, L.; Feng, P.; Zhang, J.; Fu, X.; Liu, Y.; Yan, X.; Wang, T., Three-dimensional functionalized tetrapod-like ZnO nanostructures for plasmid DNA delivery. *Small* **2006**, 2, (5), 621-5.



12. Wang, Z. L., Functional oxide nanobelts: materials, properties and potential applications in nanosystems and biotechnology. *Annu Rev Phys Chem* **2004**, 55, 159-96.
13. Bhatia, S. K.; Shriver-Lake, L. C.; Prior, K. J.; Georger, J. H.; Calvert, J. M.; Bredehorst, R.; Ligler, F. S., Use of thiol-terminal silanes and heterobifunctional crosslinkers for immobilization of antibodies on silica surfaces. *Anal Biochem* **1989**, 178, (2), 408-13.
14. Shriver-Lake, L. C.; Donner, B.; Edelstein, R.; Breslin, K.; Bhatia, S. K.; Ligler, F. S., Antibody immobilization using heterobifunctional crosslinkers. *Biosensors & Bioelectronics* **1997**, 12, (11), 1101-1106.
15. Luzinov, I.; Julthongpiput, D.; Liebmann-Vinson, A.; Cregger, T.; Foster, M. D.; Tsukruk, V. V., Epoxy-terminated self-assembled monolayers: Molecular glues for polymer layers. *Langmuir* **2000**, 16, (2), 504-516.
16. Tsukruk, V. V.; Luzinov, I.; Julthongpiput, D., Sticky Molecular Surfaces: Epoxysilane Self-Assembled Monolayers. *Langmuir* **1999**, 15, (9), 3029-3032.
17. Ruan, C. M.; Yang, L. J.; Li, Y. B., Immunobiosensor chips for detection of Escherichia coli O157 : H7 using electrochemical impedance spectroscopy. *Analytical Chemistry* **2002**, 74, (18), 4814-4820.
18. Yang, L.; Li, Y., AFM and impedance spectroscopy characterization of the immobilization of antibodies on indium-tin oxide electrode through self-assembled monolayer of epoxysilane and their capture of Escherichia coli O157:H7. *Biosens Bioelectron* **2005**, 20, (7), 1407-16.
19. Mutin, P. H.; Guerrero, G.; Vioux, A., Organic-inorganic hybrid materials based on organophosphorus coupling molecules: from metal phosphonates to surface modification of oxides. *Comptes Rendus Chimie* **2003**, 6, (8-10), 1153-1164.
20. Aziz, M. A.; Yang, H., Electrochemical immunosensor using the modification of an amine-functionalized indium tin oxide electrode with carboxylated single-walled carbon nanotubes. *Bulletin of the Korean Chemical Society* **2007**, 28, (7), 1171-1174.
21. Guerrero, G.; Mutin, P. H.; Vioux, A., Anchoring of phosphonate and phosphinate coupling molecules on titania particles. *Chemistry of Materials* **2001**, 13, (11), 4367-4373.
22. Kim, P.; Jones, S. C.; Hotchkiss, P. J.; Haddock, J. N.; Kippelen, B.; Marder, S. R.; Perry, J. W., Phosphonic acid-modified barium titanate polymer nanocomposites with high permittivity and dielectric strength. *Advanced Materials* **2007**, 19, (7), 1001-+.
23. Demir, M. M.; Koynov, K.; Akbey, U.; Bubeck, C.; Park, I.; Lieberwirth, I.; Wegner, G., Optical properties of composites of PMMA and surface-modified zincite nanoparticles. *Macromolecules* **2007**, 40, (4), 1089-1100.
24. Breen, T. L.; Fryer, P. M.; Nunes, R. W.; Rothwell, M. E., Patterning Indium Tin Oxide and Indium Zinc Oxide Using Microcontact Printing and Wet Etching. *Langmuir* **2002**, 18, (1), 194-197.
25. Krishnamoorthy, S.; Bei, T.; Zoumakis, E.; Chrousos, G. P.; Iliadis, A. A., Morphological and binding properties of interleukin-6 on thin ZnO films grown on (100) silicon substrates for biosensor applications. *Biosens Bioelectron* **2006**, 22, (5), 707-14.
26. Thomsen, L.; Watts, B.; Dastoor, P. C., A NEXAFS orientation study of gamma-aminopropyltriethoxysilane on zinc oxide surfaces. *Surface and Interface Analysis* **2006**, 38, (7), 1139-1145.

27. Watts, B.; Thomsen, L.; Fabien, J. R.; Dastoor, P. C., Understanding the Conformational Dynamics of Organosilanes: gamma-APS on Zinc Oxide Surfaces. *Langmuir* **2002**, 18, (1), 148-154.
28. Kornherr, A.; French, S. A.; Sokol, A. A.; Catlow, C. R. A.; Hansal, S.; Hansal, W. E. G.; Besenhard, J. O.; Kronberger, H.; Nauer, G. E.; Zifferer, G., Interaction of adsorbed organosilanes with polar zinc oxide surfaces: a molecular dynamics study comparing two models for the metal oxide surface. *Chemical Physics Letters* **2004**, 393, (1-3), 107-11.
29. Sadik, P. W.; Pearton, S. J.; Norton, D. P.; Lambers, E.; Ren, F., Functionalizing Zn- and O-terminated ZnO with thiols. *Journal of Applied Physics* **2007**, 101, (10), 104514-5.
30. Liu, T. Y.; Liao, H. C.; Lin, C. C.; Hu, S. H.; Chen, S. Y., Biofunctional ZnO Nanorod Arrays Grown on Flexible Substrates. *Langmuir* **2006**, 22, (13), 5804-5809.
31. Soares, J. W.; Steeves, D. M.; Ziegler, D.; DeCristofano, B. S., Surface modification of nanocrystalline zinc oxide for bio-sensing applications. *Nanomaterial Synthesis and Integration for Sensors, Electronics, Photonics, and Electro-Optics* **2006**, 6370, 637011-9.
32. Tsai, M. Y.; Lin, J. C., Surface characterization and platelet adhesion studies of self-assembled monolayer with phosphonate ester and phosphonic acid functionalities. *Journal of Biomedical Materials Research* **2001**, 55, (4), 554-565.
33. Tlili, A.; Abdelghani, A.; Aguir, K.; Gillet, M.; Jaffrezic-Renault, N., Adsorption characteristics of self-assembled thiol and dithiol layer on gold. *Materials Science & Engineering C-Biomimetic and Supramolecular Systems* **2007**, 27, (4), 620-624.
34. Porter, M. D.; Bright, T. B.; Allara, D. L.; Chidsey, C. E. D., Spontaneously organized molecular assemblies. 4. Structural characterization of n-alkyl thiol monolayers on gold by optical ellipsometry, infrared spectroscopy, and electrochemistry. *J. Am. Chem. Soc.* **1987**, 109, (12), 3559-3568.

## **2008 AACR Annual Meeting, San Diego, CA, April 10-16**

**Title:** A microelectronic bulk acoustic wave biosensor array for the detection of PSA in complex solutions

**Authors:** Anthony Dickherber<sup>1</sup>, Christopher D. Corso<sup>2</sup>, John Petros<sup>3</sup>, Milton W. Datta<sup>4</sup>, William D. Hunt<sup>1</sup>

<sup>1</sup>Departments of Electrical Engineering, Georgia Institute of Technology, Atlanta, GA

<sup>2</sup>Departments of Biomedical Engineering, Georgia Institute of Technology, Atlanta, GA

<sup>3</sup>Department of Urology and Winship Cancer Institute, Emory University, Atlanta, GA & the Atlanta VA Medical Center

<sup>4</sup>Department of Pathology, Abbott Northwestern Hospital and University of Minnesota, Minneapolis, MN

**INTRODUCTION:** Microelectronics offers the opportunity to develop inexpensive biosensors for portable disposable biomarker assays that are easily multiplexed, highly sensitive, and highly specific. Such biosensors could impact clinical diagnosis through point of care testing for biomarkers that predict tumor diagnosis or clinical recurrence. We have previously demonstrated such technology using quartz crystal microbalance (QCM) sensors. Here we extend our findings with a bulk acoustic wave (BAW) sensor that provides magnitudes of greater potential sensitivity with multiplexing capabilities. In this research we present a mass produced inexpensive 8-device array and demonstrate detection of the biomarker PSA from LnCap conditioned medium.

**METHODS:** The ZnO BAW sensor chip platform involves an 8-device array that can be used as a biosensor in complex solutions such as serum. The sensors utilize molecular perturbation of acoustic waves generated by electrodes as the detection mechanism. An appropriate surface-preparation process was determined for covalently binding monoclonal antibodies to the zinc oxide crystal to functionalize each sensor toward a specific target. The sensor arrays were then used to assay for the presence of PSA (sc-52170) and FITC (negative control, sc-69871) in conditioned medium from LNCaP prostate cancer cells.

**RESULTS:** Covalent immobilization of monoclonal antibodies to the ZnO crystal surface via a crosslinker and an organosilane monolayer was assessed via atomic force microscopy, confocal laser scanning microscopy and contact angle measurements. Results indicate the significant presence of antibodies bound to the surface. Subsequent exposure of the device arrays to LnCap conditioned medium demonstrated a significant device response of the PSA-targeted sensor over the FITC-targeted sensor. The antibody immobilization process currently requires only about 3 steps and takes roughly 1 day to prepare. Detection of targeted markers in the sample is evident nearly instantaneously once presented to the device surface. Binding of conjugated PSA from the conditioned medium yielded an easily measured 12 kHz shift on average.

**CONCLUSIONS:** Here we present an inexpensive BAW sensor array that can be rapidly and efficiently conjugated with antibodies and used for the detection of circulating biomarkers in complex solutions such as serum. This extends our prior proof of concept work with quartz crystal microbalances to a smaller inexpensive device while offering potentially greater sensitivity by several orders of magnitude. We have demonstrated an appropriate protocol for the rapid and efficient covalent binding of monoclonal antibodies to the sensor surface and the subsequent detection of PSA in LnCap conditioned medium. This system allows for multi-component biomarker array formation for rapid multiplex testing and extensive statistical data analysis.

# Anthony Dickherber

356 Foxfire Drive, Smyrna, GA 30082

404.783.0881 | [tonyd@gatech.edu](mailto:tonyd@gatech.edu)

---

## Academic Background

Georgia Institute of Technology, Atlanta, GA 2003 - Present

### **PhD Candidate in Bioengineering**

Thesis Advisor: Professor William D. Hunt

Thesis: Design and implementation of an acoustic resonator based biosensor for the early detection of prostate cancer

Minor: Public Policy (Graduate Certificate, pending)

Georgia Institute of Technology, Atlanta, GA June 2002

### **Master of Science in Electrical and Computer Engineering (Non-thesis)**

Specialization: Digital Signal Processing and Bioengineering

Georgia Institute of Technology, Atlanta, GA June 1999

### **Bachelor of Science in Electrical and Computer Engineering**

Specialization: Analog circuit design and Bioengineering

Coop Program: Scientific Atlanta, Inc.

Undergraduate Research Opportunity Program

## Research Experience

Georgia Institute of Technology, Atlanta, GA 2004 - Present

### **Graduate Teaching Assistant, Department of Biomedical Engineering**

- Head TA for BMED 3500: Biosensor and Instrumentation lab
- TA for ECE 2025: Intro to Digital Signal Processing, ECE 3741: Analog circuit design lab
- Prepared and delivered numerous lectures for ECE 3711: Bioelectronics

Georgia Institute of Technology, Atlanta, GA 2003 - Present

### **Graduate Research Assistant, Microelectronics Research Center**

- Development of novel bulk acoustic wave device technology and application towards medical and national security applications as sensing devices
- Investigation of chemically specific surface treatments of resonators for biosensor applications

Georgia Tech Research Institute, Atlanta, GA 1999 - 2003

### **Research Engineer, Information Technology & Telecommunication Laboratory**

- Extensive digital signal analysis using government-issue XMIDAS software package for communications research for classified government projects
- Extensive experience with GSM communication standard and analysis of GMSK waveforms using software radio
- Survey current technology in a variety of areas such as digital voice recorder technology and laser technology and participated in defining the international communications standards: Dedicated Short Range Communication (DSRC) standard
- Maintain a secret-level government security clearance for general technology assessment and analysis of devices on classified government projects

### **Undergraduate Research Assistant**

- Built and tested prototype analog and digital circuits for research engineers in the international set-top box research and development laboratory
- Built, calibrated and maintained equipment to simulate cable television provider networks, including digital control hubs, modulators, and signal scramblers

### **Leadership & Service Experience**

- Director of NSF ERC (GTEC) Student Leadership Council: Bioengineering and Bioscience Unified Graduate Students (managing a budget of ~\$20K towards professional and social activities organized by 6 different student committees) 2006-2007
- Biotechnology Policy Forum, member 2004 – 2008, Chair 2006-2008
- Sam Nunn Security Program Fellow, a MacArthur Foundation initiative, 2006-2007
- Bioengineering Graduate Student Advisory Committee 2004-2006
- GTEC (Georgia Tech/ Emory Center) Education & Outreach volunteer 2004-2005
- Winner of National University of Singapore annual International Business Plan competition (2002) involving an approach to apply emerging sensor technology to address port security as well as company logistics issues
- Volunteer for Hedge Funds vs. Malaria conference hosted by Emory University and sponsored by the Malaria Foundation International 2005
- Active volunteer for Trees Atlanta, Georgia Public Broadcasting/National Public Radio, Medshare International and Habitat for Humanity
- Philippine Refugee Processing Center Volunteer: Taught English and lectured on American culture to large groups of refugees varying in age from 18-75 while living in a Vietnamese refugee camp 1993
- Worked full time as a research engineering for GTRI while pursuing M.S.ECE 1999-2002
- Worked part time to cover living expenses while pursuing undergraduate degree full time (worked in engineering R&D, food service, construction, real estate advertising, student research, and managing personal investments) 1994-1999

### **Selected Publications/Presentations**

Christopher D. Corso, Anthony Dickherber, Peter Hotchkiss, Seth Marder, William D. Hunt, “A comparison of antibody immobilization methods employing organosilanes and phosphonic acids on planar crystalline ZnO surfaces,” *Lanmuir*, under review 2008

Anthony Dickherber, Christopher D. Corso, John Petros, William D. Hunt, “A microelectronic bulk acoustic wave biosensor array for the detection of PSA in complex solutions,” *2008 Annual Meeting of American Association for Cancer Research*, San Diego, CA, April 10-16, 2008

Anthony Dickherber, Christopher D. Corso, William D. Hunt, “Optimization and characterization of a ZnO biosensor array,” *Sensors & Actuators A: Physics*, Feb 5, 2008

Christopher D. Corso, Peter J. Edmonson, Anthony Dickherber, William D. Hunt, “A multi-element acoustic wave device sensor based on a filter network configuration,” *IEEE Sensors Journal*, pending acceptance, submitted September 2007

Anthony Dickherber, Christopher D. Corso, and William Hunt, "Stability of a RF sputtered ZnO solidly mounted resonator sensor in varying temperature and conductivity environments," *IEEE Sensors Conference*, Atlanta GA, Oct 29-31 2007

Christopher D. Corso, Anthony Dickherber, and William D. Hunt, "A thickness shear mode zinc oxide liquid sensor with off-axis excitation," *IEEE Sensors Conference*, Atlanta GA, Oct 29-31 2007

Cleon E. Davis, Anthony J. Dickherber, William D. Hunt, and Gary S. May, "An acoustic temperature sensor to monitor variable frequency microwave curing of polymer dielectrics," *IEEE Sensors Conference*, Atlanta GA, Oct 29-31 2007

Anthony J. Dickherber, Christopher D. Corso, William D. Hunt, Ira Pastan, Mitchell Ho, Raffit Hassan, "Mesothelin-fc fusion protein detection using a novel microelectronic acoustic sensor platform," *2007 AACR International Conference on Molecular Diagnostics in Cancer Therapeutic Development*, Atlanta, GA Sept 17-20, 2007

Christopher Corso, Anthony Dickherber, William Hunt, "Lateral field excitation thickness shear mode waves in a thin film ZnO solidly mounted resonator," jointly in *Journal of Applied Physics*, Vol. **101**(5), 1 Mar. 2007 & *Virtual Journal of Biological Physics Research*, 15 Mar 2007

Anthony Dickherber, Christopher Corso, William Hunt, "Dual Mode Sensing," *IEEE Engineering in Medicine and Biology Conference 2006*, NYC NY, Aug 28-Sep3 2006

Anthony Dickherber, William Hunt, "Breaking Down Cost Barriers to Improve Public Health," *The Sam Nunn Bank of America Policy Forum*, Atlanta, GA March 27 2006

Christopher Corso, Anthony Dickherber, Payal Shah, Alexandra Migdal, Milton Datta, Sumana Datta, William Hunt, "Development of a Simple Inexpensive Bulk Acoustic Wave Nanosensor for Cancer Biomarkers: Detection of Secreted Sonic Hedgehog from Prostate Cancer Cells," *2006 Annual Meeting of American Association for Cancer Research*, Washington DC, April 4, 2006

William Hunt, Christopher Corso, Anthony Dickherber, "Piezoelectric Bulk Acoustic Wave Biosensors for Real-Time Biomarker Detection in Complex Media," *Moving Biosensors to Point-of-Care Cancer Diagnostics* (National Cancer Institute Conference), Rockville, MD, June 8-9, 2005

Anthony Dickherber, "Towards Integration of ZnO Resonator Components with GaAs Microelectronics," *Motorola University Partnership in Research Program Conference*, Chicago, IL, October 2004

## **Grants Awarded**

- Pre-doctoral training award, US Army Medical Research and Materiel Command Prostate Cancer Research Program, *Development of Highly Sensitive Bulk Acoustic Wave Device Biosensor Arrays*, Award:\$67,824.00; Duration: 1/1/2007 to 12/31/2008

## Patents

- Provisional patent: *A Novel High Quality Bulk Acoustic Wave Thickness Shear Mode Resonator/Transducer by Lateral Field Excitation of a Multi-layer Piezoelectric Bulk*, Filed: July, 2006
- United States Patent Application No.11/822045, “An acoustic wave sensor assembly utilizing a multi-element structure,” filed July 2, 2007
- Patent (6754487), *Radio network test analysis system*, Issued: Jun 22, 2004

## Technical/Specialized Skills

- Device fabrication and testing: expert technician of most microelectronic clean-room equipment, including RF/DC sputtering system, electron-beam evaporation system, x-ray diffraction, contact photolithography, lift-off patterning, etching, wafer dicing, wafer profiling, and wafer probe testing using probing station and vector network analyzer and various rough/mechanical pumps and cryopumps
- Regularly attend weekly urological oncology board meetings of multiple major hospital systems in the Atlanta, GA, metro-area to review ongoing patient care
- Biological lab experience including use of confocal microscopy, fluorescence labeling, atomic force microscopy, scanning electron microscopy, antibody-antigen system development, various capture molecule systems development, cancer proteomics research
- Engineering tools: MATLAB, Microwave Office, Advanced Design System software, SPICE, LabVIEW, FEMLAB (Comsol Multiphysics Finite Element Analysis software), ImageJ, Microsoft Office suite
- General electrical diagnostic equipment: proficiency with a broad array of standard lab equipment, including signal and vector generators, spectrum and vector network analyzers, analog and digital oscilloscopes, digital multi-meters and supply units, power generators, and general electromechanical control systems
- Amateur automotive mechanic and general home contractor